©Copyright 2020
Andrew M. Pace

Stepping Towards Control of Systems Undergoing Impact for Legged Locomotion

Andrew M. Pace

A dissertation
submitted in partial fulfillment of the
requirements for the degree of

Doctor of Philosophy

University of Washington

2020

Reading Committee:

Samuel A. Burden, Chair

Aleksandr Aravkin

J. Nathan Kutz

Program Authorized to Offer Degree:
Electrical Engineering

University of Washington

Abstract

Stepping Towards Control of Systems Undergoing Impact for Legged Locomotion

Andrew M. Pace

Chair of the Supervisory Committee:
Dr. Samuel A. Burden
Electrical Engineering

This dissertation focuses on bringing control theory to mechanical systems subject to unilateral constraints, with the focus on legged locomotion. The key feature of these systems is the impact that occurs, causing a sudden change in the velocity of the object and a potential change in its underlying vector fields. The primary challenge for such systems arises from constraint activation, in other words, when a leg transitions from moving through the air to the ground. Throughout this dissertation, the dynamics are captured using the modelling paradigm of hybrid dynamical systems. In the language of hybrid dynamical systems, a *reset* occurs causing instantaneous change in the systems velocity. In addition, when a constraint activates or deactivates, the underlying vector field discontinuously changes. Such discontinuities violate continuity and smoothness assumptions many classical control techniques impose. This dissertation focuses on developing three aspects of control for legged locomotion: developing a control law about a desired trajectory undergoing simultaneous constraint activation, such as a pronk gait, determining the complete state, both discrete and continuous, of the system from noisy measurements, and finding a control law to track a desired trajectory through contact.

TABLE OF CONTENTS

LIST OF FIGURES

LIST OF TABLES

ACKNOWLEDGMENTS

The work of this dissertation, while mine, was never mine alone. I want to take this opportunity who explicitly and implicitly played some role in completing this dissertation. I will start with thanking my adviser, Professor Sam Burden, for the immense guidance he gave, the continuous support, and the encouragement to look beyond existing tools and techniques to come up with novel methods. Additionally, I want to thank the remainder of my committee: Professor Sasha Aravkin, for showing me the development of an objective function goes hand in hand with the optimization algorithm, Professor Nathan Kutz, for making me think of how to make hybrid dynamics more widely used, and Professor Mike Brett, for teaching me the French roll (and for taking the time to serve as GSR!).

Next, I want to thank my other collaborators Jize Zhang for tolerating the many iterations of our paper's figures, Rahul Malik [1] for patiently explaining how Dual Active Bridge (DAB) converters works over and over again, and both for their immeasurable patience with explaining new concepts.

The many people who have come through the "Burden Group," Bora Banjanin, Yana Sosnovskaya, Momona Yamagami, Ben Chasnov, Joey Sullivan, Shruti Misra, Tianqi Li, and Liam Han; to all of you, I am greatly indebted. Without our frequent conversations and chats that go far beyond research, I may not have completed this dissertation. To the many people both in and outside of BRL who have supported and encouraged me throughout this process, Andy Lewis, Nava Agadhasi, Kevin Huang, Astrini Sie, Dianmu Zhang, David Caballero, Vijeth Rai, Katherine Pratt, Sarah Li, Yohan Min, Gaurav Mukherjee, and all the members

[1] The work from the collaboration with Rahul unfortunately does not appear in this dissertation. Instead, it can be found in [69] and perhaps in a part Rahul's future dissertation.

of Seattle Cattle, I thank you; all of our conversations, from the general companionship to the advice, helped me push through. I thank Brandon Larson and Jennifer Huberman for advising me and helping me figure out all the necessary forms needed to actually graduate. Additionally, I would like to thank the creators and contributors of NumPy [81, 104] and Matplotlib [47], whose use was necessary for the computational examples throughout this dissertation.

Finally, I thank my family. My parents for humoring me on this journey and their unending support throughout my life. My sister for and bringing along Patch, who helped me adjust to walking in the constant Seattle drizzle.

Chapter 1

INTRODUCTION

In this dissertation I seek to solve of the challenges facing control of legged robots. The challenge of such systems is the sudden change in velocity whenever a leg touches down, particularly when running with legs of significant mass. Many current control techniques for legged locomotion attempt to minimize or remove these discontinuities, either through modeling (massless limbs, multi-level control such as templates and anchors [36]) or control that minimizes impact velocity. As part of the goal of this dissertation, I seek to enable control that at the model level does not require such workarounds.

Throughout this dissertation, I will be assuming the robot is made of rigid mechanical components, neglecting the rich subfield of soft robotics. This assumption makes possible the use of *hybrid dynamical systems*[1] in a straightforward manner. Additionally, modeling the physical system as a hybrid dynamical system, in particular a mechanical system subject to unilateral constraints, captures the salient features of the real world dynamics. That is, the flow of such models are left-continuous.[2]

Three critical components, but by no means the only critical component, of any closed loop control system are tracking a reference, state estimation, and generating the control signal. Classical control[3] focuses on controlling continuous flows. For each of these three problems, classical solution has several solutions for. While hybrid dynamics is not a new field and has been used for control, most of the early motivation was for continuous systems and later work seeks general control techniques for all hybrid dynamics. It is my view, much

[1] Also *hybrid system* or *hybrid dynamics*

[2] As will be briefly touched on in chapter 4, hybrid dynamics is but one modeling choice for such systems, complementarity and measure differential inclusion are two others.

[3] Which I lump so called *modern* control theory as part of.

can be gained by incorporating knowledge from mechanics into the control techniques. This dissertation will not solve these challenges for legged robots but to provide feasible paths forward.

1.1 A brief overview of rigid mechanical systems modeled as Hybrid Dynamical Systems

Before proceeding, I will provide an overview of the relevant portions of hybrid dynamics as will be useful in this dissertation. See [39] for a general introduction to hybrid dynamics and [50] for a more detailed account of modeling legged robots with hybrid dynamics. The hybrid domain, which in this dissertation may sometimes be referred to as mode or discrete state, indexes into the set of underlying vector fields. To account for this additional information, I will refer to the state of a hybrid system as the continuous state and discrete state. A guard is a set of sets within the hybrid domain specifies when the state change, either the discrete or continuous or both change[4] may change. For a legged robot, guard generally correspond to when unilateral constraints are *active*, which is equal to zero. When a unilateral constraint becomes active, an *impact* occurs which causes a jump in state's velocity such that the unilateral constraint is not violated. In hybrid systems, this jump in state is referred to as a *reset* and what causes the discontinuous trajectories.

1.2 Dissertation Content

Chapter 2 (Aim 1) This chapter focuses on showing tracking a feasible trajectory for a very particular system, the nonplastic inelastic billiard. We show that while the well known *mirror law* [35] for the elastic billiard uses a technique of extending the tracked trajectory past unilateral constraints, a similar method is not possible for inelastic billiards. From this example, we conjecture geometric control techniques for continuous systems [1, 22] cannot be used for mechanical systems with inelastic collisions.

[4]There can be guards and corresponding resets that don't cause either to change, that is not the norm.

1.2.1 Chapter 3 (Aim 2)

The aim of this chapter is to develop an estimator for the complete state. In it, we incorporate the discontinuous jumps in continuous state into the process noise by using the Student's t distribution. Additionally, we formulate the state estimation problem as an optimization problem, relaxing the restriction the discrete state from being nodes of the simplex to lying anywhere within the simplex. This relaxation, results in a *smooth*-nonconvex objective function. We provide demonstration of the state estimation technique of simulated data for a mechanical hopper.

1.2.2 Chapter 4 (Aim3)

This chapter focuses on differentiability for legged robots, particularly in cases where simultaneous activation occurs. In it we[5] show that for *admissible* trajectories undergoing simultaneous impacts of lift-offs the flow is piecewise–differentiable. Under more restricted assumptions, we show the flow is at least once (classically) differentiable. Additionally, we provide two example systems. One, a biped like model, we provide three variations demonstrating discontinuous, piecewise–differentiable, and differentiable flow. The other, the double pendulum, we develop a controller for using the implicit function for piecewise–differentiable functions.

[5]All work in this dissertation comes out of collaborations with my adviser, Professor Sam Burden, and others as indicated at the beginning of the chapters.

Chapter 2

NONPLASTIC INELASTIC BILLIARDS MUST HAVE A NEW DISTANCE FUNCTION[1]

2.1 Abstract

In this chapter, we show the nonexistence of an *extended* distance function *compatible* (defined below) with the constrained distance function under a projection preserving trajectories in the constrained space for the 1-DOF nonplastic inelastic billiard. We show the nonexistence by extending the system past the point of impact in a manner similar to the mirror law [35] and then construct a projection from the extended state space to the constrained state space such that a trajectory undergoing one impact in the constrained space maps uniquely to a trajectory in the extended space. We then show there does not exist a distance function on the extended space by showing any function on the extended space cannot be both *compatible* with the constrained space distance function and continuous. Hence, classical geometric tracking techniques [1, 22] cannot be used for tracking (or state estimation of) inelastic billiards. Furthermore, we conjecture for any rigid mechanical system undergoing impacts, there does not exist a local continuous extension of any nonplastic inelastic mechanical system with a consistent distance function as essential features of the dynamics of the 1-DOF billiard embed in such systems around impact.

2.2 Introduction

A common technique in tracking a desired trajectory or in observer design uses *distance* between the current state and the desired state (tracking) or between the estimated state and observed state (estimation); for mechanical systems state includes both position and

[1]The results of this chapter stem from several enlightening discussions with Todd D. Murphey.

velocity. Many methods exist for determining distance, and hence error, for a continuous trajectory of a mechanical system. For these smooth systems with continuous trajectories, the underlying differential geometric structure of the mechanical system can be used to develop a tracking controller [22] or observer [1].[2] For rigid mechanical systems subject to unilateral constraints, discontinuity at points of impact distinguishes these trajectories from other smooth mechanical systems. The impact times for the desired trajectory and the reference trajectory generally differ. While the position distance remains constant at the point of impact, the velocity error will jump discontinuously. For perfectly elastic collisions, the *mirror law* [35] accounts for the discontinuity in error at points of impact by extending the trajectory of either the desired trajectory or the actual trajectory past the unilateral constraint when only one of the trajectories has undergone impact. The error distance used for reference tracking then uses this extended trajectory. Within this chapter we seek to show for billiards undergoing nonplastic inelastic impacts, no similar method exists.

In this chapter, we present the 1-DOF billiard, the simplest possible example of a mechanical system undergoing impact. We detail the dynamics and state space of the system and then describe the extended state space. Next, we motivate the definition of *compatible* by equating points in $T\widetilde{C}$ with corresponding points along a trajectory in TC. After which we present the main result of this chapter in section 2.3.3: for the nonplastic inelastic 1-DOF billiard, there does not exist an extended distance function that is compatible with the distance function on the constrained state space. We conclude with a conjecture that no mechanical system undergoing inelastic impact has an extension with a compatible function and a brief overview of other methods of tracking trajectories for mechanical systems undergoing impact and more general hybrid dynamical systems.

---

[2]While both of these techniques are mathematically sound, implementation issues remain, such as determining the geodesic on the underlying Riemannian manifold. Outside of the examples given in [22], closed form solutions for geodesics are scarce. First order approximations of the geodesic distance and parallel transport between two points near each other are provided in [1, II.C].

2.3 Nonplastic Inelastic 1-DOF Billiard

In this section, we construct a distance function for the 1-DOF billiard[3] with no external forcing, undergoing an inelastic impact. Constructing an appropriate distance function is a key aspect of any tracking controller. We then show no distance function can exist for the complete trajectory when either the reference or the nominal trajectory undergoes impact.

REMARK 1. *We aim to simplify the exposition of this example. With this goal in mind, we relegate much of the technical nuances of extending the example to more complicated systems to the footnotes. We hope that the citations included in these footnotes may enable future readers to formalize this extension.*

2.3.1 Constrained Billiard

We begin by describing the 1-DOF billiard system. Let $q \in Q = \mathbb{R}$ be the position of the billiard and let $a\colon Q \to R$ with $a(q) = q \geq 0$ be the unilateral constraint.[4] The motion of the billiard is restricted such that the unilateral constraint is satisfied for all time. The feasible configuration space of the system is then $C = \mathbb{R}^+ = \{q | q \geq 0\}$. The overall feasible state space of the system is then $TC = \mathbb{R}^+ \times \mathbb{R} \ni (q, \dot{q})$.[5] Fig. 2.1 provides a visual representation of the feasible configuration and state spaces for the billiard system.

Next, we describe the dynamics of the billiard. For simplicity, let the mass matrix[6] $M(q) = I$. Hence, the distance between two points $x, y \in TC$ is given by

$$d\colon TC \times TC \to \mathbb{R}^+ \qquad d(x, y) = \|x - y\|_2 \,, \tag{2.1}$$

[3]Billiards is game with a long history of generating mathematical problems. See [62] for one such early example.

[4]In an effort to simplify notation, we will overload a to have domain of Q or $TQ \supset TC$. By $a\colon TQ \to R$ we mean $a \circ \Pi_Q$, where $\Pi_Q\colon TQ \to Q$ is the canonical projection operator onto manifold Q.

[5]TC notation denotes the tangent bundle in the context of smooth manifolds [60, App. A].

[6] In geometric mechanics, the mass matrix determines the distance between two points on the underlying space [65, §2.4]. A constant mass matrix, also referred to as a flat metric, greatly simplifies the challenge of finding this distance. A Riemannian manifold is said to have a flat metric (or be flat) if it is locally isometric to an Euclidean space [60, pg. 12].

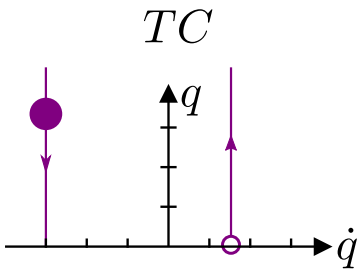

Figure 2.1: A graphical representation of a trajectory in TC. The arrows indicate the direction of travel with increasing time t.

the ℓ^2-norm.[7] Additionally, we assume no external forces act on the billiard. With some abuse of notation,[8]

$$M(q)\ddot{q} = \ddot{q} = 0. \tag{2.2}$$

Finally, let the coefficient of restitution $\gamma \in (0, 1)$. That is, the billiard undergoes neither a perfectly plastic[9] $\gamma = 0$ nor perfectly elastic $\gamma = 1$ impact. The impact law is

$$\dot{q}^+ = -\gamma \dot{q}^- \tag{2.3}$$

and impact occurs when $a(q) = 0$ and $\dot{q} < 0$, where $\dot{q}^+$ and $\dot{q}^-$ denote the right- and left-handed limits, respectively. We adopt the convention that the trajectories generated by eqs. (2.2) and (2.3) are right-continuous. Without loss of generality, we will assume for

[7] In general, the metric for a Riemannian manifold M does not give a unique metric on the tangent bundle TM, also a Riemannian manifold. A metric is used to calculate the distance of the infimal path between two points on a manifold. In order to calculate the distance for both position and velocity between a reference and a controlled trajectory, that is the distance on TC, a metric on TC is needed. See [1, 22] for methods of calculating the distance between two points in TC with applications in tracking and observers, respectively. For a general discussion on constructing a *natural Riemannian metric* on TC, see [77] for a brief overview.

[8] For a mechanical system with dynamics given by differential geometry, external forces are cotangent vectors [65, §2.3] and the Levi-Civita connection [65, §2.4] provides a way of defining acceleration giving a choice of coordinates. See [60, Chp. 4] for an explanation of why acceleration differs from the time derivative of the velocity vector on a general smooth manifold.

[9] For reasons that will not be discussed in this paper, a perfectly plastic impact gives rise to a sub-Riemannian metric [74].

any trajectory[10] the time of impact occurs at $t = 1$, $a(\zeta(t = 1)) = 0$. Additionally, we will consider only trajectories that undergo impact. Equivalently, the trajectories under consideration are those with nonzero velocity. These two assumptions imply the velocity for any considered trajectory at $t = 0$ is negative.

REMARK 2. *As $\gamma \neq 0$ and the force is constant, any trajectory can be extended to any time. That is, for a given trajectory $\zeta\colon [a, b] \to TC$ with $a, b \in \mathbb{R}$ and $a < b$, there exists a unique trajectory $\overline{\zeta}\colon \mathbb{R} \to TC$ such that $\overline{\zeta}|_{[a,b]} = \zeta$. That is for all $q, \dot{q} \in TC$, there exists a trajectory $\zeta\colon \mathbb{R} \to TC$ such that $\zeta(0) = (q, \dot{q})$. Without loss of generality, we will assume all trajectories have domain $\mathbb{R}$ and $a(\zeta(t = 1)) = 0$. That is the impact for all trajectories occurs at time $t = 1$.*

2.3.2 Extended Billiard

We now introduce the extended billiard system, a system that does not undergo impacts resulting in continuous trajectories. The two key characteristic of trajectories for the extended system are equality with a unique trajectory on the constrained system TC under the defined projection and continuity.[11]

Let the extended configuration space be denoted with $\widetilde{C} = \mathbb{R} \ni \tilde{q}$. There are no unilateral constraints for the extended system. The extended state space is then $(\tilde{q}, \dot{\tilde{q}}) \in T\widetilde{C} = \mathbb{R} \times \mathbb{R}$. For notational purposes, we partition the extended state space into two nonoverlapping half-spaces with

$$\begin{aligned} T\widetilde{C}_+ &= \left\{(\tilde{q}, \dot{\tilde{q}}) : \tilde{q} \geq 0\right\} \\ T\widetilde{C}_- &= \left\{(\tilde{q}, \dot{\tilde{q}}) : \tilde{q} < 0\right\}, \end{aligned} \tag{2.4}$$

$T\widetilde{C} = T\widetilde{C}_+ \bigsqcup T\widetilde{C}_-$.[12] Fig. 2.2 provides a visual representation of the extended state space

[10] As this assumption is not used to generate a tracking controller, it is not the same as assuming the reference and nominal (or plant) trajectory impact at the same time.

[11] The idea for the extended system is inspired by [85].

[12] By $T\widetilde{C} = T\widetilde{C}_+ \bigsqcup T\widetilde{C}_-$, we mean $T\widetilde{C} = T\widetilde{C}_+ \bigcup T\widetilde{C}_-$ and $T\widetilde{C}_+ \bigcap T\widetilde{C}_- = \emptyset$.

and the partitions. As no external forces act on the constrained system,[13] there are no forces on the extended system, yielding

$$\ddot{\tilde{q}} = 0. \tag{2.5}$$

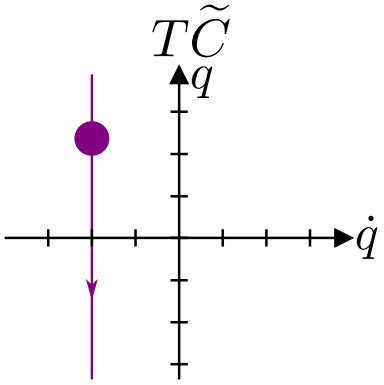

Figure 2.2: An example trajectory in $T\widetilde{C}$.

We construct a projection operator $P\colon T\widetilde{C} \to TC$ such that a trajectory in $T\widetilde{C}$, $\widetilde{\zeta}\colon \mathbb{R} \to T\widetilde{C}$ maps to a unique trajectory in TC, $\zeta\colon \mathbb{R} \to TC$. Equivalently, the projection operator is such that a trajectory in TC, which undergoes exactly one impact, corresponds to one trajectory in $T\widetilde{C}$. That is $P \circ \widetilde{\zeta} = \zeta$. We define P as

$$P(\tilde{q}, \dot{\tilde{q}}) = \begin{cases} (\tilde{q}, \dot{\tilde{q}}) & \text{if } \tilde{q} \geq 0 \\ (-\gamma\tilde{q}, -\gamma\dot{\tilde{q}}) & \text{if } \tilde{q} < 0. \end{cases} \tag{2.6}$$

That is $P|_{T\widetilde{C}_+} = I$ and $P|_{T\widetilde{C}_-} = -\gamma I$. See Fig. 2.3 for a visualization of P.

Remark 3. *As there is no acceleration on the extended system eq.* (2.5)*, any extended trajectory* $\widetilde{\zeta}$ *that maps to a given* ζ *in* TC *under* P*,* $P \circ \widetilde{\zeta} = \zeta$*, must have the same initial condition* $\widetilde{\zeta}(t = 0) = \zeta(t = 0)$ *and be continuous. Clearly, there is only one such extended trajectory* $\widetilde{\zeta}$ *for every trajectory* ζ *with nonzero velocity. Additionally, if* $\widetilde{\zeta}(t) \in T\widetilde{C}_+$*, then*

[13] In general, if there are forces on the constrained system, the extended system will experience forces mapped with the projection operator P eq. (2.6). For instance, in the bouncing ball system the sign of the force will switch. See [68, § 1.6] for how dynamics change under a smooth mapping.

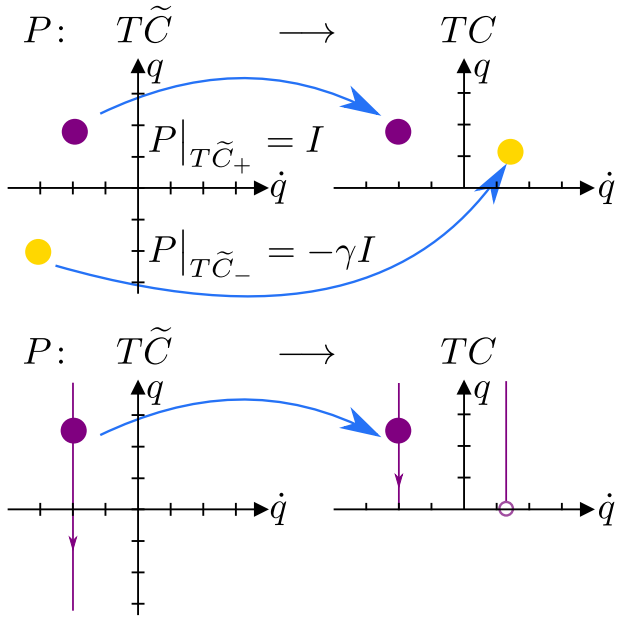

Figure 2.3: Visual representation of the projection P on two points in $T\widetilde{C}$ and their corresponding points in TC(top) and for a trajectory (bottom).

the point on the corresponding trajectory $\zeta(t)$ has not yet undergone impact. Likewise, if $\widetilde{\zeta}(t) \in T\widetilde{C}_-$, then $\zeta(t) = (P \circ \zeta)(t)$ is post-impact.

REMARK 4. *The position after projection for $P|_{T\widetilde{C}_-}$ changes as any $(\tilde{q}, \dot{\tilde{q}}) \in T\widetilde{C}_-$ violates the unilateral constraint, $a(\tilde{q}) < 0$. As TC is the codomain of P, the unilateral constraint is not violated after projection, $a\left(P(\tilde{q}, \dot{\tilde{q}})\right) \geq 0$ for all $(\tilde{q}, \dot{\tilde{q}}) \in T\widetilde{C}$.*

REMARK 5. *With the assumptions the time of impact for trajectory ζ occurs at $t = 1$, $a(\zeta(t = 1)) = 0$, and ζ has nonzero velocity, the unique (Remark 3) corresponding extended trajectory $\widetilde{\zeta}$ will remain in the left-half plane;*[14] *for all $t \in \mathbb{R}$, $\widetilde{\zeta}(t) = \left(\tilde{q}, \dot{\tilde{q}}\right)(t), \dot{\tilde{q}}(t) < 0$.*

[14]This is not the case when extending the trajectories for systems with force. See footnote 13 for a brief comment and systems with nonzero forces.

2.3.3 A compatible *function under P on $T\widetilde{C}$ does not exist*

As $T\widetilde{C}$ and TC are not the same space,[15] we provide a definition relating distance on $T\widetilde{C}$ to distance on TC, using the idea points in $T\widetilde{C}$, TC lie along trajectories. In particular, we focus on when both points $x, y \in T\widetilde{C}_+$ or both $x, y \in T\widetilde{C}_-$. Following from Remark 3, if both $x, y \in T\widetilde{C}_+$ then both points along their corresponding trajectories in TC have not undergone impact. Likewise, if both points are in $T\widetilde{C}_-$, then both points occur after each respective trajectory has undergone impact. In these two instances, the two points along their corresponding trajectories have both either undergone or not undergone an impact, and as such we wish to preserve the corresponding distance in TC under the projection P.

Definition 1. *A function $\widetilde{d}$ on $T\widetilde{C}$ is* compatible *with distance function d on TC under P when*

$$\widetilde{d}(x, y) = d\left(P(x), P(y)\right) \text{ if } x, y \in T\widetilde{C}_+ \text{ or if } x, y \in T\widetilde{C}_-. \tag{2.7}$$

Fig. 2.4 gives a visual representation of the two cases for when functions d and $\widetilde{d}$ are compatible.

Remark 6. *The definition of $\widetilde{d}$* compatible *with d under P does not restrict the definition of $\widetilde{d}$ everywhere, e.g. $\widetilde{d}(x, y)$ when $x \in T\widetilde{C}_-$ and $y \in T\widetilde{C}_+$.*

We now provide the main result of this paper, for the constructed extended state space $T\widetilde{C}$ and projection P, there does not exist a function that is compatible with d.[16] We prove this fact by showing any compatible function cannot be continuous and hence is not a distance function. Fig. 2.5 provides a visual representation for the proof of theorem 1.

Theorem 1. *There does not exist a distance function $\widetilde{d}\colon T\widetilde{C} \times T\widetilde{C} \to \mathbb{R}^+$ that is compatible with the distance function $d\colon TC \times TC \to \mathbb{R}^+$ eq. (2.1) under $P\colon T\widetilde{C} \to TC$ eq. (2.6) for nonplastic inelastic impacts $\gamma \in (0, 1)$.*

[15] For instance, topologically TC has a boundary and $T\widetilde{C}$ does not.

[16] All distance functions are continuous [76, Chp. 2 §20 Exercise 3].

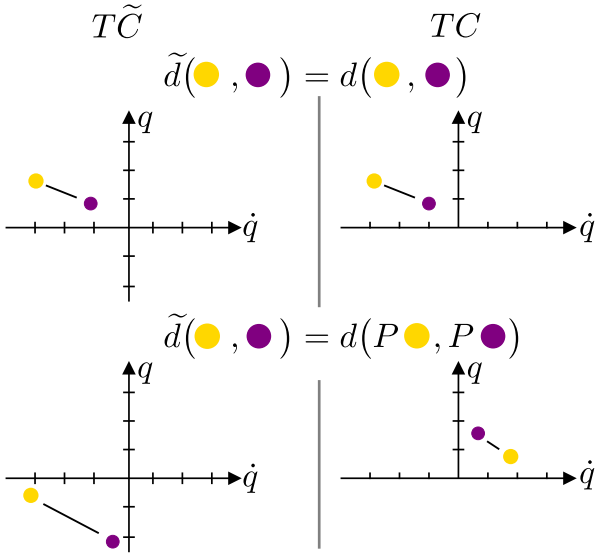

Figure 2.4: A visual representation of function $\widetilde{d}$ *compatible* with d under P, (top) when both points are in $T\widetilde{C}_+$ (bottom) when both points are in $T\widetilde{C}_-$.

Proof. Let $\widetilde{d}\colon T\widetilde{C} \times T\widetilde{C} \to \mathbb{R}^+$ be a distance function on $T\widetilde{C}$. Assume for the sake of contradiction $\widetilde{d}$ is compatible with d under P. Let $x = (0, -v)$ and $y = (0, -v - \delta)$ for some $v, \delta > 0$; $x, y \in T\widetilde{C}$.

$$\widetilde{d}(x, y) = d\left(P(x), P(y)\right) = d\left((0, -v), (0, -v - \delta)\right) = \delta \tag{2.8}$$

Let $z_n = (-1/n, -v)$ and $w_n = (-1/n, -v - \delta)$ for $n \in \mathbb{N}$; $z_n, w_n \in T\widetilde{C}$. Then $\lim_{n\to\infty} z_n = x$ and $\lim_{n\to\infty} w_n = y$. Finally,

$$\begin{aligned}
\lim_{n\to\infty} \widetilde{d}(z_n, w_n) &= \lim_{n\to\infty} d\left(P(z_n), P(w_n)\right) \\
&= \lim_{n\to\infty} d\Big(\left(1/n, \gamma v\right), \left(1/n, \gamma(v + \delta)\right)\Big) \\
&= \lim_{n\to\infty} \gamma\delta \\
&\neq \delta \\
&= \widetilde{d}(x, y),
\end{aligned} \tag{2.9}$$

where the inequality holds as $\gamma \in (0, 1)$. This completes the proof as $\widetilde{d}$ is not continuous and

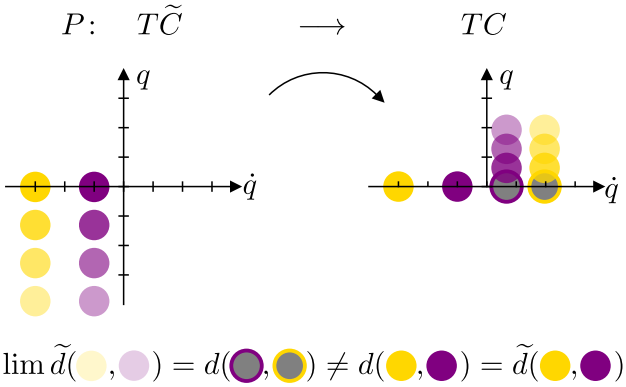

Figure 2.5: **Assuming a function $\widetilde{d}: T\widetilde{C} \times T\widetilde{C} \to R^+$ is *compatible* with d, $\widetilde{d}$ cannot be continuous and hence is not a distance function.** with the desired properties of *continuity* and *compatibility* can not exist. The two sequences in $T\widetilde{C}$, the semi-filled blue and green circles, converge to the filled blue and green circles, yet with the distance measure $\widetilde{d}$ having the *compatibility* property the distance on the convergent series does not equal the distance of the converged points.

hence cannot be a distance function. □

REMARK 7. *For perfectly elastic impacts $\gamma = 1$, the above proof does not hold. For $\gamma = 1$, $P|_{T\widetilde{C}_-} = -I_d$. With $\widetilde{d}(x, y) = \|x - y\|_2$ for all $x, y \in T\widetilde{C}$, $\widetilde{d}$ is compatible with d under P. The given extended distance $\widetilde{d}$ is equivalent to the well known* mirror law *[35] for a 1-DOF billiard.*

REMARK 8. *The proof of theorem 1 does not specify how $\widetilde{d}(x, y)$ is defined. Hence, for any $\widetilde{d}$ that is compatible with d, $\widetilde{d}$ cannot be continuous.*

2.4 Discussion

REMARK 9. *One possible method of extending the billiard system is to consider mappings $N: T\widetilde{C} \to TC$ such that $N \circ \widetilde{\zeta} \neq \zeta$. If such mappings were considered, then it is possible to*

define a continuous and compatible function on $T\widetilde{C}$. *Clearly, one such* $N\colon T\widetilde{C} \to TC$ *is*

$$N(q,\dot{q}) = \begin{cases} (q,\dot{q}) \text{ if } \dot{q} \geq \epsilon \\ (-\gamma q, -\gamma\dot{q}) \text{ if } \dot{q} < -\epsilon \\ \left(-(1-\frac{1-\gamma}{\epsilon}q)q, -\left(1-\frac{1-\gamma}{\epsilon}q\right)\dot{q}\right) \text{ otherwise} \end{cases} \tag{2.10}$$

for any $\epsilon > 0$. *As the motivation is tracking, we do not consider such mappings.*

The example we provide in section 2.3.3 demonstrates classical geometric tracking techniques [1,22] cannot be used on the 1-DOF billiard undergoing nonplastic inelastic collisions. The 1-DOF billiard exhibits the key characteristic of mechanical systems subject to unilateral constraints, a discontinuous trajectory due to an impact As such, we make the following conjecture:

Conjecture 2. *For any rigid mechanical system subject to unilateral constraints and corresponding state space* TC *with the distance function* $d\colon TC \times TC \to \mathbb{R}^+$ *undergoing a nonplastic inelastic collision, there does not exist a local extension* $T\widetilde{C}$, *projection operator* $P\colon T\widetilde{C} \to TC$, *and distance function* $\widetilde{d}\colon T\widetilde{C} \times T\widetilde{C} \to R^+$ *such that*

(i) trajectories $\widetilde{\zeta}$ *on the extended domain* $T\widetilde{C}$ *are continuous,*

(ii) $P \circ \widetilde{\zeta} = \zeta$ *locally,*

(iii) $\widetilde{d}$ *is a distance function (and hence continuous), and*

(iv) $\widetilde{d}$ *is compatible with* d *under* P.

This conjecture does not imply tracking on mechanical systems with impacts cannot be done, only that different techniques from continuous control must be used. Indeed many such techniques exist with varying levels of generality.

We conclude with a brief summary of these techniques, mentioning only methods that do not assume both desired and nominal trajectories impact at the same time. For tracking

trajectories for a general hybrid dynamical system, [53] takes the approach of *gluing* pre- and post-impact states and extends the method to deforming the underlying domain such that all trajectories are now continuous. Instead of designing a metric, the problem is shifted to designing a *gluing function*. In [17] demonstrates when the distance function takes into account the instantaneous change in state, Lyapunov-based techniques can be used to show global stability.

Another technique for handling impulsive events is to extend either the reference or nominal trajectory past the point of impact. *Reference spreading* [88, 89] extends the idea to multiple potentially simultaneous impacts and general hybrid dynamical systems by extending the reference trajectories beyond and prior to impacts as if the impact does not occur. Regardless of how the extended reference trajectory is generated, to first order the controller maintains asymptotic tracking. Another method of extending the trajectory is through a nonlinear coordinate transformation, Zhuralev-Ivanov transformation [20, Chpt. 1, §1.4.3]. For the inelastic bouncing ball [46] demonstrates control using Zhuravlev-Ivanon transformation. Additionally, there have been several methods developed for tracking trajectories specifically developed for mechanical systems subject to unilateral constraints, see [70] for tracking periodic mechanical impacts, [37] for a method using an internal model principle based controller, and [75] when the system as a complementarity Lagrangian system.

Chapter 3

STATE ESTIMATION IN HYBRID DYNAMICAL SYSTEMS[1]

3.1 Abstract

We propose an offline algorithm that simultaneously estimates discrete and continuous components of a hybrid system's state. We formulate state estimation as a continuous optimization problem by relaxing the discrete component and using a robust loss function to accommodate large changes in the continuous component during switching events. Subsequently, we develop a novel nonsmooth variable projection algorithm with Gauss-Newton updates to solve the state estimation problem and prove the algorithm's global convergence to stationary points. We demonstrate the effectiveness of our approach by comparing it to a state-of-the-art filter bank method, and by applying it to simple piecewise-linear and -nonlinear mechanical systems undergoing intermittent impact.

3.2 Introduction

This paper considers the problem of using noisy measurements from a piecewise-continuous trajectory to estimate a hybrid system's state. A *hybrid* dynamical system switches between dynamic regimes at time- or state-triggered events. The state estimation problem has been extensively studied in *classical* dynamical systems whose states evolve according to one (possibly time–varying) smooth model. This problem is fundamentally more challenging for hybrid systems since the set of discrete state[2] sequences generally grows combinatorially in

[1]Joint work with J. Zhang and A. Aravkin. This chapter appeared in [107]. Additional discussion of the derived optimization algorithm can be found in [106, Chp. 4].

[2]The state of the hybrid system is specified by the discrete and continuous components. We refer to the discrete component of the hybrid system state as the *discrete state*, and refer to the continuous component as the *continuous state*.

time.

When the discrete state sequence and switching times are known *a priori* or directly measured, only the continuous state needs to be estimated, yielding a classical state estimation problem; this approach has been applied to piecewise-linear systems [100, Chap. 4.5] and to nonlinear mechanical systems undergoing impacts [71]. When the discrete state is not known or measured, estimating both the discrete and continuous states simultaneously improves estimation performance. One approach uses a bank of filters, each tuned to one discrete state, and selects the discrete states as the filter with the lowest residual [13, §4.1]. This filter bank method has been applied to hybrid systems with linear dynamics [11, §4.1] [41], nonlinear dynamics [14], and jumps in the continuous state when the discrete state changes [12]. Likewise, particle filter methods for hybrid systems [18,29,97] use a collection of filters, identified as particles, and are applicable to more general nonlinear process dynamics. Particle filters and filter banks are effective when the number of discrete states and dimension of continuous state spaces are small.

Another approach formulates a moving-horizon estimator over both the continuous and discrete states, resulting in a mixed-integer optimization problem [16]. The inherently discrete nature of the problem formulation enables estimation of the exact sample when the discrete state switches, at the expensive of combinatorial growth of the set of discrete decision variables as the horizon increases. Multiple methods have been developed to mitigate the challenge posed by this combinatorial complexity. One approach entails summarizing past measurements and state estimates with a penalty term in the the objective function [32]. Another approach, applicable to systems with bounded noise, entails restricting the set of possible discrete state sequences using *a priori* knowledge of the system [3, 4].

An alternative approach to circumventing the combinatorial challenge entailed by exactly estimating the discrete state sequence involves *relaxing* the discrete state estimate to take on continuous values as in [9, 51]. The latter reference uses a sparsity-promoting convex program whose objective incorporates a nonsmooth penalty across all possible discrete state sequences, and guarantees the estimate converges to the true continuous and discrete states.

Both approaches are formulated for piecewise-linear systems whose continuous states do not jump when switching between subsystems; in the language of hybrid systems, the continuous states are *reset* using the identity function.

Our approach and contributions

We propose an offline algorithm for estimating the state of hybrid systems with nonlinear dynamics, non–identity resets, and noisy process and observation models. Although prior work accommodates aspects of our problem formulation, to the best of our knowledge no work simultaneously allows nonlinear dynamics and non–identity resets: [12] does not allow nonlinear dynamics, [18] and [33] do not allow non–identity reset, and [9] does not allow either nonlinear dynamics nor non–identity resets. Our starting point is the optimization perspective on generalized and robust state estimation [5, 6]. To formulate state estimation as a continuous optimization problem, we relax the discrete state to take on continuous values as in prior work. Unlike prior work on state estimation for hybrid systems, we model process noise using the Student's t distribution, which allows large innovations and makes the method applicable to systems with non–identity resets.

In combination, these elements yield a nonsmooth nonconvex continuous optimization formulation for offline state estimation (Sec. 3.3). We develop a Gauss-Newton type algorithm to solve this problem and prove the algorithm globally converges to stationary points (Sec. 3.4). The algorithm is compared to a class of state-of-the-art algorithms (Sec. 3.6) and evaluated on piecewise-linear and -nonlinear hybrid system models (Sec. 3.7).

3.3 Problem formulation

We consider observational data periodically sampled from a continuous-time hybrid dynamical system [39] that undergoes occasional jumps in continuous state, such as a mechanical system undergoing intermittent impacts [50]. We utilize a *discrete-time switched system* as the process model for this sampled data. The process model is chosen to capture the salient features of a hybrid dynamical system model, e.g. the continuous-time dynamics differing

between discrete states, while shifting the challenge of non–identity resets to the process noise. As we explain below, combining this process model with a Student's t distribution for the process noise captures the salient features of the underlying system dynamics while enabling our derivation of a computationally efficient state estimation algorithm.

3.3.1 Process and observation models

We use a *discrete-time switched system*

$$\begin{aligned} x_{t+1} &= \sum_{m=1}^{M} \mathcal{F}_m(x_t) w_t[m] + \sigma_t \\ y_t &= \mathcal{H}_t(x_t) + \delta_t \end{aligned} \tag{3.1}$$

where $m \in \{1, ..., M\}$ indexes the continuously-differentiable process model $\mathcal{F}_m \colon \mathbb{R}^n \to \mathbb{R}^n$, $M \in \mathbb{N}$ is the number of process models, $\mathcal{H}_t \colon \mathbb{R}^n \to \mathbb{R}^d$ is the continuously-differentiable observation model that generates observations $y_t \in \mathbb{R}^d$ of the hidden continuous state $x_t \in \mathbb{R}^n$, σ_t, δ_t are process and measurement noises, and $w_t \in \mathcal{D}^M$ is a *one-hot* vector[3]that indicates which process model is active at time t. Note that the observation model does not depend explicitly on the active model $\mathcal{F}_m$, which must be inferred from measurements of the continuous state x_t.

The model $\mathcal{F}_m$ that is active during each time step may be determined by an exogenous signal, prescribed as a function of time or state, or some combination thereof. Thus, the equation in (3.1) can represent the process and observation models of a wide variety of hybrid systems. Appendix A.1 provides an overview of the construction of a switched system by sampling a general hybrid dynamical system. We are motivated theoretically and experimentally to focus on cases where the active model $\mathcal{F}_m$ is constant for many time steps, only occasionally switching to a new model. When the sampling rate of a continuous-time hybrid dynamical system is much faster than the *dwell-time* [43], consecutive measurements will often be from the hybrid system in the same discrete state.

[3] $w \in \mathbb{R}^M$ is *one-hot* if $w[i] \in \{0, 1\}$ for all $i \in \{1, \ldots, M\}$ and $1^T w = 1$; $\mathcal{D}^M \subset \mathbb{R}^M$ denotes the set of one-hot vectors.

The problem of when measurements from a switched-system as in (3.1) with no process noise $\sigma_t \sim 0$, and no measurement noise $\delta_t \sim 0$, can reconstruct the true discrete and continuous state (i.e. when is the system is observable) is well studied continuous time switched linear systems [105] [51, Chpt. 2]. For the more general linear hybrid system, when the continuous state undergoes occasional jumps, observability tests with particular assumptions have been proposed [11]. To the best of our knowledge there is not a general observability test that applies to nonlinear hybrid systems with non–identity resets; a class of hybrid systems considered in this paper.

When the discrete state changes in a hybrid system, the continuous state may change abruptly according to a *reset* map. As an example, the velocity of a rigid mass changes abruptly when it impacts a rigid surface [66]. Empirically, these discrete reset dynamics are much more poorly characterized than their continuous counterparts. For instance, whereas the ballistic trajectory of a rigid mass is well-approximated by Newton's laws, the abrupt change in velocity that occurs at impact is not consistent with any established impact law [31]. Including such a reset in the system model (3.1) will introduce bias into the state estimate because the model will generate erroneous predictions at resets, diminishing the accuracy of estimated states at nearby times. This observation motivates us in the next section to account for the effect of unknown resets as part of the process noise.

3.3.2 Process noise and observation noise models

Instead of incorporating continuous state resets explicitly into the model (3.1), we introduce a distributional assumption on the process noise σ_t that accepts large instantaneous changes in the continuous state estimate. Specifically, we assume that process noise σ_t follows a Student's t distribution. However, we emphasize that this is a modeling assumption. It does not imply that process noise from real hybrid system has to follow this distribution. Compared with the commonly-used Gaussian distribution, the *heavy-tailed* Student's t is tolerant to large deviations in the estimate of the hidden continuous state x_t [8]. Hence, the Student's t error model allows an instantaneous change in the state that is consistent

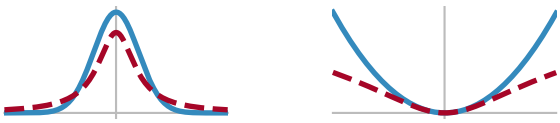

probability density negative log-likelihood

Figure 3.1: Probabability density and negative log-likelihood functions for Gaussian (solid blue) and Student's t (dashed red; degree-of-freedom $r = 1$) distributions.

with (3.1) before and after the change. The negative log-likelihood of the Student's t (as a function of σ_t) is given by

$$r \log \left(r + \left\| Q^{-1/2} \sigma_t \right\|^2 \right) - C(r), \tag{3.2}$$

where r is the degrees-of-freedom parameter of the Student's t, and Q is the covariance matrix, and $C(r)$ is a term independent of σ_t.

If the continuous state x_t was known, then any residual between the predicted observations $\mathcal{H}_t(x_t)$ and actual measurements y_t at time t is due to measurement noise; in particular, the residual does not exhibit large deviations due to continuous state resets at switching times. Thus, we assume the measurement noise δ_t follows the usual Gaussian distribution, with negative log-likelihood

$$\frac{1}{2} \left\| R^{-1/2} \delta_t \right\|^2, \tag{3.3}$$

where R is the covariance matrix. Figure 3.1 provide a comparison between the probability density (left) and the negative log-likelihood (right) for the scalar Gaussian (solid blue) and Student's t distributions (dashed red; degree-of-freedom $r = 1$).

3.3.3 State estimation problem formulation

We derive the objective function for estimating states of (3.1) using *maximum a posteriori* (MAP) likelihood. Including the constraint on w, we obtain the optimization problem

$$\min_{x_t \in \mathbb{R}^n, w_t \in \mathcal{D}^m} \sum_{t=0}^{T-1} l_{\text{meas}}(x_t, y_t) + l_{\text{proc}}(x_t, y_t, w_t) \tag{3.4}$$

where

$$l_{\text{meas}}(x_t, y_t) = \frac{1}{2} \left\| R^{-1/2} \left(y_t - \mathcal{H}_t(x_t) \right) \right\|^2$$

and

$$l_{\text{proc}}(x_t, y_t, w_t) = \\ r \log \left(r + \left\| Q^{-1/2} \left(x_{t+1} - \sum_{m=1}^{M} \mathcal{F}_m(x_t) w_t[m] \right) \right\|^2 \right).$$

Problem (3.4) is a nonlinear mixed-integer program with respect to both the continuous (x_t) and discrete (w_t) decision variables, with the discrete variable constrained to be a one-hot vector ($w_t \in \mathcal{D}^M$). We can significantly simplify the structure by establishing the following lemma.

LEMMA 1 (FORMULATION EQUIVALENCE). *Given $w \in \mathcal{D}^M$, any vectors x_1, x_2, models $\mathcal{F}_i$, and any penalty functional g, we have*

$$\begin{aligned} &\min_{w \in \mathcal{D}^M} \quad g \left(x_2 - \sum_{m=1}^{M} w[m] \mathcal{F}_m(x_1) \right) \\ =& \min_{w \in \mathcal{D}^M} \quad \sum_{m=1}^{M} w[m] g \left(x_2 - \mathcal{F}_m(x_1) \right) \end{aligned}$$

and

$$\begin{aligned} &\operatorname*{argmin}_{w \in \mathcal{D}^M} g \left(x_2 - \sum_{m=1}^{M} w[m] \mathcal{F}_m(x_1) \right) \\ =& \operatorname*{argmin}_{w \in \mathcal{D}^M} \quad \sum_{m=1}^{M} w[m] g \left(x_2 - \mathcal{F}_m(x_1) \right). \end{aligned}$$

Proof:

Since $w \in \mathcal{D}^M$ for both problems, there are only M possible values for both objective functions, i.e.

$$g(x_2 - \mathcal{F}_1(x_1)), \quad g(x_2 - \mathcal{F}_2(x_1)), \quad \ldots, \quad g(x_2 - \mathcal{F}_M(x_1)).$$

Hence, the minimum objective value for both problems will be $\min_m g(x_2 - \mathcal{F}_m(x_1))$ and every minimizer is a one-hot vector that selects a minimum value. □

Based on Lemma 1, an equivalent formulation to (3.4) is given by

$$\begin{aligned} \min_{x_t \in \mathbb{R}^n, w_t \in \mathcal{D}^M} \sum_{t=0}^{T-1} \Bigg(& \frac{1}{2} \left\| R^{-1/2} \left(y_t - \mathcal{H}_t(x_t) \right) \right\|^2 + \\ & \sum_{m=1}^{M} w_t[m] r \log \left(r + \left\| Q^{-1/2} \left(x_{t+1} - \mathcal{F}_m(x_t) \right) \right\|^2 \right) \Bigg). \end{aligned} \tag{3.5}$$

Although still a mixed-integer program, this reformulation exhibits linear coupling between the discrete variables w_t and continuous variables x_t. We will leverage this linear coupling when we develop our estimation algorithm based on the relaxed problem formulation introduced in the next section.

3.3.4 Relaxed state estimation problem formulation

Ultimately, the discrete state estimate will be specified as a one-hot vector, $w_t \in \mathcal{D}^M \subset \mathbb{R}^M$. To formulate a continuous optimization problem that approximates the mixed-integer problem formulated in the previous section, we relax the decision variable w_t to take values in the convex hull Δ^M of $\mathcal{D}^M$.We use $\Delta^M := \{w \in [0,1]^M : 1^T w = 1\}$ to denote the simplex in $\mathbb{R}^M$. The optimal relaxed w_t will generally lie on the interior of the simplex, so we project the result from our relaxed optimization problem to return the one-hot discrete state estimate. Since this relaxation-optimization-projection process tends to induce frequent changes in the discrete state estimate, we introduce a smoothing term on w_t,

$$\nu \| w_{t+1} - w_t \|_2^2,$$

yielding the continuous relaxation of (3.5) given by

$$\begin{aligned}\min_{x_t\in\mathbb{R}^n, w_t\in\Delta^M} f(x,w) := \sum_{t=0}^{T-1}\Bigg(&\frac{1}{2}\left\|R^{-1/2}\left(y_t-\mathcal{H}_t(x_t)\right)\right\|^2\\ &+\sum_{m=1}^{M} w_t[m] r\log\left(r+\left\|Q^{-1/2}\left(x_{t+1}-\mathcal{F}_m(x_t)\right)\right\|^2\right)\\ &+\nu\|w_{t+1}-w_t\|_2^2\Bigg),\end{aligned} \tag{3.6}$$

where x is the concatenated variable containing all x_t, w is the concatenated variable containing all w_t, and ν is a parameter controlling the strength of smoothing. The optimal relaxed discrete state estimate $w_t \in \Delta^M$ is projected onto $\mathcal{D}^M$ by choosing the (unique) one-hot vector whose $\operatorname{argmax}_m w_t[m]$ component is equal to 1.

3.4 State estimation algorithm

In this section, we derive an algorithm to solve the relaxed state estimation problem formulated in (3.6) using two key ideas:

1. nonsmooth variable projection;

2. Gauss-Newton descent with Student's t penalties.

These two ideas are explained in the next two subsections, followed by a convergence analysis in the third subsection.

3.4.1 Nonsmooth variable projection

The first idea is to pass to the *value function*, projecting out (partially minimizing over) the w variables, so as to reduce the number of variables to optimize over. Define

$$v(x) := \min_w f(x,w) \tag{3.7}$$

with $f(x, w)$ as in (3.6). The objective $f(x, w)$ is convex in w, but not strictly convex. To guarantee differentiability of $v(x)$, we add a smoothing term and consider

$$v_\beta(x) := \min_w f(x, w) + \frac{\beta}{2}\|w\|^2. \tag{3.8}$$

where β is usually taken to be a very small number (e.g. 10^{-4} or smaller) so that the added term has minimal effect on the original value function. (The minimizer of v_β is different from that of v.) The function $v_\beta(x)$ is a *Moreau envelope* [93, Def 1.22] of the true value function v; we refer the interested reader to [7] for details and examples concerning the Moreau envelope specifically (and nonsmooth variable projection more broadly). The unique minimizer $w(x)$ can be found quickly and accurately since the minimization problem with respect to w is strongly convex: projected gradient descent converges linearly and can be accelerated using the Fast Iterative Shrinkage-Thresholding Algorithm (FISTA) [15]. With the minimizer $w(x)$, the gradient of v_β is readily computed as

$$\nabla v_\beta(x) = \partial_x f(x, w)|_{w=w(x)}. \tag{3.9}$$

Plugging $w(x)$ back into (3.6) we obtain the problem

$$\begin{aligned}\min_x v_\beta(x) =& \frac{1}{2}\sum_{t=0}^{T-1}\|y_t - \mathcal{H}(x_t)\|^2_{R^{-1}} + \nu\|w_{t+1}(x) - w_t(x)\|_2^2 \\ &+ \sum_{m=1}^{M} w_{t,m}(x) r \log\left(1 + \frac{\|x_{t+1} - \mathcal{F}_m(x_t)\|^2_{Q^{-1}}}{r}\right) \\ &+ \frac{\beta}{2}\|w(x)\|^2,\end{aligned} \tag{3.10}$$

where $w_{t,m}(x) \equiv w_t[m](x)$.

3.4.2 Gauss-Newton descent with Student's t penalties

We derive a Gauss-Newton descent algorithm to solve (3.10) based on a line search method first proposed in [27] for convex composite problems. To apply the method we first cast the objective in (3.10) into a convex composite function, let $v_\beta = \rho \circ F$, where

$$F(x) = \begin{pmatrix} f_1(x) \\ f_2(x) \end{pmatrix}$$

with

$$\begin{aligned} f_1(x) =& \frac{1}{2}\sum_{t=0}^{T-1}\sum_{m=1}^{M} w_{t,i}(x) r \log\left(1+\frac{\|x_{t+1}-\mathcal{F}_m(x_t)\|^2_{Q^{-1}}}{r}\right) \\ &+ \nu\|w_{t+1}(x)-w_t(x)\|_2^2 + \frac{\beta}{2}\|w(x)\|^2 \\ f_2(x) =& \mathcal{H}(x) - y \end{aligned}$$

and

$$\rho\begin{pmatrix} c \\ u \end{pmatrix} = c + \frac{1}{2}\|u\|^2_{R^{-1}} + \delta_{[0,+\infty]}(c).$$

At each iteration, we choose a search direction $d^*(x)$ that

$$\begin{aligned} d^* \in \operatorname{argmin}_d \quad & \rho(F(x)+F^{(1)}(x)d) + \frac{1}{2}d^T U(x) d \\ \in \operatorname{argmin}_d \quad & f_1(x) + \nabla f_1(x) d + \frac{1}{2}\|f_2(x)+\nabla f_2(x)d\|^2_{R^{-1}} \\ & + \frac{1}{2}d^T U(x) d \\ \in \operatorname{argmin}_d \quad & \frac{1}{2}d^T\left(U(x)+\nabla\mathcal{H}(x)^T R^{-1}\nabla\mathcal{H}(x)\right)d \\ & + \nabla v_\beta(x)^T d \end{aligned} \tag{3.11}$$

where the equivalence is obtained by dropping terms independent of d. In general $U(x)$ can be any positive semidefinite matrix that varies continuously with respect to x, but for our particular objective function involving Student's t penalty, $U(x)$ is chosen to be a Hessian approximation of the Student's t term in $f_1(x)$. Therefore the update can be interpreted as a Gauss-Newton style update. This approximation, proposed in [8, (5.5), (5.6)], is employed here because of its significant computational advantage; it is of the form

$$U = \begin{bmatrix} U_1 & A_2^T & 0 & \\ A_2 & U_2 & A_3^T & 0 \\ 0 & \ddots & \ddots & \ddots \\ & 0 & A_T & U_T \end{bmatrix} \tag{3.12}$$

with

$$A_t = -r\sum_{m=1}^{M} w_{t-1,m}(x)\frac{Q^{-1}\nabla\mathcal{F}_m(x_{t-1})}{r+\|x_t-\mathcal{F}_m(x_{t-1})\|^2_{Q^{-1}}},$$

$$U_t = r \sum_{m=1}^{M} \frac{w_{t,m}(x) \nabla \mathcal{F}_m(x_t)^T Q^{-1} \nabla \mathcal{F}_m(x_t)}{r + \|x_{t+1} - \mathcal{F}_m(x_t)\|^2_{Q^{-1}}} + \frac{w_{t-1,m}(x) Q^{-1}}{r + \|x_t - \mathcal{F}_m(x_{t-1})\|^2_{Q^{-1}}}$$

for $1 \leq t \leq T-1$, and

$$U_T = \frac{r w_{T-1,m}(x) Q^{-1}}{r + \|x_T - \mathcal{F}_m(x_{T-1})\|^2_{Q^{-1}}}.$$

We can rewrite $U(x)$ as

$$U(x) = \sum_m \mathcal{F}_m(x)^T \tilde{Q}_m(w(x))^{-1} \mathcal{F}_m(x),$$

where

$$G_m(x) = \begin{bmatrix} I & 0 & 0 & \\ -\nabla \mathcal{F}_m(x_2) & I & 0 & 0 \\ 0 & \ddots & \ddots & \ddots \\ \dots & 0 - \nabla \mathcal{F}_m(x_T) & & I \end{bmatrix}$$

and

$$\tilde{Q}_m(w(x))^{-1} = \mathrm{diag}(\tilde{Q}_{m,t}(w(x))^{-1})$$
$$\tilde{Q}_{m,t}(w(x))^{-1} = \frac{r w_{t-1,m}(x) Q^{-1}}{r + \|x_t - \mathcal{F}_i(x_{t-1})\|^2_{Q^{-1}}}.$$

Clearly $U(x)$ is positive semidefinite; we show in Lemma 3 that $U(x)$ is actually positive definite, so problem (3.11) reduces to the block tridiagonal linear system

$$\left(U(x) + \nabla \mathcal{H}(x)^T R^{-1} \nabla \mathcal{H}(x)\right) d + \nabla v_\beta(x) = 0.$$

Given $d^*(x)$, the new x^+ is of the form

$$x^+ = x + \delta d^*,$$

where δ is a step size selected using the *Armijo*-type [79, Sec. 3.1] line search criterion.

$$\delta = \max\{\gamma^l : \rho(F(x + \gamma^l d^*)) \leq \rho(F(x)) + c\gamma^l \Delta(x; d^*) \text{ and } c \in (0,1)\} \tag{3.13}$$

with

$$\Delta(x;d) = \rho(F(x) + F^{(1)}(x)d) + \frac{1}{2}d^T U(x)d - \rho(F(x)).$$

When $d = 0$, we have $\Delta(x;0) = 0$[4], and since we choose the minimizing

$$d^* = \underset{d}{\operatorname{argmin}} \ \rho(F(x) + F^{(1)}(x)d) + \frac{1}{2}d^T U(x)d,$$

we have $\Delta(x;d^*) \leq 0$. Further,

$$\begin{aligned}\Delta(x;d^*) = 0 &\Leftrightarrow 0 \in \underset{d}{\operatorname{argmin}}\, \rho(F(x) + F^{(1)}(x)d) + \frac{1}{2}d^T U(x)d \\ &\Leftrightarrow 0 \in \partial\rho(F(x))F^{(1)}(x)\end{aligned}$$

by [27, Thm. 3.6]. In other words, stationarity is achieved when $\Delta(x;d^*) = 0$. When $\Delta(x;d) < 0$, we are guaranteed to have descent

$$\rho(F(x) + F^{(1)}(x)d) < \rho(F(x))$$

since $U(x)$ is positive semidefinite. This condition ensures that the line search step (3.13) is well-defined [27, Lemma 2.3].

Our approach is summarized in Algorithm 1. The positive parameter ϵ in the algorithm specifies the stopping condition. Finally, we project the relaxed discrete state estimate $w_t \in \Delta^M$ to obtain a discrete state estimate in $\mathcal{D}^M$ as described in Section 3.3.4.

3.4.3 Convergence of state estimation algorithm

In this section we show the convergence of the proposed algorithm. The convergence of Algorithm 1 to a stationary point for a general class of convex composite objective functions is established in [27] and [8]. In particular [8, Theorem 5.1] establishes the possible outcomes when applying this type of algorithm; informally, either the algorithm converges or the search direction d_k diverges. In the remainder of this section we provide two technical results needed to formalize this intuition and to apply the aforementioned theorem:

[4]We overload Δ here to match the notation in [8, 27]; $\Delta(x;d^*)$ should not be confused with Δ^M, which is used to denote the simplex containing relaxed state estimates.

Algorithm 1 Variable Projection for (3.6).

Require: $x, w, Q, R, r, \nu, \beta, \epsilon$

for $k = 1, 2, 3, ...$ **do**

  $d^{(k)} \leftarrow$ Gauss-Newton direction for $x^{(k)}$

  $x^{(k+1)} \leftarrow x^{(k)} + \delta d^{(k)}$

  $w^{(k+1)} \leftarrow \text{InnerSolver}_{\Pi_t \Delta}(w^{(k)})$

  $\text{loss}_k \leftarrow f(x^{(k+1)}, w^{(k+1)})$

Iterate till $\Delta(x^{(k)}; d^{(k)}) \geq -\epsilon$.

- Lemma 2 establishes a set of sufficient conditions that prevent divergence ($\|d^{(k)}\| \to \infty$);
- Lemma 3 proves that the sufficient conditions are satisfied.

LEMMA 2. *Let* $\Lambda = \{y | \rho(y) \leq v_\beta(x^{(0)})\}$. *If* $F^{-1}(\Lambda) = \{x | F(x) \in \Lambda\}$ *is bounded and* $U(x)$ *is positive definite for all* $x \in F^{-1}(\Lambda)$, *then the hypotheses in [8, Theorem 5.1] are satisfied and the sequence of search directions* $\{d^{(k)}\}$ *is bounded.*

Proof: The hypotheses in [8, Theorem 5.1] require that $F^{(1)}$ to be bounded and uniformly continuous on the set $S = \bar{co}(F^{(-1)}(\Lambda))$ where $\bar{co}$ stands for the closed convex hull. $F^{(1)}$ is continuous on S since $f_1^{(1)}$ exists and is continuous by property of Moreau envelope and proximal operator, and $f_2^{(1)}$ is continuous trivially. Further, given that S is closed by definition and bounded by assumption, it is compact. Hence $F^{(1)}$ is bounded and uniformly continuous on S.

Now we need to show that the sequence of search direction is bounded. At any iteration, the search direction d we choose satisfies

$$0 \leq \rho(F(x) + F^{(1)}(x)d) + \frac{1}{2} d^T U(x) d \leq \rho(F(x)) \leq \rho(F(x^0))$$

where the first inequality relies on $\rho \geq 0$ and on the positive semidefinite property of $U(x)$; the second inequality comes from $\Delta(x; d) \leq 0$; the third inequality results from the line search condition that creates a decreasing sequence $\{\rho(F(x^{(k)})\}$.

Since $\rho(F(x^0))$ is finite, $d^T U(x)d < \infty$ for all iterations. Because Λ is closed by closedness of ρ and F is continuous, $F^{-1}(\Lambda)$ is also closed. Along with its boundedness by assumption, $F^{-1}(\Lambda)$ is compact. Since $x \in F^{-1}(\Lambda) \mapsto \lambda_{\min}(U(x))$ is continuous, its image is bounded, hence given that $U(x)$ is positive definite there exists some $\lambda_{\min} > 0$ for all $x \in F^{-1}(\Lambda)$. Therefore $0 < \lambda_{\min}\|d\|^2 \leq d^T U(x)d < \infty$, which implies that $d^{(k)}$ cannot be unbounded. □

LEMMA 3. *$F^{-1}(\Lambda)$ is bounded for problem (3.10) and $U(x)$ is positive definite for all $x \in F^{-1}(\Lambda)$.*

Proof: First note that Λ is bounded by the coercivity of ρ. This implies that for an unbounded sequence $\|x^{(k)}\| \to \infty$, we still have $f_1(x^{(k)}) < \infty$ and $\|f_2(x^{(k)})\| < \infty$.

If $\|x^{(k)}\| \to \infty$, then we can find some $t+1$ and a subsequence J such that $\lim_{k\in J}\|x_{t+1}^{(k)}\| = \infty$. By the definition of f_1 and $f_1(x^{(k)}) < \infty$, $\lim_{k\in J}\|\mathcal{F}_i(x_t^{(k)})\| = \infty$, which further implies that $\lim_{k\in J}\|x_t^{(k)}\| = \infty$. Iteratively this means that $\lim_{k\in J}\|x_t^{(k)}\| = \infty$ for all t, in particular for the given starting point x_0, but that is not possible.

To show that $U(x)$ in (3.12) is positive definite, recall that we can rewrite $U(x)$ as

$$U(x) = \sum_m G_m(x)^T \tilde{Q}_m(w(x))^{-1} G_m(x) \succeq 0.$$

If there exists some d such that $d^T U(x)d = 0$, then

$$\begin{aligned}
&d^T \left(\sum_m G_m(x)^T \tilde{Q}_m(w(x))^{-1} G_m(x) \right) d \\
=&\sum_m \underbrace{d^T G_m(x)^T}_{z_m(x)^T} \tilde{Q}_m(w(x))^{-1} \underbrace{G_m(x)d}_{z_m(x)} \\
=&\sum_m z_m(x)^T \tilde{Q}_m(w(x))^{-1} z_m(x) = 0, \\
\Rightarrow& z_m(x)^T \tilde{Q}_m(w(x))^{-1} z_m(x) = 0 \ \forall i \\
\Rightarrow& z_{m,t}(x)^T \tilde{Q}_{m,t}(w(x))^{-1} z_{m,t}(x) = 0 \forall t \ \forall i
\end{aligned}$$

since $\tilde{Q}_m(w(x))^{-1} = \text{diag}(\tilde{Q}_{m,t}(w(x))^{-1})$, and

$$\tilde{Q}_{m,t}(w(x))^{-1} = \frac{r w(x)_{t,m} Q^{-1}}{r + \|x_{t+1} - \mathcal{F}_m(x_t)\|^2_{Q^{-1}}}$$

are positive semidefinite. However because each $w_t \in \Delta$, there has to be some $\tilde{Q}_{m,t}^{-1} \succ 0$ for each t. Therefore $U(x)$ must be positive definite for all $x \in F^{-1}(\Lambda)$. $\square$

3.5 Parameter Tuning for Proposed Algorithm

Before we present numerical results, we include a general guidance on parameter tuning for the new algorithm. We discuss both standard parameters (e.g. Q, R) that must be tuned by any algorithm for this application, as well as the parameters ν and r which are specific to our approach. We first give a rough outline of steps we have taken to tune the parameters, followed by more detailed guidelines to tune each individual parameter.

1. Start with large r for Student's t, i.e. distribution close to Gaussian.

2. If Q and R are unknown, they are tuned such that the smooth part of trajectories can be well approximated.

3. Decrease degrees of freedom r of Student's t so that the nonsmooth part of trajectories can be captured.

4. Adjust smoothing coefficient ν to reduce number of switches.

For degrees of freedom r, one can start with a large value, meaning that the distribution is close to Gaussian, and decrease it later to capture jumps in the continuous state.

For covariance matrices Q and R, if empirical estimations are available, they can be supplied to the model directly. There is existing literature on estimation methods for noise covariance matrices [30]. When such estimations are not available, we usually assume the matrices to be diagonal for simplicity, in which case the inverse of diagonal entries can also be interpreted as weights. The diagonal values of R represent variance for measurements. When choosing R, we consider the relative scale of measurements, e.g. measurements with smaller magnitude usually have smaller variance. For choices of diagonal values of Q, we

usually assign smaller variance for observed states, e.g. positions in our examples,and larger variance for unobserved states.

The choice of smoothing coefficient ν depends on modeler's belief in frequency of switches. One can start with a small value of ν (i.e. little penalty on frequent switches), and gradually increase it, till the pattern of switches is close to modeler's belief.

We recommend having a short piece of manually labeled trajectories as a training set for the purpose of parameter tuning. After tuning, the user can apply the same parameters on larger dataset collected from similar scenarios.

In terms of sensitivity of estimation results on parameters, we had the following observations when running our experiments:

- The estimation result is not very sensitive to r. We were able to decrease r fairly aggressively during parameter tuning.

- For the diagonals of Q and R, we found that it was important to have values in the correct ranges, but the exact values taken were not crucial.

- For smoothing coefficient ν, we noticed that the switching times were sensitive to ν when ν was very small relative to the diagonal entries of Q^{-1} and R^{-1}. Since we assumed that the discrete states should not change too frequently, we used a slightly larger ν.

3.6 Comparison with the Interacting Multiple Model (IMM) method

We compare the nonsmooth variable projection algorithm[5] (Algorithm 1) with the Interacting Multiple Model (IMM) [19] algorithm implemented in the open-source package `filterpy` [58]. We consider two examples, in both cases the continuous state x is a scalar, and there are two discrete states. In the first example, the continuous state x undergoes no jumps, i.e. the

[5]We provide an implementation of Algorithm 1 and the comparison results in this section at `https://github.com/jizezhang/hds-state-estimation` (and duplicated at `https://github.com/apace2/hds-state-estimation`).

reset is the identity function. In the second example, the continuous state x undergoes an instantaneous jump when the discrete state changes; i.e. a non–identity reset. The dynamics of the two discrete state process models are:

$$\dot{x} = -1 \qquad \mathcal{F}_{w=1},$$
$$\dot{x} = 1 \qquad \mathcal{F}_{w=2}.$$

For the second example with non–identity resets, when a discrete state switch occurs, the continuous state decreases by 5. In both examples the discrete state switches at $t = 1$ and $t = 2$. Additionally, the measurement noise has a variance of $R = [.0001]$, which is used as the measurement noise covariance for all models. IMM_1 uses a process noise model of covariance $Q = [.001]$ for both the internal Kalman filters and IMM_2 uses a process normal process noise model with covariance $Q = [.2]$.

In the first example, Algorithm 1 (VP) and IMM perform nearly identically (Figure 3.2). Both methods accurately recover the continuous state and discrete state. When the system undergoes instantaneous jumps in the continuous state at discrete state changes, Algorithm 1 outperforms IMM (Figure 3.3). For IMM, there is a clear trade–off exists between recovering the continuous state and recovering the discrete state. When using a process noise model with large covariance, as in the case of IMM_2, the continuous state can be recovered at the expense of the discrete state. In the top subplot of Figure 3.3, $\widetilde{w}_{IMM_2}$ is nearly the same value for the duration of the simulation, with slight separation between the two modes. With a smaller covariance, as in IMM_1, the discrete state can be recovered. From $t = 1$ to near $t = 1.25$, IMM_1 incorrectly identifies the discrete state due to the continuous state jump direction being opposite of the continuous state dynamics for discrete state $w = 2$.

Both Algorithm 1 and IMM require a similar number of parameters from the user. For both methods, covariance matrices for the process error model Q and measurement error model R need to be provided. IMM adjusts the estimated frequency of switching between the discrete states via a probability transition matrix while Algorithm 1 uses the smoothing parameter ν, Sec. 3.3.4. Algorithm 1 has one additional parameter r due to the process noise

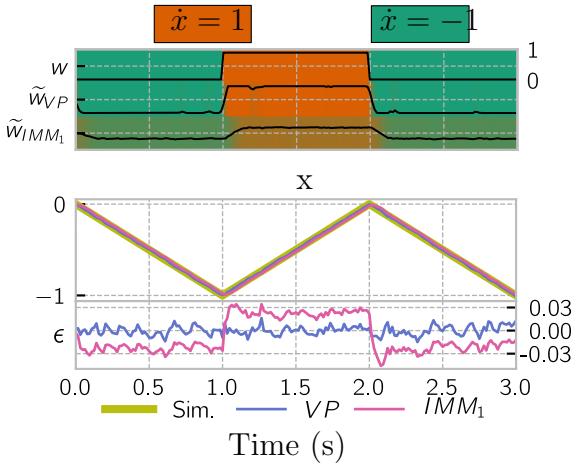

Figure 3.2: **Algorithm 1 (VP) performs comparably to IMM when the continuous state does not undergo any resets.** The top plot shows the true state w and the simplex estimate of the true state from both methods $\widetilde{w}_{VP}$, $\widetilde{w}_{IMM_1}$. The simplex estimate is shown in color and the probability estimate of the discrete state being $w = 1$ is superimposed as a black line. The middle plot shows the actual value of the continuous state of the simulation and the estimates. The bottom plot shows the residual between true continuous state and the estimated continuous state.

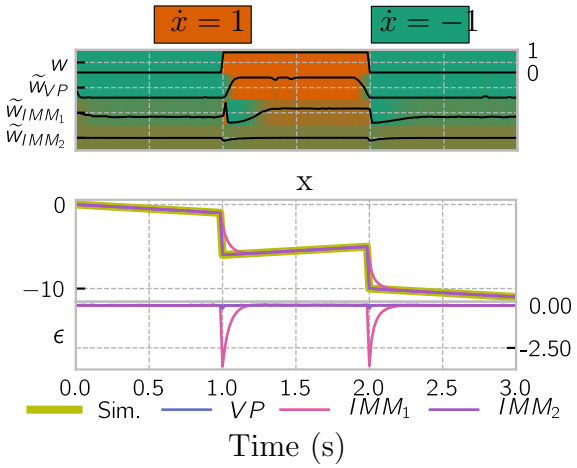

Figure 3.3: **Algorithm 1 (VP) outperforms the IMM when there are jumps in the continuous state.** The plots follow the convention laid out in Figure 3.2.

model being Student's t distribution, which is crucial for obtaining accurate estimates with non–identity resets, Sec. 3.3.2.

3.7 Experiments with hybrid system models

To evaluate the proposed approach to state estimation for hybrid systems, we apply our algorithm to linear and nonlinear impact oscillators. In addition to being well-studied ([28, §1.2], [95]), these mechanical systems were chosen since they are among the simplest physically-relevant models that have non–identity reset maps. The parameter and trajectory regime considered in what follows is representative of a jumping robot constructed from one limb of a commercially-available quadrupedal robot [52] and controlled with an event-triggered stiffness adjustment; Figure 3.4a contains a photograph of the limb. The jumping robot's hip and foot are constrained to move vertically in a gravitational field, so the rigid pantograph mechanism depicted in Figure 3.4b has two mechanical degrees-of-freedom (DOF) coupled through nonlinear pin-joint constraints. These two DOF are preserved, but their nonlinear coupling is neglected, in the piecewise-linear model illustrated in Figure 3.4c. The hybrid dynamics of these linear and nonlinear impact oscillators are specified in Section 3.7.1

We perform two sets of experiments. The first set of experiments in Sec. 3.7.2 concern the piecewise-linear model depicted in Figure 3.4c and explore the consequences of our modeling assumptions and the efficacy of our proposed algorithm:

- Sec. 3.7.2 demonstrates the advantage of employing a Student's t distribution for process noise as compared to a Gaussian distribution;

- Sec. 3.7.2 demonstrates the superior convergence rate yielded by Gauss-Newton descent directions as compared to gradient (steepest) descent;

- Sec. 3.7.2 demonstrates the advantage of smoothing the relaxed discrete state estimate; and

(a)

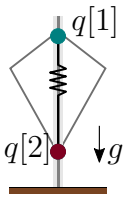

(b)

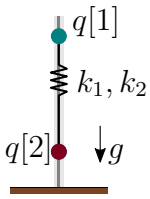

(c)

Figure 3.4: **Jumping robot and impact oscillator hybrid system models** (Sec. 3.7.1). (a) Photograph of the physical robot (one leg from a Minitaur [52]) that inspired the simulation models. (b) Nonlinear model consisting of two masses coupled with a linear spring and a nonlinear pantograph mechanism. (c) Linear model consisting of two masses coupled with a linear spring.

- Sec. 3.7.2 demonstrates the algorithm's performance when *onboard* measurements are used instead of *offboard* measurements.

The second set of experiments in Sec. 3.7.3 evaluate our proposed approach using the nonlinear model depicted in Figure 3.4b.

Since this section is devoted to comparing estimated states to ground truth simulation results, and since our approach entails the determination of a relaxed discrete state estimate *en route* to obtaining the discrete state estimate, we now introduce notation that distinguishes these quantities:

- $w_t \in \mathcal{D}^M$ denotes the ground truth discrete state;
- $\widetilde{w}_t \in \Delta^M$ denotes the relaxed discrete state estimate;
- $\widehat{w}_t \in \mathcal{D}^M$ denotes the discrete state estimate.

This notational distinction was not introduced previously in the interest of readability since there was no ambiguity entailed by overloading notation in the problem formulation and algorithm specification.

3.7.1 Impact oscillator hybrid system models

The continuous state $x = (q, \dot{q}) \in \mathbb{R}^4$ for the jumping robot hybrid system model consists of the two-dimensional configuration vector $q \in \mathbb{R}^2$ and corresponding velocity $\dot{q} \in \mathbb{R}^2$, where $q[1]$ and $q[2]$ denote the vertical height of the hip and foot, respectively. The foot is not permitted to penetrate the ground, $q[2] \geq 0$, so the first part of the discrete state indicates whether this constraint is active: A (air) if $q[2] > 0$, G (ground) if $q[2] = 0$. To compensate for energy losses at impact, an event-triggered controller stiffens or softens a spring based on which direction the hip is traveling, so the second part of the discrete state indicates the direction of travel for $q[1]$: $\uparrow$ if up, $\downarrow$ if down. With $\ddot{q}_m(q, \dot{q}) \in \mathbb{R}^2$ denoting the acceleration of the hip and foot in discrete state $m \in \{\mathrm{A}\downarrow, \mathrm{G}\downarrow, \mathrm{G}\uparrow, \mathrm{A}\uparrow\}$,[6] formula for this acceleration are given in Table 3.1. At the moment of impact (when the discrete state changes from $w_t \in \{\mathrm{A}\downarrow, \mathrm{A}\uparrow\}$ to $w_{t+1} \in \{\mathrm{G}\downarrow, \mathrm{G}\uparrow\}$) the foot velocity $\dot{q}[2]$ is instantaneously *reset* to 0, corresponding to perfectly *plastic* impact. An example of the jump in continuous state when transitioning from $\mathrm{A}\downarrow$ to $\mathrm{G}\downarrow$ on the foot velocity $\dot{q}[2]$ is shown in Figure 3.5 near time 17.5s.

3.7.2 Piecewise-linear impact oscillator experiment

In this subsection, we employ the linear spring laws

$$k_1(q, \dot{q}) = 10(q[1] - q[2]) - 3,$$

and

$$k_2(q, \dot{q}) = 15(q[1] - q[2]) - 3,$$

with parameter values $m_h = 3, m_t = 1, g = 2$. Appendix A.2 contains a complete definition of the hybrid system.

In our first demonstration the observed states are $q[1]$ and $q[2]$, position of the hip and foot, leaving the velocities unobserved:

$$\mathcal{H}_{\mathrm{pos}}(x) = q. \tag{3.14}$$

[6] To simplify exposition we identify $m = \mathrm{A}\downarrow$ with $m = 1$, $m = \mathrm{G}\downarrow$ with $m = 2$, $m = \mathrm{G}\uparrow$ with $m = 3$, and $m = \mathrm{A}\uparrow$ with $m = 4$.

Discrete state w	**Icon**	$\ddot{q}_w(x)$
$w = \text{A}\downarrow$		$\begin{bmatrix} \frac{1}{m_h}\left(-k_1(q,\dot{q})\right) - g \\ \frac{1}{m_t}\left(k_1(q,\dot{q})\right) - g \end{bmatrix}$
$w = \text{G}\downarrow$		$\begin{bmatrix} \frac{1}{m_h}\left(-k_1(q,\dot{q})\right) - g \\ 0 \end{bmatrix}$
$w = \text{G}\uparrow$		$\begin{bmatrix} \frac{1}{m_h}\left(-k_2(q,\dot{q})\right) - g \\ 0 \end{bmatrix}$
$w = \text{A}\uparrow$	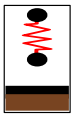	$\begin{bmatrix} \frac{1}{m_h}\left(-k_2(q,\dot{q})\right) - g \\ \frac{1}{m_t}\left(k_2(q,\dot{q})\right) - g \end{bmatrix}$

Table 3.1: **Discrete states and continuous dynamics for impact oscillator hybrid system models** (Sec. 3.7.1). Note that the continuous dynamics $\ddot{q}$ have the same general form for both the piecewise-linear and -nonlinear models, with the spring law k being a linear or nonlinear function of the continuous state $x = (q, \dot{q})$ depending on which model is considered.

State estimation results for this system are shown in Figure 3.7b.

In the remainder of this subsection, we demonstrate the effects of the choices we made in our problem formulation (Sec. 3.3) and algorithm derivation (Sec. 3.4) using the piecewise-linear model as a running example. We also consider a variation where the measurements correspond to the leg length and velocity, which are more representative of the *onboard* measurements available to an autonomous robot operating outside of the laboratory.

Student's t versus Gaussian process noise

Figure 3.5 compares the estimation of foot velocity using Student's t with $r = 0.01$ versus using Gaussian for the process noise distribution; in both cases the true discrete state is given. The estimated trajectory for both distributions match the true simulated trajectory away from jumps, while near jumps, such as around times 16.6s and 17.5s, using the Student's t distribution enables closer tracking of the instantaneous change in the true foot velocity $\dot{q}[2]$

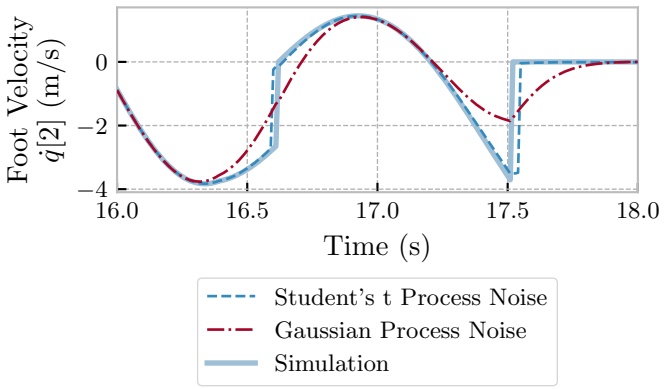

Figure 3.5: **The Student's t distribution process noise yields better estimates of instantaneous changes in continuous state** (Sec. 3.7.2). In this plot, estimates of the foot velocity are shown near two impacts ($\approx$ 16.6s, 17.5s).

than when using a Gaussian distribution.

Gauss-Newton versus gradient (steepest) descent

We empirically compared convergence rates for continuous state x_t updates obtained using Gauss-Newton and gradient (steepest) descent directions (Algorithm 1, line 2). Figure 3.6 shows the log loss versus algorithm iteration for the two methods; the actual discrete state w_t was taken as given to perform this comparison. As expected, the objective value decreases significantly faster when the search direction is determined by the Gauss-Newton scheme as compared to the direction of steepest descent, reaching the stopping criterion in ten times fewer iterations in our tests.

Smoothing the relaxed discrete state versus not

If the continuous states are given, the discrete state estimate returned by our algorithm (skipping lines 2 and 3 of Algorithm 1) is very close to the true discrete state regardless of whether a smoothing term is included in the relaxed problem formulation. When simul-

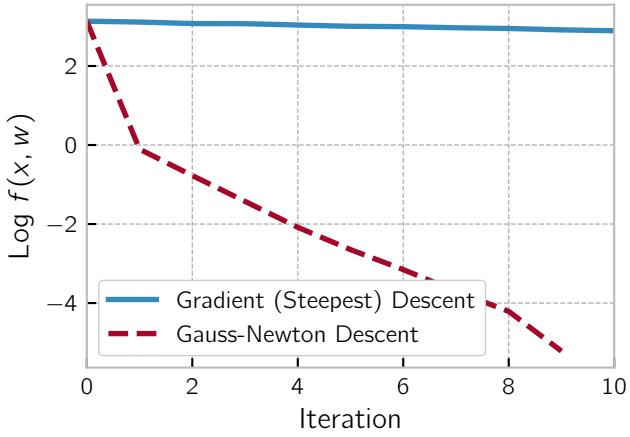

Figure 3.6: **Gauss-Newton descent directions yield faster convergence than gradient (steepest) descent** (Sec. 3.7.2). In this plot, the discrete state variables w are given and the second line of Algorithm 1 is modified to use either Gauss-Newton descent directions or gradient (steepest) descent to estimate the continuous state variables x by minimizing the relaxed objective function $f(x, w)$ (3.6).

taneously estimating both the continuous and discrete states, the smoothing term becomes crucial, as illustrated by comparing the discrete state estimates ($\widehat{w}_t$) in Figure 3.7a (without smoothing) and Figure 3.7b (with smoothing). In particular, the estimated discrete state switches rapidly without smoothing, whereas with smoothing the discrete state tends to remain constant for many samples and change mostly near ground-truth switching times.

Onboard versus offboard measurements

In the laboratory, the positions of the robot hip and foot can be directly measured *offboard*, e.g. with an external camera system. Outside of the laboratory, only the relative position of the hip and foot can be directly measured onboard our robot. Thus, we are motivated by this practical consideration to evaluate our algorithm's performance in the case where only the relative position and velocity of the hip and foot are measured,

$$\mathcal{H}_{\text{relative}}(x) = \begin{bmatrix} q[1] - q[2] \\ \dot{q}[1] - \dot{q}[2] \end{bmatrix}. \tag{3.15}$$

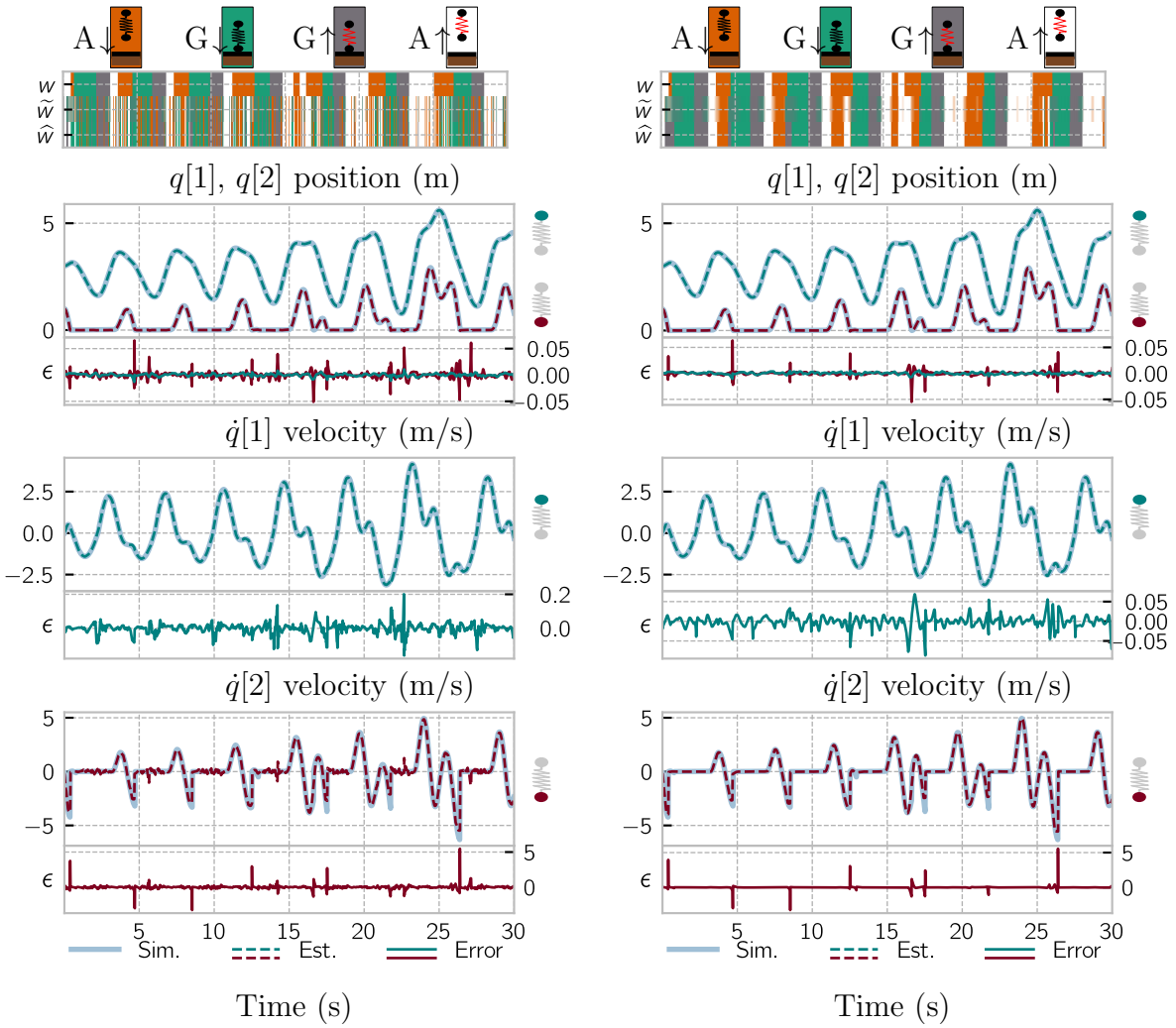

(a) Without Smoothing ($\nu = 0$)

(b) With switching ($\nu > 0$)

Figure 3.7: **Without smoothing ($\nu = 0$), the discrete state estimate switches frequently** (Sec. 3.7.2). **With smoothing ($\nu > 0$), the discrete state estimate mostly switches near the true switching times.** (Sec. 3.7.2). The top plot shows the true discrete state of the system $w \in D^M$, the relaxed discrete state estimate $\widetilde{w} \in \Delta^M$, and the discrete state estimate $\widehat{w} \in D^M$ for a simulation of the piecewise-linear system. The subsequent plots show the estimate, simulation, and error ϵ values for position and velocity of the hip $q[1]$ and foot $q[2]$.

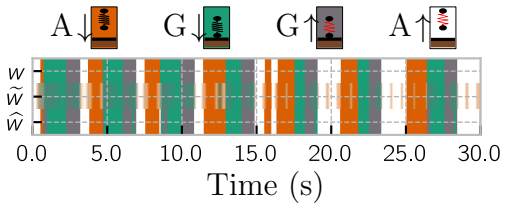

Figure 3.8: **Estimated discrete state using onboard (relative position and velocity) measurements $\mathcal{H}_{\text{relative}}$ (3.15) for the piecewise-linear system closely matches true discrete state.** (Sec. 3.7.2). Continuous state estimates are not shown since they are formally unobservable using only onboard measurements (in practice, they drift away from ground truth over time).

Although the full hybrid system state is formally unobservable with these relative measurements, our algorithm nevertheless yields good estimates of the discrete state as shown in Figure 3.8; due to large errors in the estimate of (unobservable) continuous states, we omit those results from the figure.

3.7.3 Piecewise-nonlinear impact oscillator experiment

To test Algorithm 1 on a nonlinear model, we included the kinematic constraints depicted in Figure 3.4b, resulting in a nonlinear spring force. In this model we set the two spring laws to be the same $k_1 = k_2$, decreasing the number of discrete states from four to two: $w = \text{A}$ when $q[2] > 0$ and $w = \text{G}$ when $q[2] = 0$. Appendix A.3 contains the complete hybrid system description for the model. State estimation results compare favorably with the analogous results from the piecewise-linear system when using either absolute position measurements $\mathcal{H}_{\text{pos}}$ (3.14) (compare Figure 3.9a with Figure 3.7b) or relative measurements $\mathcal{H}_{\text{relative}}$ (3.15) (compare Figure 3.9b with Figure 3.8).

In Figure 3.9a we see that the model can estimate continuous and discrete states in the nonlinear setting. However, we do notice that the estimated trajectories are not as close to ground truth as in the linear case. In particular, when $q[2]$ has a value only slightly greater than 0 (e.g. between times 3s and 4s), the algorithm fails to detect the transition between

$w = \mathrm{A}$ and $w = \mathrm{G}$.

3.8 Conclusion

We proposed a new state estimation algorithm for hybrid systems, analyzed its convergence properties, compared with IMM, and evaluated its performance on piecewise-linear and -nonlinear hybrid systems with non–identity resets. The algorithm leverages a relaxed state estimation problem formulation where the decision variables corresponding to the discrete state are allowed to take on continuous values. This relaxation yields a continuous optimization problem that can be solved using recently-developed nonsmooth variable projection techniques. The effectiveness of the approach was demonstrated on hybrid system models of mechanical systems undergoing impact.

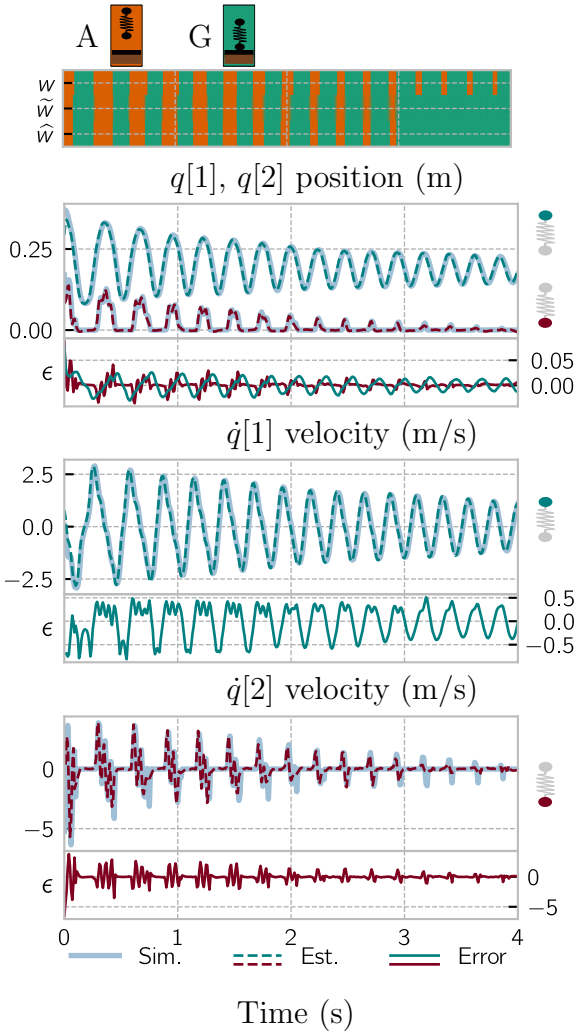

(a) **Continuous and discrete states estimated for the piecewise-nonlinear model** (Sec. 3.7.3). Notational and plotting conventions are adopted from Figure 3.7.

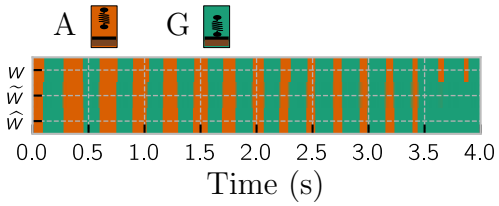

(b) **Estimated discrete state using onboard (relative position and velocity) measurements $\mathcal{H}_{\text{relative}}$ (3.15) for the piecewise-nonlinear system closely matches true discrete state.** (Sec. 3.7.2). As with Figure 3.8, continuous state estimates are not shown since they drift from the true values over time.

Figure 3.9: State estimatotion for a piecewise-nonlinear model (Sec. 3.7.1); note the nonlinear model only has two discrete states.

Chapter 4

PIECEWISE–DIFFERENTIABLE FLOW[1]

4.1 Abstract

The goal of this paper is to present the conditions under which a mechanical system with unilateral constraints is PC^r and under which it is at least once C^1. Additionally we provide an example of such systems.

4.2 Introduction

In this paper we handle rigid mechanical systems subject to unilateral constraints, a type of mechanism with many applications including locomotion and manipulation. One key characteristic of such system is the discontinuous trajectories that result from impact with unilateral constraints. While the trajectories themselves are discontinuous, under certain circumstances away from points of impact, the flow is differentiable. Ignoring grazing, it is well known that the flow is classically differentiable near trajectories undergoing independent contacts [2]. The same is not the case near trajectories with simultaneous impacts, one example is the flow for a rocking block [67] which is discontinuous along such trajectories. When unilateral constraints are *orthogonal with respect to the mass inverse matrix* the flow is at least continuous even for simultaneous impacts [10]. In this work we show that along *admissible trajectories* the flow is piecewise–differentiable, a class of differentiability stronger then directional differentiable and weaker than classical differentiable. We use the notion of piecewise–differentiable from [91,96], which provides similar properties as classically differentiable, e.g. composition, chain rule, and implicit function theorem [96, Chp. 3] We next show with even greater restriction to the system, of which *limbs decoupled through the body* is a

[1]Portions of this chapter originally appeared in [83, 84]

subset of [83], the flow is classically differentiable along trajectories even with simultaneous impacts.

Much work has gone into characterizing flows for systems with switching vector fields. [2] The work in [2] shows the existence of a first-order approximation for a continuous trajectory undergoing a discontinuous change in the underlying vector field when all nearby trajectories undergo the same sequence of vector field changes; [2, (2.5)] is the well known saltation (or jump update) matrix. This result is extended to continuous left-hand side trajectories in [49].[2] [23] generalizes the result of [2] to cases where nearby trajectories may undergo differing switching orders and shows the flow to be piecewise–differentiable. Similar result are shown in [90, 94], where sensitivity analysis is provided for fixed mode sequences and potentially varying mode sequences respectively. All the above results come from hybrid dynamics. [57] provides a differentiability result when the dynamics stem from a complementarity problem.

4.3 Background

Within this section we cover well known properties of mechanical systems interacting with unilateral constraints. We utilize two common formalisms for modeling mechanical systems undergoing impacts (i) measure differential equations / inclusion and (ii) hybrid dynamical systems.[3] Measure differential inclusion provides the key result of existence and uniqueness [10, Thm. 10] and continuity [10, Thm. 20] of flow.[4]

The section is organized as follows, we first define constraints and what contact is and provide a key assumption *orthogonality of constraints*. Next, we introduce the well known dynamics of the system, and introduce assumptions to guarantee existence and uniqueness of the flow followed by a reiteration of [10, Thm. 20]. Next we state key assumptions on what makes a given trajectory *admissible*.

---

[2]In [49], the notion of *piecewise*–differentiable is introduced for trajectories undergoing up to two simultaneous impacts but means *directional* derivative as opposed to the stronger notion provided by [91].

[3]Other modeling conventions are *singular perturbations* and *complementarity systems* [61, Chp. 1].

[4]To the best of the authors' knowledge, there are no comparable results to [10, Thm. 20] using the hybrid dynamical systems formalism for mechanical systems subject to unilateral impacts.

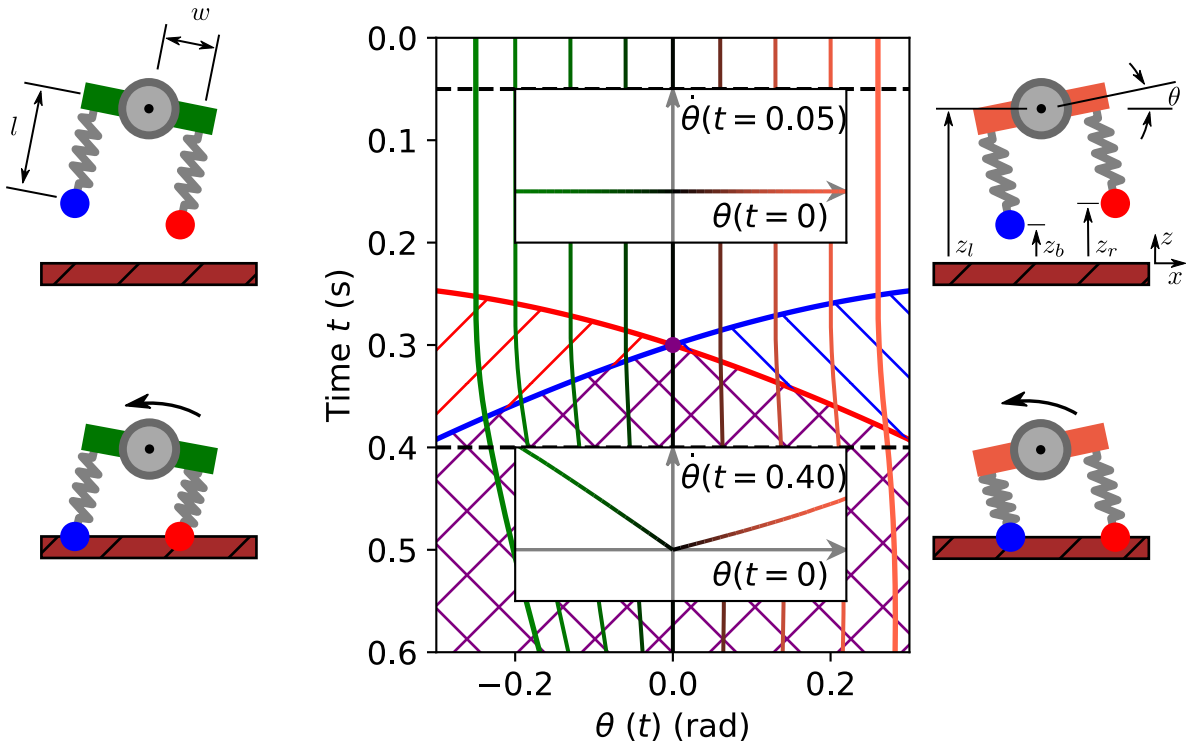

Figure 4.1: Figure of a basic example piecewise differentiable flow. The pictured system is described in detail in section 4.5.1

4.3.1 Mechanical Systems Subject to Unilateral Constraints

In this paper, we study the dynamics of a mechanical system with configuration coordinates $q \in \mathbb{Q} = \mathbb{R}^d$ subject to n (perfect, holonomic, scleronomic)[5] unilateral constraints

$$a_i(q) \geq 0, \forall i \in \{1, 2, \cdots, n\}, \tag{4.1}$$

where $a_i \colon Q \to \mathbb{R}$ is differentiable and $n, d \in \mathbb{N}$. We are primarily interested in systems with $n > 1$ constraints. Given any ordered set $J \subset \{1, \ldots, n\}$ with the natural ordering, and letting $|J|$ denote the number of elements in J, we let $a_J \colon Q \to \mathbb{R}^{|J|}$ denote the function defined by

$$(a_J)_i (q) = a_{J_i}(q) \tag{4.2}$$

for all $i \in J$ and $q \in Q$, with $a_\emptyset(q) = 0$.

Definition 2 (contact modes). *With $A = \{q \in Q | a_i(q) \geq 0 \ \forall i \in \{1, \ldots, n\}\}$ denoting the set of* admissible *configurations, the constraint functions $\{a_j\}_{j=1}^n$ partition A into a finite collection[6] $\{A_J\}_{J \in 2^n}$ of* contact modes*:*

$$\forall J \in 2^n : A_J = \{q \in Q \mid a_J(q) = 0, \forall i \notin J : a_i(q) > 0\}. \tag{4.3}$$

We let $TA = \{(q, \dot{q}) \in TQ : q \in A\}$ and $TA_J = \{(q, \dot{q}) \in TQ : q \in A_J\}$ for each $J \in 2^n$.

Definition 3 ((in)active constraints). *For an admissible configuration $q \in A_J \subset A$, we refer to the J as the set of* active *constraints and the set $\{j \in \{1, 2, \ldots, n\} | a_j(q) > 0\}$ as the set of* inactive *constraints.*

Remark 10. *In definition 2, $J = \{1, \ldots, n\}$ indexes the maximally constrained contact mode and $J = \emptyset$ indexes the unconstrained contact mode.*

---

[5] A constraint is: *perfect* if it only generates force in the direction normal to the constraint surface; *holonomic* if it varies with configuration but not velocity; *scleronomic* if it does not vary with time. We will discuss the inclusion of *imperfect*, *nonholonomic*, or *nonscleronomic* constraints in section 4.6.

[6] We let $2^n = \{J \subset \{1, \ldots, n\}\}$ denote the *power set* (i.e. the set containing all subsets) of $\{1, \ldots, n\}$.

ASSUMPTION 1 (INDEPENDENT CONSTRAINTS [10, §3.4]). *The constraints are independent:*

$$\forall J \in 2^n,\ q \in a_J^{-1}(0) : \{Da_j(q)\}_{j\in J} \subset T_q^*Q \text{ is linearly independent.} \tag{4.4}$$

REMARK 11. *Algebraically, Assumption 1 (independent constraints) implies that the constraint forces λ_J are well–defined, and that there are no more constraints than degrees–of–freedom, $n \leq d$. Geometrically, it implies for each $J \in 2^n$ that $a_J^{-1}(0) \subset Q$ is an embedded codimension–$|J|$ submanifold, and that the codimension–1 submanifolds $\left\{a_j^{-1}(0)\right\}_{j\in J}$ intersect transversally; this follows from [59, Thm. 5.12] since* (4.4) *states that $a_J \colon Q \to \mathbb{R}$ is constant–rank on its zero section.*

ASSUMPTION 2 (ORTHOGONAL CONSTRAINTS [10, THM. 20]). *Constraint surfaces intersect orthogonally:*

$$\forall i,j \in \{1,\dots,n\},\ i \neq j,\ q \in a_i^{-1}(0) \cap a_j^{-1}(0) : \langle Da_i(q), Da_j(q)\rangle_{M^{-1}} = 0. \tag{4.5}$$

REMARK 12. *Note that Assumption 2 (orthogonal constraints) is strictly stronger than Assumption 1 (independent constraints). Physically, the assumption can be interpreted as asserting that any two independent limbs that can undergo impact simultaneously must be inertially decoupled. This can be achieved in artifacts by introducing series compliance in a sufficient number of degrees–of–freedom.*

It is well–known (see e.g. [10, Sec. 3] or [50, Sec. 2.4, 2.5]) that for a constant contact mode with $J = \{j \in \{1,\dots,n\} : a_j(q) = 0\}$, the set of active constraints, the system's dynamics take the form

$$M(q)\ddot{q} = f(q,\dot{q}) - c(q,\dot{q})\dot{q} + Da_J(q)^\top \lambda_J(q,\dot{q}), \tag{4.6a}$$

$$\dot{q}^+ = \Delta_J(q,\dot{q}^-)\dot{q}^-, \tag{4.6b}$$

where $M \colon Q \to \mathbb{R}^{d\times d}$ specifies the mass matrix (or *inertia tensor*) for the mechanical system in the q coordinates, $f \colon TQ \to \mathbb{R}^d$ is termed the *effort map* [10] and specifies[7] the internal

[7] We let $TQ = \mathbb{R}^d \times \mathbb{R}^d$ denote the *tangent bundle* of the configuration space Q; an element $(q,\dot{q}) \in TQ$ can be regarded as a pair containing a vector of generalized configurations $q \in \mathbb{R}^d$ and velocities $\dot{q} \in \mathbb{R}^d$; we write $\dot{q} \in T_qQ$.

and applied forces, $c\colon TQ \to \mathbb{R}^{d\times d}$ denotes the *Coriolis matrix* determined[8] by M, $Da_J\colon Q \to \mathbb{R}^{|J|\times d}$ denotes the (Jacobian) derivative of the constraint function a_J with respect to the coordinates, $\lambda_J\colon TQ \to \mathbb{R}^{|J|}$ denotes the reaction forces generated in contact mode J to enforce the set of active unilateral constraints, $a_J(q) = 0$ [66, (4.5)],

$$\lambda_J(q,\dot{q}) = -\Lambda_J(q)\bigg(Da(q)M^{-1}(q)\left(f(q,\dot{q}) - c(q,\dot{q})\dot{q}\right) + \frac{d}{dt}(Da_J)(q)\dot{q}\bigg), \tag{4.7}$$

$\Delta_J\colon TQ \to \mathbb{R}^{d\times d}$ specifies the collision restitution law that resets velocities to ensure compatibility with the active unilateral constraints, and $\dot{q}^+$ (resp. $\dot{q}^-$) denotes the right– (resp. left–)handed limits of the velocity vector with respect to time.

Given Assumption 2 (orthogonal constraints), the impact law eq. (4.6b) has a unique solution [50, Sec. 2.5]

$$\Delta(q,\dot{q}) = I_d - (1+\gamma(q))\, M(q)^{-1} Da_J(q)^\top \Lambda_J(q) Da_J(q),$$

where I_d is the d–dimensional identity matrix, $\gamma\colon Q \to [0,1]$ is a continuous function specifying the *coefficient of restitution*,and $\Lambda_J\colon Q \to \mathbb{R}^{d\times d}$ is given by

$$\Lambda_J(q) = \left(Da_J(q)M(q)^{-1}Da_J(q)^\top\right)^{-1},$$

and $\Lambda_\emptyset(q) = 0$

Remark 13. *When only constraint deactivations occur, $\dot{q}^+ = \Delta_J(q,\dot{q}^-)\dot{q}^- = \dot{q}^-$. In a similar vain, we adopt the convention $\Delta_\emptyset(q,\dot{q}) = I_d$ since any velocity is allowable in the unconstrained mode.*

Remark 14. *Equation eq.* (4.6) *generates a right hand continuous flow, with discontinuities whenever a constraint is activated. It is import to note eq.* (4.6b) *does not apply only when the constraint mode changes, indeed at every instant in time eq.* (4.6b) *for a constant mode J $\dot{q}^+ = \Delta_J(q,\dot{q}^-)\dot{q}^- = \dot{q}^-$ as λ_J ensures $a_J(q) = 0$.*

---

[8]For each $\ell, m \in \{1,\dots,d\}$ the (ℓ,m) entry $c_{\ell m}$ is determined from the entries of M via

$$c_{\ell m} = \frac{1}{2}\sum_{k=1}^{d}\left(D_k M_{\ell m} + D_m M_{\ell k} - D_\ell M_{km}\right).$$

In the present paper, we will assume that appropriate conditions have been imposed to ensure trajectories of eq. (4.6) exist on a region of interest in time and state.

ASSUMPTION 3 (EXISTENCE AND UNIQUENESS [10, THM. 10]). *There exists a* flow *for eq.* (4.6)*, that is, a function* $\phi : \mathcal{F} \to TA$ *where* $\mathcal{F} \subset [0, \infty) \times TA$ *is an open subset containing* $\{0\} \times TA$ *and for each* $(t, (q, \dot{q})) \in \mathcal{F}$ *the restriction* $\phi|_{[0,t]\times\{(q,\dot{q})\}} \colon [0, t] \to TQ$ *is the unique left–continuous trajectory for eq.* (4.6) *initialized at* $(q, \dot{q})$*.*

REMARK 15. *The problem of ensuring trajectories of eq.* (4.6) *exist and are unique has been studied extensively; we refer the reader to [10, Thm. 10] for a specific result and [50] for a general discussion of this problem.*

Since we are concerned with differentiability properties of the flow, we assume the elements in eq. (4.6) are differentiable.

ASSUMPTION 4 (C^r VECTOR FIELD AND RESET MAP [10, §3.4]). *The vector field eq.* (4.6a) *and reset map eq.* (4.6b) *are continuously differentiable to order* $r \in \mathbb{N}$*.*

REMARK 16. *If we restricted our attention to the continuous–time dynamics in eq.* (4.6)*, then Assumption 4 would suffice to provide the local existence and uniqueness of trajectories imposed by Assump. 3; as illustrated by [10, Ex. 2], Assumption 4 does not suffice when the vector field eq.* (4.6a) *is coupled to the reset map eq.* (4.6b)*.*

REMARK 17. *The problem of ensuring trajectories of* (4.6) *exist and are unique has been studied extensively; we refer the reader to [10, Thm. 10] for a specific result and [50] for a general discussion of this problem.*

4.3.2 Differentiability for constant contact mode sequence

It is possible to satisfy the hypothesis of Assumption 3 (existence and uniqueness of flow) under mild conditions that allow trajectories to exhibit phenomena such as *grazing* (wherein the trajectory activates a new constraint without undergoing impact) or *Zeno* (wherein the

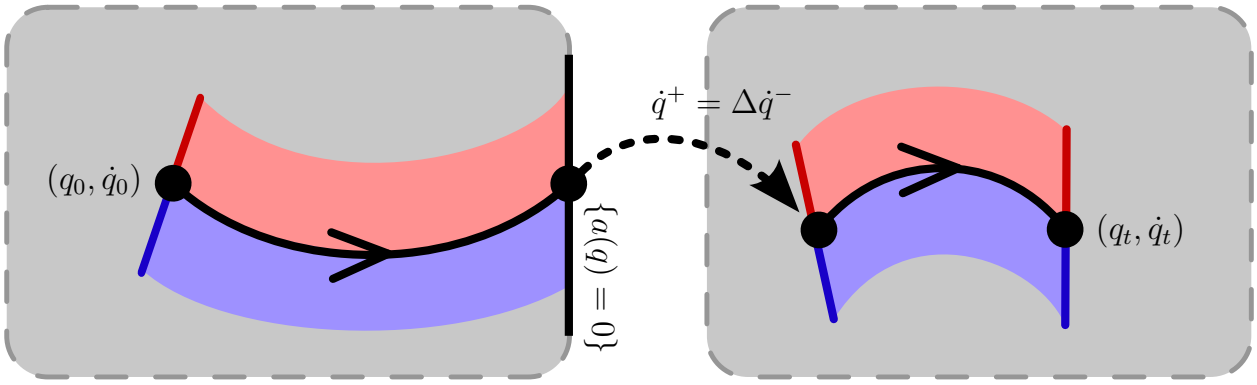

Figure 4.2: Example of what a constant contact mode sequence means for differentiation and why differentiable

trajectory undergoes an infinite number of impacts in a finite time interval). In this and subsequent sections, where we seek to study differentiability properties of the flow, we will not be able to accommodate grazing and Zeno phenomena. Therefore we proceed to restrict the trajectories under consideration.

One import reminder is that while we seek criteria that denote differing concepts of differentiability of the flow, this does not imply the flow is everywhere continuous. Importantly, permissible trajectories with constraint activations must be discontinuous. Instead, the restrictions of considering trajectories will enforce continuity of final condition with respect to perturbations of the initial condition. That is, under assumptions laid out in this section, ϕ is a continuous function nearby $(t, (q, dotq))$, Fig. 4.2 provides an example of a classically differentiable flow with a discontinuous trajectory.

DEFINITION 4 (CONSTRAINT ACTIVATION/DEACTIVATION). *The trajectory $\phi^{(q,\dot{q})}$ initialized at $(q, \dot{q}) \in TA_J \subset TQ$* activates constraints *$I \in 2^n$* at time *$t > 0$*[9] *if (i) no constraint in I was active immediately before time t and (ii) all constraints in I become active at time t.*

[9]We also informally refer to a constraint activating as *impacting constraints I* due to, once excluding grazing trajectories, all constraint activations cause a discontinuity in the velocity according to eq. (4.6b).

Formally,[10]

$$\begin{aligned}\exists \varepsilon > 0 :\ I \cap J = \emptyset,\ \textit{(i)}\ \phi\left((t-\varepsilon, t), (q, \dot{q})\right) \subset TA_J, \\ \textit{(ii)}\ \phi(t, (q, \dot{q})) \in TA_{I \cup J}.\end{aligned} \tag{4.8}$$

We refer to t as a constraint activation time *for $\phi^{(q,\dot{q})}$. Similarly, the trajectory $\phi^{(q,\dot{q})}$* deactivates constraints $I \in 2^n$ at time $t > 0$ *if (i) all constraints in I were active at time t and (ii) no constraint in I remains active immediately after time t. Formally,*

$$\begin{aligned}\exists \varepsilon > 0 :\ I \subset J,\ \textit{(i)}\ \phi(t, (q, \dot{q})) \in TA_J, \\ \textit{(ii)}\ \phi\left((t, t+\varepsilon), (q, \dot{q})\right) \subset TA_{J \setminus I}.\end{aligned} \tag{4.9}$$

Definition 5 (Admissible (de)activation). *A constraint activation time $t > 0$ for $\phi^{(q,\dot{q})}$ is* admissible *if the constraint velocity*[11] *for all activated constraints $I \in 2^n$ is negative. Formally, with $(\rho, \dot{\rho}^-) = \lim_{s \to t^-} \phi(s, (q, \dot{q}))$ denoting the left–handed limit of the trajectory at time t,*

$$\forall i \in I : D_t \left[a_i \circ \phi\right](0, (\rho, \dot{\rho}^-)) = Da_i(\rho)\dot{\rho}^- < 0. \tag{4.10}$$

for all activated constraints $I \in 2^d$ is negative.

A constraint deactivation time $t > 0$ for $\phi^{(q,\dot{q})}$ is admissible *if, for all deactivated constraints $I \in 2^n$: (i) the constraint velocity or constraint acceleration*[12] *is positive, or (ii) the time derivative of the contact force is negative. Formally, with $(\rho, \dot{\rho}^+) = \lim_{s \to t^+} \phi(s, (q, \dot{q}))$ denoting the right–handed limit of the trajectory at time t, for all $i \in I$:*

$$\begin{aligned}D_t \left[a_i \circ \phi\right](0, (\rho, \dot{\rho}^+)) > 0 \ \textit{or} \\ D_t^2 \left[a_i \circ \phi\right](0, (\rho, \dot{\rho}^+)) > 0,\end{aligned} \tag{4.11a}$$

---

[10] $\phi((t_1, t_2), (q, \dot{q})) = \{\phi(t, (q, \dot{q})) : t \in (t_1, t_2)\} \subset TQ$ denotes the *image* of $\phi^{(q,\dot{q})}$ over the interval $(t_1, t_2) \subset [0, \infty)$.

[11] Formally, the *Lie derivative* [59, Prop. 12.32] of the constraint along the vector field specified by (4.6a). Although constraint functions are technically only functions of configuration $q \in Q$ and not the full state $(q, \dot{q}) \in TQ$, by a mild abuse of notation we allow ourselves to consider compositions $a \circ \phi$ rather than the formally correct $a \circ \pi_Q \circ \phi$ where $\pi_Q : TQ \to Q$ is the canonical projection.

[12] Formally, the second Lie derivative of the constraint along the vector field specified by (4.6a).

or

$$D_t \left[\lambda_i \circ \phi\right](0, (\rho, \dot{\rho}^+)) < 0. \tag{4.11b}$$

Remark 18. *The conditions for admissible constraint deactivation in eq.* (4.11a) *can only arise at admissible constraint activation times; otherwise the trajectory is continuous, whence active constraint velocities and accelerations are zero. Hence deactivations of the form eq.* (4.11a) *occur* contingent *upon an activation, and are thus referred to as* contingent deactivations.

Definition 6 (Admissible Trajectory). *A trajectory* $\phi^{(q,\dot{q})}$ *is* admissible *on* $[0, t] \subset \mathbb{R}$ *if (i) it has a finite number of constraint activation (hence, deactivation) times on* $[0, t]$*, and (ii) every constraint activation and deactivation is admissible; otherwise the trajectory is* inadmissible.

Remark 19 (Admissible Trajectories). *The key property admissible trajectories possess that will be leveraged in what follows is: time–to–activation and time–to–deactivation (that is the time to a constraint (de)activation) are differentiable with respect to initial conditions; the same is not generally true of inadmissible trajectories.*

Remark 20 (Grazing is not admissible). *The restriction in definition 6 (admissible trajectory)that all constraint (de)activation times be admissible precludes admissibility of grazing.*

Remark 21 (Zeno is not admissible). *The restriction in definition 6 (admissible trajectory)to a finite number of constraint activations occur on a compact time interval precludes admissibility of Zeno.*

Remark 22 (Analyticity is sufficient). *Given* Zeno *trajectories are not admissible, the necessary order of differentiation for all functions may be less than analytic, Additionally we know that the intersection of Assumption 4 (C^r vector field and reset map) and Assumption 3 (existence and uniqueness of flow) given analytic functions satisfy both. We choose not to assume all functions are analytic given that analyticity is a very restrictive assumption.*

Remark 23 (Equivalence with Complementarity). *The dynamics near a definition 6 (admissible trajectory) with Assumption 2 (orthogonal constraints) can be written without the explicit dependence on the contact mode J. That is, we can write eq.* (4.6a) *as*

$$M(q)\ddot{q} = f(q,\dot{q}) - c(q,\dot{q})\dot{q} + \sum_{i=1}^{n} \delta_i(q,\dot{q}) Da_i(q)^\top \lambda_i(q,\dot{q}), \tag{4.12}$$

where

$$\delta_i(q,\dot{q}) = \begin{cases} 1 & \text{if } a_i(q) = 0 \text{ and } Da_i(q)\dot{q} = 0 \text{ and } \lambda_i(q,\dot{q}) \leq 0 \\ 0 & \text{otherwise.} \end{cases} \tag{4.13}$$

The total force due to the set of active constraints is the superposition (that is the sum) of the forces due to the individual active constraints as the constraints are orthogonal. *The conditions on the constraint force eq.* (4.13) *are equivalent to*

$$\begin{aligned} &\lambda_i(q,\dot{q}) \leq 0, \qquad a_i(q) \geq 0, \qquad a_i(q)\lambda_i(q,\dot{q}) = 0 \\ &\lambda_i(q,\dot{q}) \leq 0, \qquad Da_i(q)\dot{q} \geq 0, \qquad \lambda_i(q,\dot{q}) Da_i(q)\dot{q} = 0, \end{aligned} \tag{4.14}$$

which are identical to the complementarity equations [66, (2.2)]. That is, for admissible trajectories *undergoing* orthogonal constraint *activations eq.* (4.6) *is equivalent to complementarity.*

Definition 7 (Contact mode sequence [50, Def. 4]). *The* contact mode sequence *associated with a trajectory $\phi^{(q,\dot{q})}$ that is admissible on $[0,t] \subset \mathbb{R}$ is the unique function*

$$\omega \colon \{0,\dots,m\} \to 2^n \tag{4.15}$$

such that there exists a finite sequence of times $\{t_\ell\}_{\ell=0}^{m+1} \subset [0,t]$ for which $0 = t_0 < t_1 < \cdots < t_{m+1} = t$ and

$$\forall \ell \in \{0,\dots,m\} : \phi((t_\ell, t_{\ell+1}), (q,\dot{q})) \subset TA_{\omega(\ell)}. \tag{4.16}$$

Remark 24. *In definition 7 (contact mode sequence), the sequence ω is easily seen to be unique by the admissibility of the trajectory; indeed, the associated time sequence consists of start, stop, and constraint activation/deactivation times. Note that successive modes in the*

sequence need not be related by set containment (i.e. $\omega(\ell) \subset \omega(\ell+1)$ or $\omega(\ell) \supset \omega(\ell+1)$) since, e.g., one constraint could activate and another deactivate at the same time instant as in Fig. 4.4. Thus, ω is not simply a discrete "counter" as in hybrid time domains *[40, §3.2].*

We now state the well–known fact[13] that, if the contact mode sequence is fixed, then admissible trajectory outcomes are differentiable with respect to initial conditions.

LEMMA 4 (DIFFERENTIABILITY FOR CONSTANT MODE SEQUENCE [2]). *Under Assumption 3 (existence and uniqueness of flow), Assumption 4 (C^r vector field and reset map), and Assumption 1 (independent constraints), with $\phi\colon [0,\infty) \times TA \to TA$ denoting the flow, if $\Sigma \subset TQ$ is a C^r embedded submanifold such that all trajectories initialized in $\Sigma \cap TA$*

(i) are admissible on $[0,t] \subset \mathbb{R}$ and

(ii) have the same contact mode sequence,

then the restriction $\phi|_{\{t\}\times\Sigma}$ is C^r.

4.3.3 (Dis)continuity with differing contact mode sequences

As stated in section 4.2, the purpose of this paper is provide sufficient conditions that ensure trajectories of eq. (4.6) vary differentiably as the contact mode varies. In this section we consider what condition must be imposed to give rise to continuity, a precondition for differentiability. We begin in section 4.3.3 by demonstrating that the trasnversality of constraints imposed by Assumption 1 (independent constraints) generally gives rises to discontinuity, then introduce an orthogonality condition in section 4.3.3 that suffices to guarantee continuity.

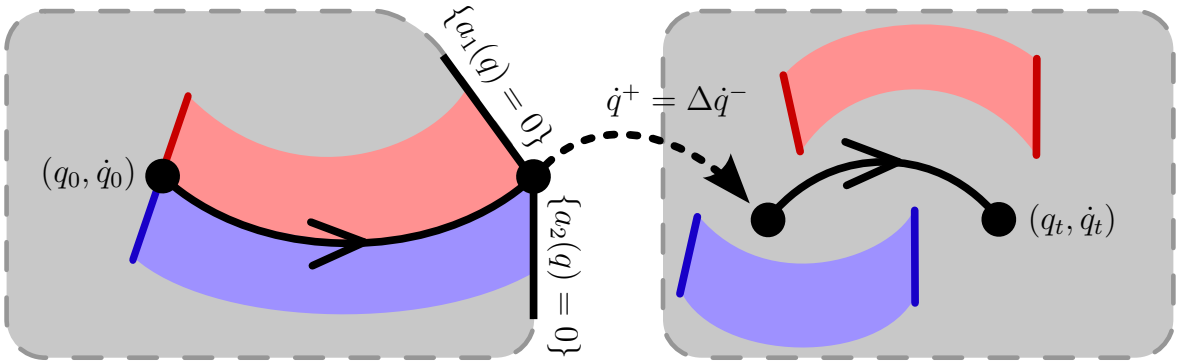

Figure 4.3: Example of a discontinuous flow

Discontinuity with differing contact mode sequences

Consider an unconstrained initial condition $(q, \dot{q}) \in TA_\emptyset \subset TQ$ that impacts (i.e. admissibly activates) exactly two constraints $i, j \in \{1, \ldots, n\}$ at time $t > 0$. With $(\rho, \dot{\rho}^-) = \phi(t, (q, \dot{q}))$, we have

$$a_{\{i,j\}}(\rho) = 0, Da_i(\rho)\dot{\rho}^0 < 0, Da_j(\rho)\dot{\rho}^- < 0. \tag{4.17}$$

The pre–impact velocity $\dot{\rho}^-$ resets via eq. (4.6b):

$$\dot{\rho}^+ = \Delta_{\{i,j\}}(\rho)\dot{\rho}^-. \tag{4.18}$$

As noted in Remark 11 (independent constraints), the constraint surfaces $a_i^{-1}(0)$, $a_j^{-1}(0)$ intersect transversally. Therefore given any $\varepsilon > 0$ it is possible to find $(q_i, \dot{q}_i)$ and $(q_j, \dot{q}_j)$ in the open ball of radius ε centered at $(q, \dot{q})$ such that the trajectory $\phi^{(q_i, \dot{q}_i)}$ impacts constraint i before constraint j and $\phi^{(q_j, \dot{q}_j)}$ impacts j before i. As $\varepsilon > 0$ tends toward zero, the time spent flowing according to (4.6a) tends toward zero, hence the post–impact velocities tend

[13]The result follows via a straightforward composition of smooth flows with smooth time–to–impact maps; we refer the interested reader to [26, App. A1] for details.

toward the twofold iteration of (4.6b):

$$\begin{aligned} \dot{\rho}_i^+ &= \Delta_{\{i,j\}}(\rho)\Delta_i(\rho)\dot{\rho}^-, \\ \dot{\rho}_j^+ &= \Delta_{\{i,j\}}(\rho)\Delta_j(\rho)\dot{\rho}^-. \end{aligned} \tag{4.19}$$

Recalling for all $J \in 2^n$ that $\Delta_J \in \mathbb{R}^{d\times d}$ is an orthogonal projection[14] onto the tangent plane of the codimension–$|J|$ submanifold $a_J^{-1}(0)$, observe that $\dot{\rho}_i^+ = \dot{\rho}^+ = \dot{\rho}_j^+$ if and only if $Da_i(\rho)$ is orthogonal to $Da_j(\rho)$. Therefore if constraints intersect transversally but non–orthogonally, outcomes from the dynamics in (4.6) vary discontinuously as the contact mode sequence varies.

Remark 25 (discontinuous locomotion outcomes). *The analysis of a saggital–plane quadruped in [87] provides an instructive example of the behavioral consequences of transverse but non–orthogonal constraints in a model of legged locomotion. As summarized in [87, Table 2], the model possesses three distinct but nearby trot (or trot–like) gaits, corresponding to whether two legs impact simultaneously (as in eq.* (4.18)*) or at different time instants (as in eq.* (4.19)*); the trot that undergoes simultaneous impact is unstable due to discontinuous dependence of trajectory outcomes on initial conditions.*

Continuity with differing contact mode sequences

To preclude the discontinuous dependence on initial conditions exhibited in section 4.3.3, we strengthen the *transversality* of constraints implied by Assumption 1 (independent constraints) by imposing *orthogonality* of constraints.

Section 4.3.3 demonstrated that Assumption 2 (orthogonal constraints) is necessary in general to preclude discontinuous dependence on initial conditions. The following result demonstrates that this assumption is sufficient to ensure continuous dependence on initial conditions, even as the contact mode varies.[15]

[14] relative to the inner product $\langle\cdot,\cdot\rangle_M$. For further discussion of orthogonal projection in constraint activation of mechanical systems, see [50, §1.3.4].

[15] We note for the interested reader that the result on continuity with respect to initial conditions in [67]

LEMMA 5 (CONTINUITY ACROSS MODE SEQ. [10, THM. 20]). *Under Assumption 3 (existence and uniqueness of flow), Assumption 4 (C^r vector field and reset map), and Assumption 2 (orthogonal constraints), with $\phi\colon [0,\infty) \times TA \to TA$ denoting the flow, if $t \in \mathbb{R}$ and $(p,\dot{p}) \in TA \subset TQ$ are such that t is not a constraint activation time for $(p,\dot{p})$, then ϕ is continuous at $(t,(p,\dot{p}))$.*

REMARK 26 (CONTINUITY WITH DIFFERING MODE SEQUENCE). *The preceding result implies that the flow ϕ is continuous almost everywhere in both time and state, without needing to restrict to admissible trajectories. Thus orthogonal constraints ensure the flow ϕ depends continuously on initial conditions, even along trajectories that exhibit grazing and Zeno phenomena.*[16] *For the reason described in Remark 19 (admissible trajectories), we will not be able to accommodate these phenomena when we study differentiability properties of trajectories in the next section.*

4.4 Differentiability with differing contact mode sequences

Within this section we present the two main results of this paper, theorem 3 (piecewise differentiability with differing contact mode sequences) and theorem 4 (at least once classically differentaible with differeing contact mode sequence). Additionally, we discuss how to calculate the piecewise–derivative of the flow and the sufficient assumption for theorem 4 (at least once classically differentaible with differeing contact mode sequence) to hold.

4.4.1 Piecewise–differentiability of trajectories

We now provide conditions that ensure trajectories depend *differentiably* on initial conditions, even as the contact mode sequence varies. In general, the flow does not possess a classical Jacobian (alternately called *Fréchet* or *F*–)derivative, i.e. there does not exist a single linear

is inapplicable along trajectories that simultaneously activate and/or deactivate more than one constraint; such trajectories do no satisfy hypothesis 4 and 5 of [67, Thm. III.2].

[16] We remark that [10, Thm. 20] implies the function ϕ is continuous everywhere with respect to the quotient metric defined in [24, Sec. III], whence the numerical simulation algorithm in [24, Sec. IV] is provably–convergent for all trajectories (even those that graze) up to the first occurrence of Zeno.

map that provides a first–order approximation for the flow. Instead, under admissibility conditions introduced in section 4.3, we show that the flow admits a *piecewise*–linear first–order approximation termed[17] a *Bouligand* (or *B*–)derivative [96, Chp. 3.1]. Though perhaps unfamiliar, this derivative is nevertheless quite useful. Significantly, unlike functions that are merely directionally differentiable, B–differentiable functions admit generalizations of many techniques familiar from calculus, including the Chain Rule [96, Thm. 3.1.1] (and hence Product and Quotient Rules [96, Cor. 3.1.1]), Fundamental Theorem of Calculus [96, Prop. 3.1.1], Implicit Function Theorem [96, Thm. 4.2.3], and the B–derivative can be employed to implement scalable algorithms [54] for optimization or learning.

We proceed by showing that the flow is piecewise–differentiable in the sense defined in [96, Chp. 4.1] and recapitulated here; functions that are piecewise–differentiable in this sense are always B–differentiable [96, Prop. 4.1.3]. Let $r \in \mathbb{N} \bigcup \{\infty\}$ denote an oder of differentiability[18] and $D \subset \mathbb{R}^m$ be open. A continuous function $\psi \colon D \to \mathbb{R}^\ell$ is called *piecewise–*C^r if the graph of ψ is everywhere locally covered by the graphs of a finite collection of functions that are r–times continuously differentiable (C^r–functions).[19] Formally, for every $x \in D$ there must exist an open set $U \subset D$ containing x and a finite collection $\left\{\psi_\omega \colon U \to \mathbb{R}^\ell\right\}_{\omega \in \Omega}$ of C^r–functions such that for all $x \in U$ we have $\psi(x) \in \{\psi_\omega(x)\}_{\omega \in \Omega}$. We now state and prove one of the two main results of this paper: whenever the flow of a mechanical system subject to unilateral constraints is continuous and admissible, it is piecewise–C^r; see Fig. 4.4 for an illustration.

THEOREM 3 (PIECEWISE–DIFFERENTIABLE FLOW). *Under Assumption 3 (existence and uniqueness of flow), Assumption 4 (C^r vector field and reset map), and Assumption 2*

---

[17] This terminology was introduced, to the best of our knowledge, by Robinson [91].

[18] We let context specify whether $r = \infty$ indicates "mere" smoothness or the more stringent condition of analyticity.

[19] The definition of piecewise–C^r may at first appear unrelated to the intuition that a function ought to be piecewise–differentiable precisely if its "domain can be partitioned locally into a finite number of regions relative to which smoothness holds" [92, Section 1]. However, as shown in [92, Theorem 2], piecewise–C^r functions are always piecewise–differentiable in this intuitive sense.

(orthogonal constraints), with $\phi\colon [0,\infty) \times TA \to TA$ *denoting the flow, if* $t \in [0,\infty)$, $(p,\dot{p}) \in TA \subset TQ$, *and* $\Sigma \subset TQ$ *is a* C^r *embedded submanifold containing* $(p,\dot{p})$ *such that*

(i) the trajectory $\phi^{(p,\dot{p})}$ *activates and/or deactivates constraints at a finite set of times* $\{t_i | t_i \in (0,t)\}$,

(ii) $\phi^{(p,\dot{p})}$ *has no other activation or deactivation times in* $[0,t]$,

(iii) trajectories initialized in $\Sigma \cap TA$ *are admissible on* $[0,t]$, *and*

(iv) the set Ω *of contact mode sequences for trajectories initialized in* $\Sigma \cap TA$ *is finite,*

then the restriction $\phi|_{[0,\infty)\times\Sigma}$ *is piecewise–*C^r *at* $(t,(p,\dot{p}))$.

Proof. We seek to show that the restriction $\phi|_{[0,\infty)\times\Sigma}$ is piecewise–C^r at $(t,(p,\dot{p}))$. We first show the result when there is only one instant of time $s \in (0,t)$ when constraints activate and/or deactivate. We will proceed by constructing a finite set of r times continuously differentiable selection functions for ϕ on $[0,t] \times \Sigma$. In the example given in Fig. 4.4, there are two selection functions, one corresponding to a perturbation along $(v_r, \dot{v}_r)$, colored red, and the other along $(v_b, \dot{v}_b)$, colored blue. Let $m \in \{1,\dots,n\}$ be the number of constraints undergoing (de)activation at time s. These selection functions will be indexed by a pair of functions (ω,η) where: $\omega\colon \{0,\dots,m\} \to 2^n$ is a contact mode sequence, (de)activating at time s. i.e. $\omega \in \Omega$; $\eta\colon \{0,\dots,m-1\} \to \{1,\dots,n\}$ indexes constraints that undergo admissible activation or deactivation[20] at the contact mode transition indexed by $\ell \in \{0,\dots,m-1\}$. For instance, in Fig. 4.4 the index functions for the (de)activation sequence starting from $(v_r,\dot{v}_r)$, in red, are $\omega_r(0) = \{1\}, \omega_r(1) = \emptyset, \omega_r(2) = \{2\}$, $\eta_r(0) = 1, \eta_r(1) = 2$, and the

[20]In light of Remark 18, we only consider deactivations of type (ii) in definition 5 (admissible constraint activation/deactivation). In some systems, a deactivation of type (ii) may only arise following a (simultaneous) activation; it suffices to restrict to functions η that do not index such deactivations. This restriction of η is the only constraint we impose on the (ω,η). We do not attempt to find the set of feasible (ω,η) and instead show the result holds for all possible (ω,η) pairs.

index functions for the (de)activation sequence starting from $(v_b, \dot{v}_b)$, in blue, are $\omega_b(0) = \{1\}, \omega_b(1) = \{1,2\}, \omega_b(2) = \{2\}$, $\eta_b(0) = 2, \eta_b(1) = 1$. Note that for each $\omega \in \Omega$ the set $H(\omega)$ of possible η's is finite; since the set Ω is finite by assumption, the set of pairs (ω, η) is finite.

Let $(\omega\colon \{0,\dots,m\} \to 2^n) \in \Omega$ and $(\eta\colon \{0,\dots,m-1\} \to \{1,\dots,n\}) \in H(\omega)$ be as described above. Let $\mu\colon \{0,\dots,m\} \to 2^n$ be defined as $\mu(k) = \bigcup_{i=0}^{k-1} \{\eta(i)\}$, where we adopt the convention that $\bigcup_{i=0}^{-1} \{i\} = \emptyset$; note that μ is uniquely determined by η. $\mu(k)$ as defined above is equivalent to the union of only activated constraints up to $k-1$ because of orthogonality of constraints and constraints undergoing deactivation must be active at some prior point for deactivation to occur.[21] For the sake of readability, we suppress dependence on η and ω until (4.26). Let $(\rho, \dot{\rho}^-) = \lim_{u \uparrow s} \phi(u, (p, \dot{p}))$. For all $k \in \{0,\dots,m\}$ define $\dot{\rho}_k = \Delta_{\mu(k)}(\rho)\dot{\rho}^-$. There exists an open neighborhood $U_k \subset TQ$ containing $(\rho, \dot{\rho}_k)$ such that the vector field determined by (4.6a) at $\omega(k)$ admits a C^r extension to $F_k\colon U_k \to \mathbb{R}^{2d}$. (Note that for $k = m$ (resp. $k = 0$) the neighborhood U_k can be taken to additionally include $\phi((s,t],(p,\dot{p}))$ (resp. $\phi([0,s),(p,\dot{p}))$).)

By the Fundamental Theorem on Flows [59, Thm. 9.12], F_k determines a unique maximal flow $\phi_k\colon \mathcal{F}_k \to U_k$ over a maximal flow domain $\mathcal{F}_k \subset \mathbb{R} \times U_k$, which is an open set that contains $\{0\} \times U_k$, and the flow ϕ_ℓ is C^r. (Note that $(t-s, (\rho, \dot{\rho}_m)) \in \mathcal{F}_m$ and $(s, (p, \dot{p})) \in \mathcal{F}_0$.)

If $\eta(\ell)$ indexes an admissible constraint activation (recall that $\ell \in \{0,\dots,m-1\}$), then there exists a time–to–activation $\tau_\ell\colon U_\ell \to \mathbb{R}$ defined over an open set $U_\ell \subset TQ$ containing $(\rho, \dot{\rho}_\ell)$ such that

$$\forall (q,\dot{q}) \in U_\ell : a_{\eta(\ell)} \circ \phi_\ell(\tau_\ell(q,\dot{q}),(q,\dot{q})) = 0. \tag{4.20}$$

If instead $\eta(\ell)$ indexes an admissible constraint deactivation, then there exists a time–to–deactivation $\tau_\ell\colon U_\ell \to \mathbb{R}$ defined over an open set $U_\ell \subset TQ$ containing $(\rho, \dot{\rho}_\ell)$ such that

$$\forall (q,\dot{q}) \in U_\ell : \lambda_{\eta(\ell)} \circ \phi_\ell(\tau_\ell(q,\dot{q}),(q,\dot{q})) = 0. \tag{4.21}$$

[21] η is not uniquely determined by ω due to the possibility of instantaneous activation/deactivation for the same constraint; consider for instance the bounce of an elastic ball [42, Chp. 2.4].

In either case, τ_ℓ exists and is C^r by the Implicit Function Theorem [59, Thm. C.40] due to admissibility of trajectories initialized in Σ. (Note for $\ell = 0$ the neighborhood U_ℓ can be extended to include $\phi([0, s), (p, \dot{p}))$ using the semi–group property[22] of the flow ϕ_ℓ.) See Fig. 4.4 for an illustration of constraint activations and deactivations.

Let $\varphi_\ell \colon \mathbb{R} \times U_\ell \to \mathbb{R} \times U_\ell$ be defined for all $(u, (q, \dot{q})) \in \mathbb{R} \times U_\ell$ by

$$\varphi_\ell(u, (q, \dot{q})) = (u - \tau_\ell(q, \dot{q}), \phi_\ell(\tau_\ell(q, \dot{q}), (q, \dot{q}))) . \tag{4.22}$$

The map φ_ℓ flows a state $(q, \dot{q})$ using the vector field from contact mode $\omega(\ell)$ until constraint $\eta(\ell)$ undergoes admissible activation/deactivation, and deducts the time required from the given budget u. The total derivative of φ_ℓ at $(0, (\rho, \dot{\rho}_\ell))$ (see also [26, § 7.1.4]) is

$$D\varphi_\ell(0, (\rho, \dot{\rho}_\ell)) = \begin{bmatrix} 1 & \frac{1}{gf} g \\ 0 & I_{2d} - \frac{1}{gf} fg \end{bmatrix}, \tag{4.23}$$

where $f = F(\rho, \dot{\rho}_\ell)$ and $g = Dh_{\eta(\ell)}(\rho, \dot{\rho}_\ell)$ where $h_\ell \colon TQ \to \mathbb{R}$ is defined for all $(q, \dot{q}) \in TQ$ by $h_\ell(q, \dot{q}) = a_{\eta(\ell)}(q)$.

Let $\Gamma_\ell \colon \mathbb{R} \times TQ \to \mathbb{R} \times TQ$ be defined for all $(u, (q, \dot{q})) \in \mathbb{R} \times TQ$ by

$$\Gamma_\ell(u, (q, \dot{q})) = (u, (q, \Delta_{\mu(\ell)}(q, \dot{q})\dot{q})). \tag{4.24}$$

The map Γ_ℓ resets velocities to be compatible with contact mode $\omega(\ell)$ while leaving positions and times unaffected. The total derivative of Γ_ℓ at $(u, (q, \dot{q}))$ is given by

$$D\Gamma_\ell(u, (q, \dot{q})) = \begin{bmatrix} 1 & 0 & 0 \\ 0 & I_d & 0 \\ 0 & D_q(\Delta_{\mu(\ell)}(q, \dot{q})\dot{q}) & \Delta_{\mu(\ell)}(q) \end{bmatrix}. \tag{4.25}$$

For each $\omega \in \Omega$ and $\eta \in H(\omega)$ define ϕ^η_ω by the formal composition

$$\phi^\eta_\omega = \phi_m \circ \prod_{\ell=0}^{m-1} (\Gamma_{\ell+1} \circ \varphi_\ell) . \tag{4.26}$$

---

[22] $\phi_\ell(u + v, x) = \phi_\ell(u, \phi_\ell(v, x))$ whenever $(v, x), (u + v, x), (u, \phi_\ell(v, x)) \in \mathcal{F}_\ell$.

We take as the domain of ϕ_ω^η the set

$$\mathcal{F}_\omega^\eta = (\phi_\omega^\eta)^{-1}(TQ) \subset \mathbb{R} \times TQ, \tag{4.27}$$

noting that $\mathcal{F}_\omega^\eta$ is (i) open since each function in the composition is continuous, and (ii) nonempty since $(t,(p,\dot{p})) \in \mathcal{F}_\omega^\eta$. The map ϕ_ω^η flows states via a given contact mode sequence for a specified amount of time; note that some of the resulting "trajectories" are not physically realizable, as they may evaluate the flows $\{\phi_k\}_{k=0}^m$ in backward time. An example of such a physically unrealizable "trajectory" is illustrated in Fig. 4.4 by $\phi_{\eta_r}^{\omega_r}(t,(v_b,\dot{v}_b))$, which first flows forward in time via the extended vector field $F_{\{1\}}$ past the constraint surface $\{a_2(q)=0\}$ until constraint 1 deactivates and then flows backwards in time until constraint 2 activates, ultimately terminating in $TA_{\{2\}}$.

With $\mathcal{F} = \bigcap \{\mathcal{F}_\omega^\eta : \omega \in \Omega, \eta \in H(\omega)\} \subset [0,\infty)\times TQ$, for any $(u,(q,\dot{q})) \in \mathcal{F} \cap ([0,\infty) \times TA)$ with contact mode sequence $\omega \in \Omega$ and constraint sequence $\eta \in H(\omega)$, the trajectory outcome is obtained by applying ϕ_ω^η to $(u,(q,\dot{q}))$, i.e. $\phi(u,(q,\dot{q})) = \phi_\omega^\eta(u,(q,\dot{q}))$. See Fig. 4.4 for an illustration of trajectories with different contact mode sequences.

The maps φ_ℓ, Γ_ℓ, and ϕ_ω^η are C^r on their domains since they are each obtained from a finite composition of C^r functions. Therefore the restriction[23] $\phi|_{[0,\infty)\times\Sigma}$ is a continuous selection of the finite collection of C^r functions

$$\{\phi_\omega^\eta : \omega \in \Omega, \eta \in H(\omega)\}$$

on the open neighborhood $\mathcal{F} \subset TQ$ containing $(t,(p,\dot{p}))$, i.e. $\phi|_{[0,\infty)\times\Sigma}$ is piecewise–C^r at $(t,(p,\dot{p}))$. See Fig. 4.1 for an illustration the piecewise–differentiability of trajectory outcomes arising from a transition between contact mode sequences.

As the composition of a finite number of piecewise–differentiable functions is piecewise–differentiable [96, Thm. 3.1.1], the above result can clearly be extended to include any finite

[23] As a technical aside, we remark that the domain of ϕ is confined to $[0,\infty) \times TA$, whence invoking the definition of piecewise–differentiability requires a continuous extension $\widetilde{\phi}$ of ϕ defined on a neighborhood of $(t,(p,\dot{p}))$ that is open relative to $[0,\infty) \times TQ$. One such extension is obtained by composing ϕ with a sufficiently differentiable retraction [59, Chp. 6] of TQ onto TA (such a retraction is guaranteed to exist locally by transversality of constraint surfaces).

set of (de)activation times $\{t_i | t_i \in (0,t)\}$. □

REMARK 27 (SATISFYING THEOREM 3 HYPOTHESES). *Models of animal or robot behaviors involving intermittent contact with terrain—walking, running, climbing, leaping, dancing, juggling, grasping—generally satisfy our hypotheses, so long as they possess sufficient compliance as in Fig. 4.5 (middle and right).*

REMARK 28 (RELAXING THEOREM 3 HYPOTHESES). *Since the class of piecewise–differentiable functions is closed under finite composition, conditions (i) and (ii) in the preceding Theorem can be readily relaxed to accommodate a finite number of constraint activation/deactivation times in the interval* $(0,t)$. *Conditions (iii) and (iv) are more difficult to relax since there are systems wherein trajectories initialized arbitrarily close to an admissible trajectory fail to be admissible themselves. As a familiar example, consider a 1 degree–of–freedom elastic impact oscillator [42, Chp. 2.4] (i.e. a bouncing ball): the stationary trajectory (initialized with* $q, \dot{q} = 0$*) is admissible for all time, but all nearby trajectories (initialized with* $q \neq 0$ *or* $\dot{q} \neq 0$*) exhibit the Zeno phenomenon. We will discuss further possible extensions in section 4.6*

Under the hypotheses of the preceding Theorem, the continuous flow ϕ is piecewise–differentiable at a point $(t,(p,\dot{p})) \in [0,\infty) \times TA$, that is, near $(t,(p,\dot{p}))$ the graph of ϕ is has an open covering by the graphs of a finite collection
$\{\phi^{\eta}_{\omega} : \omega \in \Omega, \eta \in H(\omega)\}$ of differentiable functions (termed selection functions). This implies in particular that there exists a continuous and piecewise–linear function

$$D\phi(t,(p,\dot{p})) : T_{(t,(p,\dot{p}))}\left([0,\infty) \times TA\right) \to T_{\phi(t,(p,\dot{p}))}A \tag{4.28}$$

(termed the Bouligand or B–derivative) that provides a first–order approximation for how trajectory outcomes vary with respect to initial conditions. Formally, for all $(u,(v,\dot{v})) \in T_{(t,(p,\dot{p}))}\left([0,\infty) \times TA\right)$, the vector $D\phi(t,(p,\dot{p});u,(v,\dot{v})) \in \mathbb{R}^{2d}$ is the directional derivative of $\phi(t,(p,\dot{p}))$ in the $(u,(v,\dot{v}))$ direction:

$$\lim_{\alpha \downarrow 0} \frac{1}{\alpha}\left[(\phi(t+\alpha u,(p+\alpha v,\dot{p}+\alpha\dot{v})) - \phi(t,(p,\dot{p}))) - \ D\phi(t,(p,\dot{p});u,(v,\dot{v}))\right] = 0. \tag{4.29}$$

Furthermore, this directional derivative is contained within the collection of directional derivatives of the selection functions. Formally, for all $(u,(v,\dot{v})) \in T_{(t,(p,\dot{p}))}\left([0,\infty)\times TA\right)$,

$$D\phi(t,(p,\dot{p});u,(v,\dot{v})) \in \left\{D\phi^{\eta}_{\omega}(t,(p,\dot{p});u,(v,\dot{v})) : \omega\in\Omega, \eta\in H(\omega)\right\}. \tag{4.30}$$

The selection functions are classically differentiable, hence their directional derivatives can be computed via matrix–vector multiplication between a classical (Jacobian/Fréchet) derivative matrix and the perturbation vector. Formally, for all $(u,(v,\dot{v})) \in T_{(t,(p,\dot{p}))}\left([0,\infty)\times TA\right)$ and corresponding $\omega\in\Omega$, $\eta\in H(\omega)$,

$$D\phi^{\eta}_{\omega}(t,(p,\dot{p});u,(v,\dot{v})) = D\phi^{\eta}_{\omega}(t,(p,\dot{p}))\begin{bmatrix} u \\ v \\ \dot{v}\end{bmatrix}, \tag{4.31}$$

where $D\phi^{\eta}_{\omega}(t,(p,\dot{p}))\in\mathbb{R}^{(2d)\times(1+2d)}$ is the classical derivative of the selection function ϕ^{η}_{ω}. The matrix $D\phi^{\eta}_{\omega}(t,(p,\dot{p}))$ can be obtained by applying the (classical) chain rule to the definition of ϕ^{η}_{ω} from (4.26).

Remark 29 (Calculating $D\phi(t,(p,\dot{p};u,(v,\dot{v})))$. *We will assume that for a given $(u,(v,\dot{v}))$, the corresponding constraint (de)activation and mode sequences is known, corresponding to η and ω in the proof of theorem 3 (piecewise differentiability with differing contact mode sequences).*[24] *As the component of the derivative with respect to time is the underlying vector field at $\phi(t,(p,\dot{p}))$, we will only discuss the calculation of $D_{(q,\dot{q})}\phi(t,(p,\dot{p});u,(v,\dot{v}))$. In particular, as the derivate of the flow away from constraint (de)activation is well studied (see [44, §7.2] for calculating the variational equation of a continuous flow), we will calculate the jump update, or* saltation *matrix, of the variational equation at points of admissible contact (de)activation.*

For the given $(u,(v,\dot{v}))$ and the corresponding η and ω,

$$D_{(q,\dot{q})}\phi(t,(p,\dot{p});(v,\dot{v})) = D_{(q,\dot{q})}\phi^{\eta}_{\omega}(t,(p,\dot{p}))\begin{bmatrix} v \\ \dot{v}\end{bmatrix} \tag{4.32}$$

[24] It is nontrivial to to determine η,ω from $u,(v,\dot{v})$ and to the best of the authors' knowledge, existing literature does not contain a closed form solution.

Without loss of generality, assume m simultaneous constraint (de)activations occur at time $s \in (0,t)$ and no other constraint (de)activations occur.

$$\begin{aligned}\phi_\omega^\eta(t,(p,\dot{p})) &= \phi \circ \prod_{\ell=0}^{m-1} \left(\Gamma_{\eta(\ell+1)} \circ \varphi_{\omega(\ell)}\right) \circ (t-s, \phi(s,(p,\dot{p}))) \\ &= \phi \circ \prod_{\ell=0}^{m-1} \left(\Gamma_{\eta(\ell+1)} \circ \varphi_{\omega(\ell)}\right) \circ \left(t-s, (\rho,\dot{\rho}^-)\right),\end{aligned} \tag{4.33}$$

with $(\rho,\dot{\rho}^-) = \lim_{t\uparrow s} \phi(t,(p,\dot{qp}))$, Γ_J eq. (4.24) is the impact map into mode J eq. (4.6b), $\varphi_{\omega(\ell)}$ eq. (4.22) is flowing in mode $\omega(\ell)$ until the next $\ell+1$ constraint (de)activation occurs. The calculation of $D\phi_\omega^\eta$ then follows from the chain rule

$$D\phi_\omega^\eta = D\phi(t-s,(\rho,\dot{\rho}^+)) \prod_{\ell=0}^{m-1} \left(D\Gamma_{\omega(\ell+1)} D\varphi_{\omega(\ell)}\right)(s,(\rho,\dot{\rho}^-)) D\phi(s,(p,\dot{p})), \tag{4.34}$$

where $D\Gamma$ is given in eq. (4.25) and $D\varphi$ in eq. (4.23). Let $\Xi_\omega^\eta \colon \mathbb{R} \times TQ \to \mathbb{R}^{2d}$ be given with[25]

$$\Xi_\omega^\eta = \prod_{\ell=0}^{m-1} \Xi_{\omega(\ell)}^{\eta(\ell)} = \prod_{\ell=0}^{m-1} D\Gamma_{\omega(\ell+1)} D\varphi_\ell. \tag{4.35}$$

Next, we will show the equivalence of Ξ_ω^η with the more common form of the saltation matrix S for the jump update to the variational equation on the state alone when only one constraint undergoes activation.[26] *With F^+ denoting the vector field immediately post constraint activation, F^- the vector field immediately prior to constraint, $g = D_{(q,\dot{q})}(a_i \circ \Pi_Q)$ and $R_i \colon TQ \to TQ$ denoting the reset of the state due to the activation of constraint i being defined with*

$$R_i(q,\dot{q}) = (q, \Delta_{\{i\}}(q,\dot{q})\dot{q}), \tag{4.36}$$

---

[25] We denote this jump matrix update to the variational equation of Ξ for consistency with [26].

[26] When a constraint undergoes deactivation, the underlying vector field is continuous, hence the corresponding $\Xi_{\omega(\ell)}^{\eta(\ell)} = I$.

$$
\begin{aligned}
S_i &= \begin{bmatrix} F^+ & I_{2d} \end{bmatrix} D\Gamma D\varphi \begin{bmatrix} 0 \\ I_{2d} \end{bmatrix} \\
&= \begin{bmatrix} F^+ & I_{2d} \end{bmatrix} \begin{bmatrix} 1 & 0 \\ 0 & DR \end{bmatrix} \begin{bmatrix} 1 & \frac{1}{gF^-}g \\ 0 & DR - \frac{1}{gF^-}F^-g \end{bmatrix} \begin{bmatrix} 0 \\ I_{2d} \end{bmatrix} \\
&= DR + \frac{1}{gF^-}\left(F^+ - DRF^-\right)g,
\end{aligned} \tag{4.37}
$$

which matches [49, (1.5)] and [94, (27)] for autonomous mode transitions.[27] *Clearly, for multiple simultaneous constraint (de)activations for a given mode sequence* ω *and constraint (de)activation sequence* η*,*

$$
S_\omega^\eta = \prod_{\ell=0}^{m-1} S_{\omega(\ell)}^{\eta(\ell+1)}. \tag{4.38}
$$

Then

$$
D_{(q,\dot{q})}\phi(t,(p,\dot{p});(v,\dot{v})) = D_{(q,\dot{q})}\phi(t-s,(\rho,\dot{\rho}^+))S_\omega^\eta(\rho,\dot{\rho}^-)D_{(q,\dot{q})}\phi(s,(p,\dot{p}))\begin{bmatrix} v \\ \dot{v} \end{bmatrix}. \tag{4.39}
$$

4.4.2 At least once (classically) differentiable

Under Assumptions 2 to 4 from section 4.3, previous work has shown that, when the contact mode sequence is fixed, trajectory outcomes vary continuously [10, Thm. 20] and differentiably [2] with respect to variations in initial conditions (i.e. initial states and parameters). This enables the use of scalable algorithms for optimal control [86] and reinforcement learning [102] to improve the performance of a given behavior (corresponding to the fixed contact mode sequence) using gradient descent. However, these algorithms cannot be relied upon to select among different behaviors (corresponding to different contact mode sequences) since trajectory outcomes are known to depend nonsmoothly on initial conditions theorem 3 (piecewise differentiability with differing contact mode sequences). In this section we report that Assumption 5 yields classically differentiable trajectory outcomes *even as the contact mode sequence varies*, enabling the use of scalable algorithms to select behaviors.

---

[27] In both the cited examples the reset map R is not directly written, instead using the notion that the reset is the initial state plus the change in state [49, (1.4)] or [94, (13)]. In the notation of [94], $R = I + \Delta$.

To show the flow is at least once differentiable, we introduce an assumption such that all components of the piecewise–derivative are equal.

Assumption 5 (Commuting saltation matrices).

$$\begin{aligned} &\forall i, j \in \{1, \ldots, n\}\,,\ i \neq j, q \in a_i^{-1}(0) \cap a_j^{-1}(0) : \\ &\quad \forall \dot{q} \in \{\dot{q} | Da_i(q)\dot{q} < 0\} \cap \{\dot{q} | Da_j(q)\dot{q} < 0\} : \\ &\quad S^j_{\{i\}}(q, \Delta_{\{i\}}(q, \dot{q})\dot{q}) S^i(q, \dot{q}) = S^i_{\{j\}}(q, \Delta_{\{j\}}(q, \dot{q})\dot{q}) S^j(q, \dot{q}), \end{aligned} \tag{4.40}$$

where S^i, S^j are defined in eq. (4.37).

Remark 30 (Limbs decoupled through the body). *While Assumption 5 has minimal mechanical motivation,*[28] *a weaker condition with more mechanical intuition while also yielding at least once C^1 flow is* limbs decoupled through the body *[83]. Broadly speaking, limbs decoupled through the body requires any two unilateral constraints (limbs) that undergo simultaneous activation must be intertially decoupled. This assumption is strictly stronger than Assumption 2 (orthogonal constraints). See section 4.6.3 for a further discussion of decoupled limbs.*

Remark 31 (Structure of saltation matrix S). *Given Assumption 2 (orthogonal constraints) and unilateral constraints only dependent upon positions eq.* (4.1)*, the structure of a saltation matrix S^i eq.* (4.37) *for corresponding to admissible activation for constraint i is*

$$S^i(q, \dot{q}) = \begin{bmatrix} A_i & 0 \\ B_i & C_i \end{bmatrix}, \tag{4.41}$$

where $A_i, B_i, C_i \in \mathbb{R}^{d \times d}$ and 0 is the 0 matrix.

The following is a collection of facts related to the structure of the saltation matrix with R_i as defined in eq. (4.36).

[28] It is possible to provide a set of equations which are equivalent to eq. (4.40), but those equations provide neither mechanical motivation nor elegance and only distract from the underlying idea; when the saltation matrices pairwise commute, the flow is at least C^1.

1. *Following from the chain rule and Assumption 2 (orthogonal constraints), the reset maps commute* $R_i \circ R_j = R_j \circ R_i$ *and hence*

$$DR_i(R_j(q,\dot{q}))DR_j(q,\dot{q}) = DR_j(R_i(q,\dot{q}))DR_i(q,\dot{q}). \tag{4.42}$$

2. *As coefficient of restitution only depends upon configuration,* $D_{\dot{q}}(\Delta_i(q,\dot{q})\dot{q}) = \Delta_i(q)$ *and* $C_i = \Delta_i(q)$*. Hence, for two different constraint activations* i, j *and* $i \neq j$*,* $C_iC_j = C_jC_i$*.*

3. *It can be shown,* $A_iA_j = A_jA_i$*.*

4. *If* $D_q(\Delta_i(q,\dot{q})) = 0$*, e.g. when the mass matrix is configuration independent, the determination of whether the saltation matrices commute depends on how forces change when the velocity jumps. See section 4.5.1 for an example system with constant mass matrix and non-commuting saltation matrices.*

Example 1 (Specification of $H(\omega)$ for a simple system). *Let the example system consist of* $m \in \mathbb{N}^+$ *independent bean bags and a ceiling constraint. Assume all bean bags hit their corresponding ceiling constraint at the same time, then* $\Omega = \{(\omega\colon (0,\ldots,m) = \emptyset) | m \in \{1,\ldots,n\}\}$*. In this example, the various orderings will be due to* η*. Then* $|H(\omega)| = m!$ *with two examples of the impact sequence being* $\eta_1, \eta_2\colon (1,\ldots,n) \to (1,\ldots,n)$*,*

$$\eta_1(i) = i \tag{4.43}$$

$$\eta_2(i) = n + 1 - i. \tag{4.44}$$

Theorem 4 (At least once (classically) differentiable with differing contact mode sequences). *Under Assumption 3 (existence and uniqueness of flow), Assumption 4 (*C^r *vector field and reset map), Assumption 2 (orthogonal constraints), Assumption 5 (commuting saltation matrices), with* $\phi\colon [0,\infty) \times TA \to TA$ *denoting the flow, if* $t \in [0,\infty)$*,* $(p,\dot{p}) \in TA \subset TQ$*, and* $\Sigma \subset TQ$ *is a* C^r *embedded submanifold containing* $(p,\dot{p})$ *such that*

(i) the trajectory $\phi^{(p,\dot{p})}$ *activates and/or deactivates constraints at a finite set of times* $\{t_i | t_i \in (0,t)\}$*,*

(ii) $\phi^{(p,\dot{p})}$ *has no other activation or deactivation times in* $[0,t]$*,*

(iii) trajectories initialized in $\Sigma \cap TA$ *are admissible on* $[0,t]$*, and*

(iv) the set Ω *of contact mode sequences for trajectories initialized in* $\Sigma \cap TA$ *is finite,*

then the restriction $\phi|_{[0,\infty)\times\Sigma}$ *is at least* C^1 *at* $(t,(p,\dot{p}))$*.*

Proof. We begin by stating that from theorem 3 (piecewise differentiability with differing contact mode sequences), ϕ is piecewise–differentiable at $(t,(q,\dot{q}))$. We will show $D\phi(t,(q,\dot{q});u,(v,\dot{v}))$ is a linear function of $(u,(v,\dot{v}))$. It will then follow that $D\phi(t,(q,\dot{q}))$ exists and is the classical derivative [96, § 3.1], proving the theorem. We first show the result when there is only one time instant $s \in (0,t)$ when constraints activate and/or deactivate. Let $(\rho,\dot{\rho}^-) = \phi(s,(q,\dot{q}))$, that is the impact configuration and the pre-impact velocity.

We next demonstrate that showing all possible state saltation matrices S are identical is equivalent to showing $D\phi(t,(q,\dot{q});(u,(v,\dot{v}))$ is linear as a function of $(u,(v,\dot{v}))$. $D\phi(t,(q,\dot{q};\cdot))$ is composed of two components: $D_t\phi(t,(q,\dot{q});\cdot)$; the derivative with respect to time, and $D_{(q,\dot{q})}\phi(t,(q,\dot{q});\cdot)$; the derivative with respect to state. As discussed in Remark 29, $D_t\phi$ is the underlying vector field at $\phi(t,(q,\dot{q}))$; hence independent of $(u,(v,\dot{v}))$. From eq. (4.39),

$$D_{(q,\dot{q})}\phi(t,(q,\dot{q});(v,\dot{v})) = D_{(q,\dot{q})}\phi(t-s,(\rho,\dot{\rho}^+))S^\eta_\omega(\rho,\dot{\rho}^-)D_{(q,\dot{q})}\phi(s,(q,\dot{q}))\begin{bmatrix} v \\ \dot{v} \end{bmatrix}, \tag{4.45}$$

where η,ω depend on $(v,\dot{v})$. Hence, showing $D\phi(t,(q,\dot{q};\cdot)$ is a linear function is equivalent to showing $S^\eta_\omega(\rho,\dot{\rho}^-) = S^{\eta'}_{\omega'}(\rho,\dot{\rho}^-)$ for all $\omega,\omega' \in \Omega$ and $\eta \in H(\omega), \eta' \in H(\omega')$.

We next show all the state saltation matrices are identical. Without loss of generality, assume all constraints are undergoing activation (not excluding dependent deactivations). Let m be the number of constraints undergoing activation Assume $|\omega| = |\omega'| = m$ or equivalently assume both perturbations undergo m distinct constraint activations.[29] Then by Assumption 5 (commuting saltation matrices), $S^\eta_\omega = S^{\eta'}_{\omega'}$, and $D\phi(t,(q,\dot{q}))$ exists.

[29]This assumption does not loose cause a loss of generality, as clearly if $\|omega\| < m$ simultaneous constraint activations occur and hence this theorem can be applied to those perturbation directions.

As the composition of a finite number of differentiable functions is differentiable [59, Cor. C.11], the above result can clearly be extended to include any finite set of (de)activation times $\{t_i | t_i \in (0,t)\}$. □

Example 2 (Simultaneous activation/deactivation of two different constraints). *Let* $(q, \dot{q}^-) \in TA_{\{1\}}$ *and at* $t = \tau$ *constraint* 2 *activates and constraint* 1 *deactivates. Assume constraints* 1 *and* 2 *are orthogonal. Then two of the word sequences are* $\{1\} \to \{1,2\} \to \{2\}$ *and* $\{1\} \to \emptyset \to \{2\}$.

For the flow to be continuous, the post impact velocity must be the same regardless of the word, i.e.

$$\dot{q}^+ = \Delta_{\{2\}}\Delta_{\{1,2\}}\dot{q}^- = \Delta_{\{2\}}\Delta_{\emptyset}\dot{q}^-$$

Given $(q, \dot{q}^-) \in TA_{\{1\}}$,

$$\Delta_{\{1,2\}}\dot{q}^- = \Delta_{\{2\}}\dot{q}^-$$

completing the example, as from orthogonality of constraints $\Delta_{\{1,2\}} = \Delta_{\{2\}}\Delta_{\{1\}}$.

4.5 Applications

We demonstrate the applicability of results from section 4.4 on two example systems. Section 4.5.1 provides variations of biped-like system with a constant mass matrix. The system variations demonstrate discontinuous flow, piecewise–differentiable flow, and classically differentiable flow about a trajectory undergoing simultaneous impacts. Section 4.5.2 generates a nonsmooth control law using the knowledge a piecewise–differentiable system has an implicit function. In this subsection, the example system is a double pendulum with two joint stops.

4.5.1 Demonstration of various types of flow occurring at simultaneous impact for a simple system

Our initial system is a crude approximation of a biped with two unilateral constraints as the left and right feet, blue and red dots, respectively, in Fig. 4.5(top). For this system we detail three variations, the discontinuous model, the piecewise–differentiable model, and the classically differentiable case. Fig. 4.5 gives a visualization of each system variation and a slice of the flow demonstrating the modes respective properties. In the following sections, we provide a detailed description of each of the system variations.

Rigid biped: An example of discontinuous flow

For ease of notation, we will model the system shown in Fig. 4.5(top left) using bilateral constraints and not generalized coordinates. As discussed in section 4.6.10, bilateral constraints can be incorporated into the general results. The legs, excluding the feet, are assumed to be perfectly rigid and massless. Additional parameters used in the generation of Fig. 4.5 are given in table 4.1.

The configuration parameters of the rigid biped are

$$q = \begin{bmatrix} x_b & x_l & x_r & z_b & z_l & z_r & \theta \end{bmatrix}, \tag{4.46}$$

and the equivalent location on the piecewise–differentiable biped are depicting in Fig. 4.1. The mass matrix is

$$M(q) = \operatorname{diag}\left(m_b, m_f, m_f, m_b, m_f, m_f, I_b\right), \tag{4.47}$$

where both the feet have the same mass m_f. We will assume the system undergoes perfectly plastic collisions, i.e. $\gamma(q) = 0$ for all $q \in Q$. For convenience, we will introduce the following variables:

- w, half the width of the body,
- ℓ, the leg length from the foot to the body,

- d, the distance from the center of the body (x_b, z_b) to either the right (x_r, z_r) or left (x_l, z_l) foot, $d = \sqrt{\ell^2 + w^2})$,
- ϕ_r the angle from the center of the body to the right foot $\phi_r = \cos^{-1}(w/d)$, and
- ϕ_l the angle from the center of the body to the left foot $\phi_l = \cos^{-1}(-w/d)$.

Annotation of w and ℓ are given in Fig. 4.1.

For the rigid biped, there are two sets of constraints, unilateral and bilateral. The two unilateral constraints require the two feet remain above the ground,

$$a_1(q) = z_l \geq 0, \tag{4.48a}$$

$$a_2(q) = z_r \geq 0. \tag{4.48b}$$

For ease of notation, we denote the bilateral constraints with the symbol a_i, for $i \notin \{1, 2\}$. The first two bilateral constraints a_3 and a_4 require the right foot and the center of the body remaining a fixed distance apart,

$$a_3(q) = z_b + d\cos(\phi_r + \theta) - z_r = 0 \tag{4.49a}$$

$$a_4(q) = x_b + d\sin(\phi_r + \theta) - x_r = 0. \tag{4.49b}$$

Likewise, bilateral constraints a_5 and a_6 require the left foot and the center of the body remain a fixed distance apart,

$$a_5(q) = z_b + d\cos(\phi_l + \theta) - z_l = 0, \tag{4.50a}$$

$$a_6(q) = x_b + d\sin(\phi_l + \theta) - x_l = 0. \tag{4.50b}$$

As outlined in section 4.6.10, for a system with bilateral and unilateral constraints, eq. (4.61) must be satisfied for all pairwise sets of constraints. The rigid biped does not have orthogonal constraints as for any $q \in Q$,

$$\begin{aligned} Da_1(q)^T M^{-1}(q) Da_3(q) &= -1/m_f \neq 0 \text{ and} \\ Da_2(q)^T M^{-1}(q) Da_5(q) &= -1/m_f \neq 0. \end{aligned} \tag{4.51}$$

The only applied force on the rigid biped comes from gravity $g \in \mathbb{R}$,

$$f(q, \dot{q}) = \begin{bmatrix} 0 & 0 & 0 & -m_b g & -m_l g & -m_r g & 0 \end{bmatrix}, \tag{4.52}$$

with $g > 0$. As bilateral constraints are always considered *active*, the set of possible modes is given with

$$J = \begin{cases} \{3,4,5,6\} & a_1(q) > 0 \text{ and } a_2(q) > 0 \\ \{1,3,4,5,6\} & a_1(q) = 0 \text{ and } a_2(q) > 0 \\ \{2,3,4,5,6\} & a_1(q) > 0 \text{ and } a_2(q) = 0 \\ \{1,2,3,4,5,6\} & a_1(q) = 0 \text{ and } a_2(q) = 0 \end{cases} \tag{4.53}$$

The continuous dynamics for the rigid biped are then given with eq. (4.6a). As a result of the constraints not being orthogonal, eq. (4.6b) cannot be used. Instead, the reset law follows from the rocking block [67, §II.E].

Biped with actuation: An example of PC^r flow

The biped with actuation is depicted in Fig. 4.5(top center), where the gray circle denotes an attached flywheel actuator and as opposed to the rigid legs of section 4.5.1, the legs are now massless spring. The state, mass matrix, and unilateral constraints remain the same as in section 4.5.1. As the rigid, massless legs are replaced with massless linear springs, there are no bilateral constraints. The two unilateral constraints a_1 and a_2 are clearly orthogonal with respect to the inverse of the mass matrix eq. (4.47).

Before we define the effort map f for the actuated biped, we define two convenience functions, $L_r, L_l \colon Q \to \mathbb{R}$, the length of the right and left limbs, respectively.

$$\begin{aligned} L_r(q) &= \sqrt{\left(x_r - (x_b + w\cos\theta)\right)^2 + \left(z_r - (z_b + w\sin\theta)\right)^2}, \\ L_l(q) &= \sqrt{\left(x_l - (x_b - w\cos\theta)\right)^2 + \left(z_l - (z_b - w\sin\theta)\right)^2}. \end{aligned} \tag{4.54}$$

The effort map $f\colon TQ \to \mathbb{R}^d$ is then

$$\begin{aligned} f(q,\dot{q}) = &\begin{bmatrix} 0 & 0 & 0 & -m_b g & -m_l g & -m_r g & 0 \end{bmatrix} && \text{force from gravity} \\ &+ \kappa(L_l(q) - \ell) D_q(L_l)(q) + \kappa(L_r(q) - \ell) D_q(L_r)(q) && \text{force from springs} \\ &+ \begin{bmatrix} 0 & 0 & 0 & 0 & 0 & 0 & \beta(\dot{z}_l - \dot{z}_r)^2 \end{bmatrix} && \text{force from actuator,} \end{aligned} \tag{4.55}$$

where ℓ is the nominal length of the spring, κ is the spring constants, and β is a constant parameter.

While the actuated biped meets Assumption 2 (orthogonal constraints), it does not meet Assumption 5 (commuting saltation matrices). Clearly it can be shown the two state saltation matrices do not commute and additional the cause is the force from the actuator. Hence, the assumption for theorem 3 (piecewise differentiability with differing contact mode sequences) are meet but not for theorem 4 (at least once classically differentaible with differeing contact mode sequence).[31]

Springy biped: An example of classically differentiable flow

The springy biped is depicted in Fig. 4.5(top right). The dynamics for this variation are similar to that of the actuated biped in section 4.5.1 with the exception the effort map differs. The effort map f changes to

$$\begin{aligned} f(q,\dot{q}) = &\begin{bmatrix} 0 & 0 & 0 & -m_b g & -m_l g & -m_r g & 0 \end{bmatrix} && \text{force from gravity} \\ &+ \kappa(L_l(q) - L) D_q(L_l)(q) + \kappa(L_r(q) - R) D_q(L_r)(q) && \text{force from springs.} \end{aligned} \tag{4.56}$$

to mimic the removal of the massless actuated flywheel. As the mass matrix and the unilateral constraints do not change, the unilateral constraints remain orthogonal. Additionally, it can be shown the conditions for Assumption 5 (commuting saltation matrices) are meet as the system now satisfies Remark 30 (limbs decoupled through the body).[32]

[31] To see the explicit calculation of the saltation matrices for the actuated biped, see `biped/salt_calc.py` in `https://github.com/apace2/20-mechanical-simultaneous-impact`.

[32] To see the explicit calculation of the saltation matrices for the actuated biped, see `biped/salt_calc.py` in `https://github.com/apace2/20-mechanical-simultaneous-impact`.

Table 4.1: Parameter values used in simulation to generate Fig. 4.5

Parameter	Description	Value
m_b, m_l, m_r	Mass of the body, left foot, and right foot (resp.)	1
I_b	body inertia	1
g	gravity	1
l, w	length of leg and half of the body width	$0.5, 0.25$
κ	leg spring constant	27
β	actuator parameter	1.5
T	Final time	1.4

4.5.2 Non-smooth control

In this section we seek to demonstrate the phenomenon of PC^r flow on a system with non-constant mass matrix which causes non-zero Coriolis forces. We will use the double pendulum with inelastic impacts as the basis for our example. First, we demonstrate the example system is PC^r and then we generate a nonsmooth control law controlling for a final state about a trajectory with simultaneous constraint activations.

Double pendulum and PC^r flow

For the double pendulum shown in Fig. 4.6a the configuration space is $Q = \mathbb{R}^2$ with configuration states being

$$q = \begin{bmatrix} \theta_1 & \theta_2 \end{bmatrix}^\top \tag{4.57}$$

The mass matrix for the system is given in [78, (4.10)]. The unilateral constraints are

$$\begin{aligned} a_1(q) &= \theta_1 \geq 0 \\ a_2(q) &= -\theta_2 + c \geq 0, \end{aligned} \tag{4.58}$$

[33]The code used to generate Fig. 4.6b can be found at `https://github.com/apace2/20-mechanical-simultaneous-impact` in `pendulum/PCr_plot.py`.

Table 4.2: Parameter values used in simulation to generate Fig. 4.6

Parameter	Description	Value
m_1, m_2	Mass of rod 1 and 2 (resp.)	1
l_1, l_2	Length of rod 1 and 2 (resp.)	$\frac{1}{2}, \frac{2}{7}$
γ	Coefficient of restitution	.3
$(\bar{\theta}_1, \bar{\theta}_2) = (\theta_1, \theta_2)(t = 0)$	Initial configuration	$(0.681, 1.29)$
$(\dot{\theta_1}, \dot{\theta_2})(t = 0)$	Initial velocity	$(-.992, 1.943)$
T	Final time	1.4

where $c \in \mathbb{R}$ is a carefully chosen[34] constant such that for the given choice of parameters in table 4.2, $Da_1(q)M^{-1}(q)Da_2^\top(q) = 0$ when both $a_1(q) = 0$ and $a_2(q) = 0$. It can be shown that with $b = m_2 l_1 l_2/2$ and $d = m_2 l_2^2/3 + m_2(l_1/2)^2$, with $c = \arccos(-d/b)$, $Da_1(q)^\top M^{-1}(q)Da_2(q) = 0$ when $q = \Big[0, c\Big]$.

For the sake of simplicity, the only forces on the system are Coriolis forces due to the choice of reference frame. That is, the effort map $f(q, \dot{q}) = 0$. The coefficient of restitution γ is 0.3. Due to the nature of elastic impacts, similar to the bouncing ball, whenever one constraint is activated the same constraint is deactivated due to condition eq. (4.11a), a contingent deactivation.

It can be shown[35] the described double pendulum does not satisfy Assumption 5 (commuting saltation matrices). Without explicitly calculating the necessary state saltation matrices, the configuration dependence of the mass matrix provides intuition the system may not be

[34] [98] goes into detail on designing mechanical systems such that unilateral constraints are orthogonal at points of simultaneous constraint activation.

[35] See `pendulum/DP_PCr_salt.py` in `https://github.com/apace2/20-mechanical-simultaneous-impact`. The saltation matrices in the referenced file are calculated for the two possible pairs of words and activation sequences

$$\begin{aligned} &\omega = \{\emptyset, \emptyset, \emptyset\} \\ &\eta_1 \colon \{0,1\} \to \{1,2\} \text{ with } \eta_1(0) = 1,\ \eta_1(1) = 0 \\ &\eta_2 \colon \{0,1\} \to \{1,2\} \text{ with } \eta_2(0) = 0,\ \eta_2(1) = 1. \end{aligned} \tag{4.59}$$

classically differentiable. In particular, $D_q\Delta_{\{i\}}(q) \neq 0$ for both $i = 1$ and $i = 2$ at point of simultaneous constraint activation and the lower left $d \times d$ submatrix of the saltation matrix is non-zero. See Fig. 4.6 for an example of the piecewise nature of the flow due to simultaneous constraint activation.

4.5.3 Nonsmooth Control law

One method to generate a control law for a differentiable system uses the implicit function theorem, see [63], which is another method of developing a deadbeat control law on a linear system. As implicit function theorem exists for PC^r functions [96, 4.2.1] a similar method can be used for the double pendulum.

The control parameter u is a constant torque applied to the shoulder joint as shown in Fig. 4.6a. As the system is underactuated, only one final state can be controlled using this method. For the sake of demonstration purposes, we will develop a control law to regulate final elbow angle at time T $\theta_2(T)$ with respect to the initial shoulder angle $\theta_1(0)$. We numerically calculate the control law for a range of θ_1 values about the nominal $theta_1$. The control law and the resulting final elbow $\theta_2(T)$ rotation using this control law is shown in section 4.5.3.

4.6 Discussion

While the results presented in this paper are most directly applicable to the study of locomotion and manipulation, we contend the potential of extending the results presented here to a broader class of hybrid systems. In [26], the existence of a piecewise–differentiable flow was shown to exist in nonsmooth vector fields commonly used to model neural networks and power distribution systems along with locomotion. theorem 3 (piecewise differentiability with differing contact mode sequences) extends this result for locomotion and manipulation to allow non-trivial state resets between domains and varying dimensions of the hybrid state

[36]The code used to generate this figure can be found at `https://github.com/apace2/20-mechanical-simultaneous-impact` in `pendulum/nonsmooth_controller.py`.

space. To the best of our knowledge, this is the first time a class of hybrid systems with non-trivial state resets has been shown to generate piecewise–differentiable flows. A similar proof technique may be useful to generalize the result to additional hybrid systems.

We conclude by discussing possible routes (or obstacles) to extending our results and implications.

4.6.1 Extending our results

The hypotheses used to state theorem 3 (piecewise differentiability with differing contact mode sequences) restrict either the systems or systems trajectories under consideration; we will discuss the latter before addressing the former.

Trajectories we termed admissible exhibit neither *grazing* nor *Zeno* phenomena. Since grazing generally entails constraint activation times that are not even Lipschitz continuous with respect to initial conditions, flow is not piecewise–C^r along grazing trajectories. This fact has been shown by others [28, Ex. 2.7], and is straightforward to see in an example. Indeed, consider the trajectory of a point mass moving vertically in a uniform gravitational field subject to a maximum height (i.e. ceiling) constraint. The grazing trajectory is a parabola; the time–to–activation function involves a square root of the initial position. Zeno trajectories, on the other hand, can exhibit differentiable trajectory outcomes following an accumulation of constraint activations (and, hence, deactivations); consider, for instance, the (stationary) outcome that follows the accumulation of impacts in a model of a bouncing ball with inelastic collisions [42, Chp. 2.4]. Thus we cannot at present draw any general conclusions regarding differentiability of the flow along Zeno trajectories, and speculate that it might be possible to recover piecewise–differentiability along such trajectories in the *completion* of the mechanical system [82, Sec. IV] after establishing continuity with respect to initial conditions in the intrinsic state–space metric [24, Sec. III].

The (so–called [10]) effort map f was not allowed to vary with the contact mode, while the dynamics in eq. (4.6) vary with the contact mode $J \subset \{1, \ldots, n\}$ due to intermittent activation of unilateral constraints $a_i(q) \geq 0, \forall i \in \{1, \ldots, n\}$. Contact–dependent effort can

easily introduce nonexistence or nonuniqueness. Indeed, this phenomenon was investigated thoroughly by Carathéodory and, later, Filippov [34, Chp. 1]. For a specific example of the potential challenges in allowing contact–dependent forcing, note that the introduction of simple friction models into mechanical systems subject to unilateral constraints is known to produce pathologies including nonexistence and nonuniqueness of trajectories [101]. To generalize the preceding results to allow the above phenomena, one would need to provide conditions ensuring that trajectories (i) exist uniquely, (ii) depend continuously on initial conditions, and (iii) admit differentiable selection functions along trajectories of interest.

Generalizing result to non–mechanical systems

Two key challenges need to be meet,

- the unilateral constraints must be *orthogonal* in some sense, to avoid the discontinuity challenge presented in section 4.3.3.

- Continuity must be guaranteed. To the best of our knowledge, orthogonal constraints are sufficient for continuity. [10, Thm. 20] is the only result the authors are aware of that proves continuity and it applies to mechanical systems

Including control inputs

We focused on autonomous dynamics in eq. (4.6); however, parameterized control inputs can be incorporated through a standard state augmentation technique in such a way that theorem 3 (piecewise differentiability with differing contact mode sequences) implies trajectory outcomes depend piecewise–differentiably on initial states and input parameters, even as the contact mode sequence varies.

Specifically, suppose eq. (4.6) is replaced with

$$M(q)\ddot{q} = \tilde{f}((q,\dot{q}),u) + c(q,\dot{q})\dot{q} + Da_J(q)^\top \tilde{\lambda}_J((q,\dot{q}),u), \tag{4.60a}$$

$$\dot{q}^+ = \widetilde{\Delta}_J((q,\dot{q}^-),u)\dot{q}^-, \tag{4.60b}$$

where $\tilde{f}: TQ \times U \to \mathbb{R}^d$ is an effort map that accepts a constant input parameter $u \in U = \mathbb{R}^m$, $\tilde{\lambda}_J: TQ \times U \to \mathbb{R}^{|J|}$ is the reaction force that results from applying effort $\tilde{f}(q, \dot{q}, u)$ in contact mode J, and $\widetilde{\Delta}_J: TQ \times U \to \mathbb{R}^d$ is a reset map that accepts input parameter u as well. We interpret the vector u as parameterizing an open– or closed–loop input to the system; once initialized, u remains constant.[37] It is possible to generalize the proof of theorem 3 (piecewise differentiability with differing contact mode sequences) to provide conditions under which there exists a continuous flow $\widetilde{\phi}: \widetilde{\mathcal{F}} \to TA$ for eq. (4.60) that is piecewise–differentiable with respect to initial conditions $(q, \dot{q}) \in TA$ and input parameters $u \in U$ over an open subset $\widetilde{\mathcal{F}} \subset [0, \infty) \times TA \times U$ containing $\{0\} \times TA \times U$.

4.6.2 Implications for optimization and learning

Optimization and learning algorithms have emerged in recent years as powerful tools for synthesis of dynamic and dexterous robot behaviors [55,56,64,72,103]. Since scalable algorithms leverage derivatives of trajectory outcomes, their applicability to the dynamics in eq. (4.6) has previously (i) been confined to a fixed contact mode sequence [72, 73] or (ii) relied on approximations or relaxations of the dynamics [55, 56, 103]. Neither of these approaches is entirely satisfying: (i) prevents the algorithm from automatically selecting the behavior (corresponding to the contact mode sequence) in addition to extremizing its performance; (ii) implies the model under consideration is no longer a mechanical system subject to unilateral constraints. The results we report in section 4.4 provide an analytical and computational framework within which derivative–based algorithms can be rigorously and directly applied to the dynamics of mechanical systems subject to unilateral constraints eq. (4.6) to select between permutations of constraint (de)activations. The issue of whether or not a contact needs to be activated still must be addressed. See section 4.6.4 for a discussion of difficulties associated with grazing, and hence varying the number of contacts between trajectories, is

[37] A control policy represented using a universal function approximator such as an artificial neural network [56,64] provides an example of a parameterized closed–loop input, while a control signal represented using a finite truncation of an expansion in a chosen basis [55,72] provides an example of a parameterized open-loop input.

difficult.

4.6.3 Decoupled limbs

Limbs decoupled through the body [83] meets the conditions imposed by Assumption 5 (commuting saltation matrices), and can be interpreted physically as asserting that robot segments that can undergo impact simultaneously (i.e. limbs) must be decoupled through another segment not undergoing impact (i.e. the body). Crucially, this condition is required to ensure trajectory outcomes vary continuously with respect to initial conditions [10, Thm. 20]; since continuity is a precondition for differentiability, this condition is equally necessary for the result reported in theorem 4 (at least once classically differentaible with differeing contact mode sequence). We note that this condition is violated by conventional robots constructed from rigid serial chains and non–backdrivable actuators [78]. In contrast, design methodologies that incorporate direct–drive actuators [48, 52] or series compliance [80, 99] tend to produce robotic limbs that are (approximately) decoupled.

4.6.4 Grazing contact

definition 5 (admissible constraint activation/deactivation) precludes *grazing* trajectories, i.e. those that activate constraints with zero constraint velocity, or deactivate constraints with zero instantaneous rate of change in contact force. The key technical challenge entailed by allowing constraint activation (resp. deactivation) we termed *inadmissible* lies in the fact that the time–to–activation (resp. time–to–deactivation) function is not differentiable. This fact has been shown by others [28, Ex. 2.7], and is straightforward to see in an example. Indeed, consider the trajectory of a point mass moving vertically in a uniform gravitational field subject to a maximum height (i.e. ceiling) constraint. The grazing trajectory is a parabola, whence the time–to–activation function involves a square root of the initial position.

4.6.5 Zeno phenomena

definition 5 (admissible constraint activation/deactivation) precludes *Zeno* trajectories, i.e. those that undergo an infinite number of constraint activations (hence, deactivations) in a finite time interval. The key technical challenge entailed by allowing Zeno lies in the fact that evaluating the flow requires composing an infinite number of flow–and–reset functions. Composing a finite number of smooth functions yields a smooth function, but the same is not generally true for infinite compositions. Thus although it is possible to show that the infinite composition results in a differentiable flow in simple examples like the *rocking block* [45] and *bouncing ball* [10, Sec. 6.1], we cannot at present draw any general conclusions regarding differentiability of the flow along Zeno trajectories.

4.6.6 Friction

Friction is a microscopic phenomenon that eludes first–principles understanding [38]. Phenomenological models of friction are macroscopic approximations; one popular model[38] posists a transition from *sticking* to *sliding* when the ratio of normal to tangential force drops below a parameterized threshold. The system's flow is discontinuous at this threshold, as some trajectories *slide* away from their *stuck* neighbors. Even if such transitions are avoided, the introduction of simple friction models into mechanical systems subject to unilateral constraints is known to produce pathologies including nonexistence and nonuniqueness of trajectories [101].

4.6.7 Non–Euclidean configuration spaces

We restricted the configuration space to $Q = \mathbb{R}^d$ starting in section 4.4.2 to simplify the exposition and lessen the notational overhead. Nevertheless, the preceding results apply to configuration spaces that are complete Riemannian manifolds.[39]

---

[38] Usually attributed to Coulomb, but also due to Antomons [38].

[39] Since the preceding results are not stated in coordinate–invariant terms, they are formally applicable only after passing to coordinates.

4.6.8 Contact–dependent effort

The dynamics in eq. (4.6) vary with the contact mode $J \subset \{1, \ldots, n\}$ due to intermittent activation of unilateral constraints $a_J(q) \geq 0$, but the (so–called [10]) effort map f was not allowed to vary with the contact mode. Contact–dependent effort can easily introduce nonexistence or nonuniqueness. Indeed, consider a planar system with $q \in \mathbb{R}^2$ undergoing plastic impact with the constraint surface specified by $a(q) = q_1$ subject to contact–dependent effort that satisfies $f_\emptyset(q) = (-1, +1)$ if $q_1 > 0$ and $f_{\{1\}}(q) = (+1, -1)$ if $q_1 = 0$. Every trajectory eventually activates the constraint. Once the constraint is active, the trajectory becomes ill–defined.

4.6.9 Massless limbs

To accommodate massless limbs, one must specify their unconstrained dynamics. If the unconstrained dynamics differ from the constrained dynamics, then in effect one has introduced contact–dependent effort, whence we refer to the preceding section. If the unconstrained dynamics do not differ from the constrained dynamics, then in effect one has introduced bilateral constraints the massless limbs must satisfy, whence we refer to the subsequent section. The constrained dynamics of massless limbs are derived in [21].

4.6.10 Bilateral constraints

The preceding results hold in the presence of bilateral (i.e. equality) constraints so long as they do not couple limbs. Formally, if the bilateral constraints $b(q) = 0$ are specified by a differentiable function $b : Q \to \mathbb{R}^m$, there must exist an assignment $\beta : \{1, \ldots, m\} \to \{1, \ldots, n\}$ such that for all bilateral constraints $k \in \{1, \ldots, m\}$, unilateral constraints $i, j \in \{1, \ldots, n\}$, $i \neq j$, and configurations $q \in b^{-1}(0) \cap a_i^{-1}(0) \cap a_j^{-1}(0)$:

$$\begin{aligned} \langle Da_i(q), Da_j(q) \rangle_{M^{-1}} &= 0, \\ \langle Db_{\beta(k)}(q), Da_i(q) \rangle_{M^{-1}} &= 0, \\ \langle Db_{\beta(k)}(q), Da_j(q) \rangle_{M^{-1}} &= 0. \end{aligned} \tag{4.61}$$

4.6.11 Non–autonomous dynamics

One may wish to allow the continuous and/or discrete dynamics in eq. (4.6) to vary with time or an external input. Some common cases can easily be handled. If the dynamics are time–varying, but time could be incorporated as a state variable so that the preceding assumptions hold for the augmented system determined by $\widetilde{q} = (t, q) \in \widetilde{Q} = \mathbb{R} \times Q$,

$$\widetilde{M}\left(\widetilde{q}\right) = \mathrm{diag}\left(1, M(q)\right), \ \widetilde{f}\left(\widetilde{q}, \dot{\widetilde{q}}\right) = (0, f(t, q, \dot{q})), \tag{4.62}$$

then the preceding results apply directly to the augmented system; a similar observation holds when the value of an external input is determined by time and state in such a way that the closed–loop system (possibly augmented as above to remove the time dependence) satisfied the preceding assumptions.

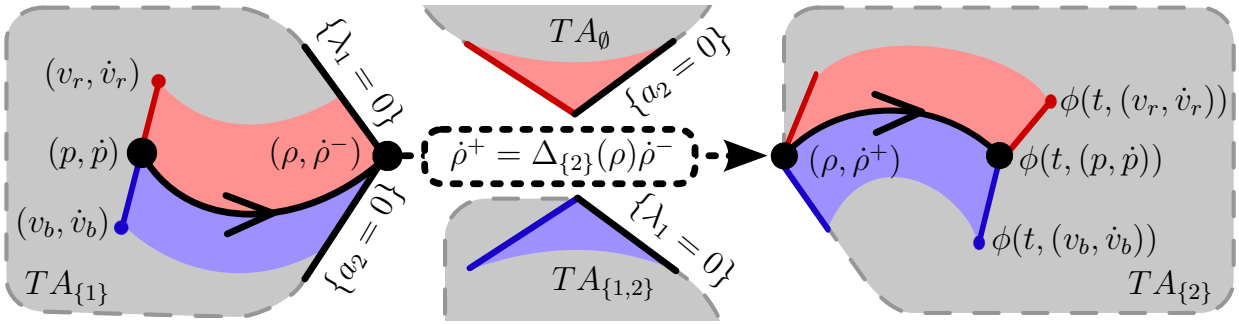

Figure 4.4: Illustration of trajectory undergoing simultaneous constraint activation and deactivation: the trajectory initialized at $(p, \dot{p}) \in TA_{\{1\}} \subset TQ$ flows via (4.6a) to a point $(\rho, \dot{\rho}^-) \in TA_{\{1\}}$ where both the constraint force λ_1 and constraint function a_2 are zero, instantaneously resets velocity via (4.6b) to $\dot{\rho}^+ = \Delta_{\{2\}}(\rho)\dot{\rho}^-$, then flows via (4.6a) to $\phi(t, (p, \dot{p})) \in TA_{\{2\}} \subset TQ$. Nearby trajectories undergo activation and deactivation at distinct times: trajectories initialized in the red region, e.g. $(v_r, \dot{v}_r)$, deactivate constraint 1 and flow through contact mode $TA_\emptyset$ before activating constraint 2—their contact mode sequence is $(\{1\}, \emptyset, \{2\})$—while trajectories initialized in the blue region, e.g. $(v_b, \dot{v}_b)$, activate 2 and flow through $TA_{\{1,2\}}$ before deactivating 1—their contact mode sequence is $(\{1\}, \{1,2\}, \{2\})$. Here, the constraint activation triggered a *plastic* impact wherein eq. (4.6b) resets the velocity normal to the activated constraint to zero; if the activation had instead been *elastic*, then the final contact mode would have been $TA_\emptyset$. Note that constraint activations generally reset the system state to the interior of a contact mode, whereas deactivations reset the system state to the boundary of a contact mode. Piecewise–differentiability of the trajectory outcome is illustrated by the fact that red outcomes lie along a different subspace than blue.

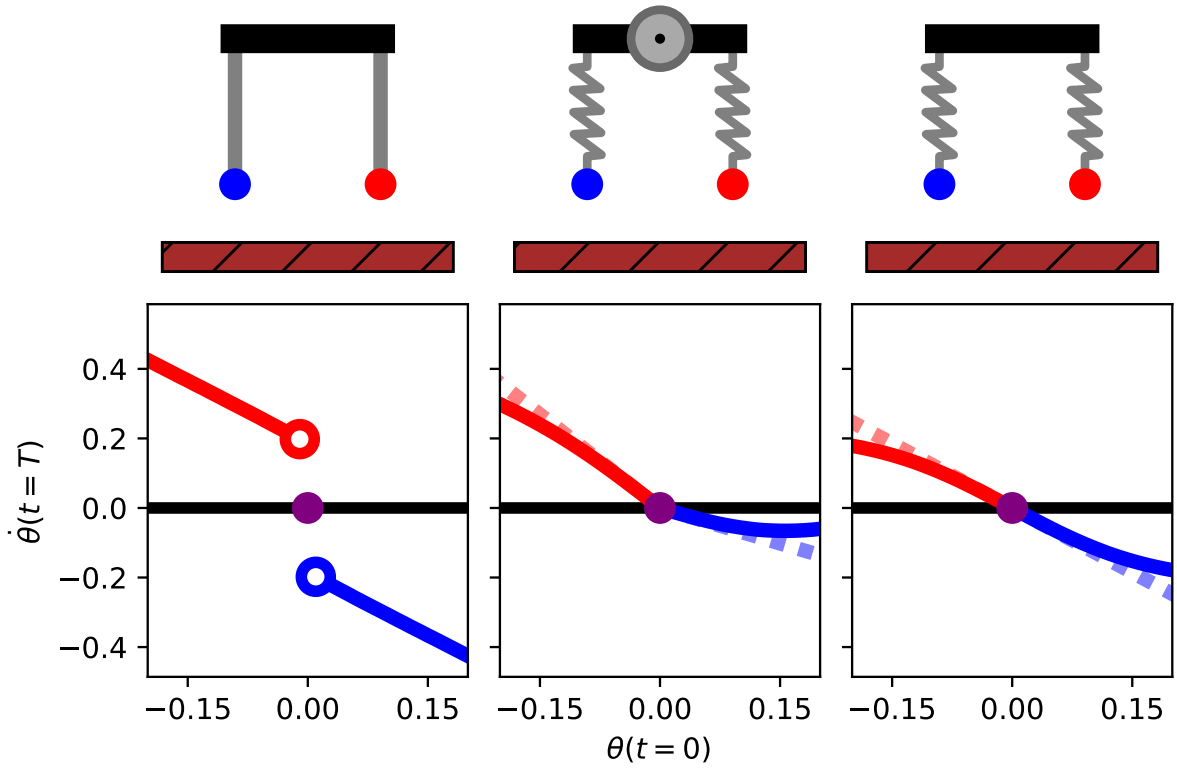

Figure 4.5: **Trajectory outcomes in mechanical systems subject to unilateral constraints.**[30](*top*) In general, trajectory outcomes depend discontinuously on initial conditions. In the pictured model for rigid–leg trotting (adapted from [87]), discontinuities arise when two legs touch down: if the legs impact simultaneously (corresponding to rotation $\theta(0) = 0$), then the post–impact rotational velocity is zero; if the left leg impacts before the right leg ($\theta(0) > 0$, blue) or vice–versa ($\theta(0) < 0$, red), then the post–impact rotational velocities are bounded away from zero. (*middle*) In the pictured model for soft–leg trotting (adapted from [26] with the addition of a nonlinear damper coupling the body and limbs), trajectory outcomes (solid lines) are continuous and piecewise–differentiable at $\theta(0) = 0$ (dashed lines). (*bottom*) When the system meets Assumption 5 (commuting saltation matrices), trajectory outcomes depend continuously and classically differentiably on initial conditions. In the pictured model for soft–leg trotting (adapted from [26]), trajectory outcomes (solid lines) are continuous and differentiable.

In each of the three cases, the entire biped is rotated by the initial body angle about the center of the body $(x_b, z_b)(t = 0) = (0, 1)$.

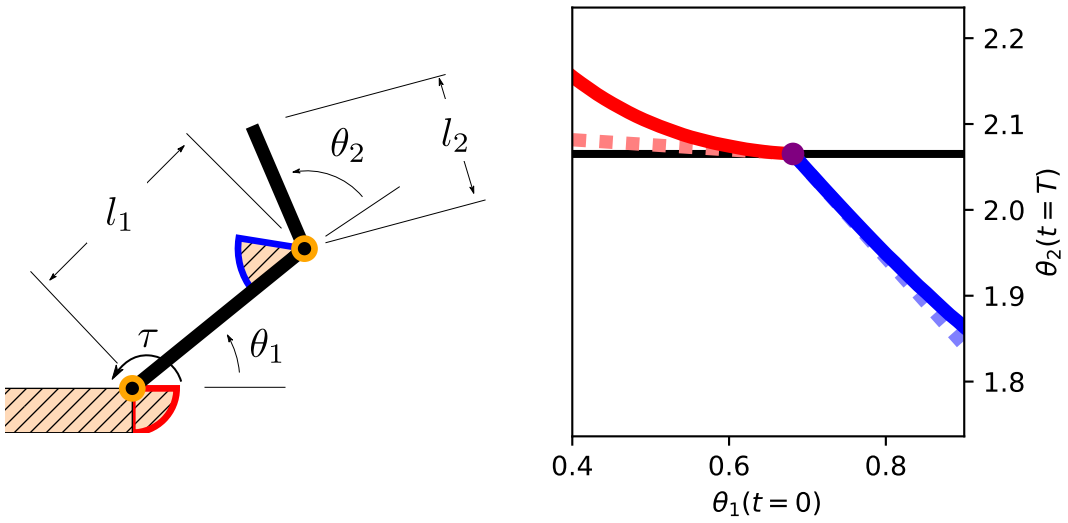

(a) Underactuated double pendulum with two stops.

(b) Piecewise dependence on initial condition. When the initial $\theta_1(t = 0) < \bar{\theta}_1$, the unilateral constraint a_1 undergoes impact before a_1. Vice versa when $\theta_1(t = 0) > \bar{\theta}_1$.

Figure 4.6: An example system a with configuration dependent mass matrix generating PC^r flow b.[33]

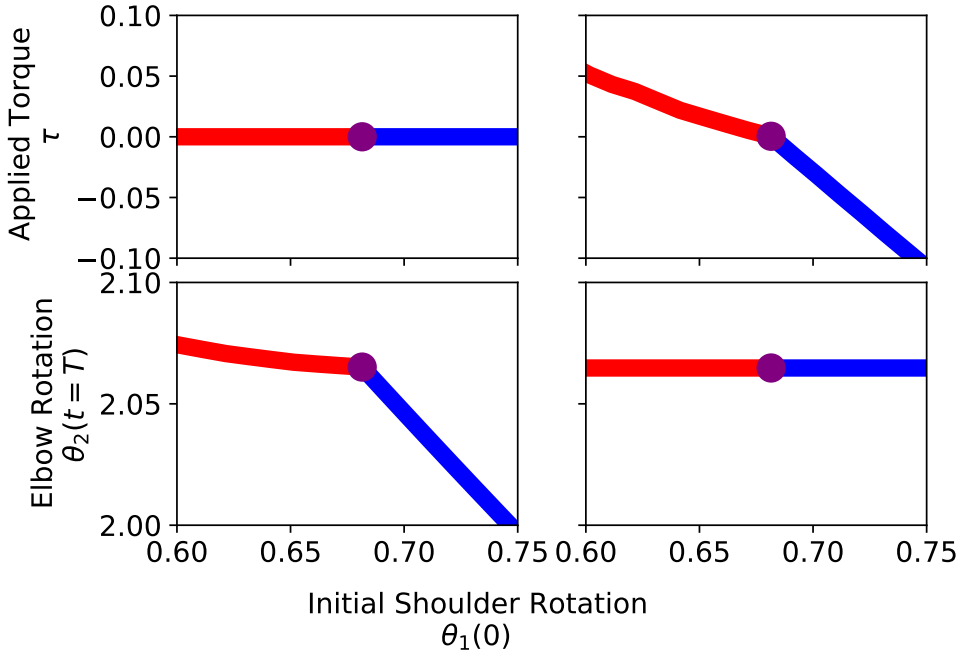

Figure 4.7: Demonstration of the nonsmooth control law[36]

Chapter 5

DISCUSSION

The goal of this dissertation is to argue legged robots are inherently a different type of dynamical system from classical mechanical systems, and provide initial steps towards developing rigorous control techniques handling impact. Legged robots are a type of rigid mechanical system undergoing impacts, trajectories will experience a rapid change in velocity at every impact. These trajectories, while continuous in the physical world, are highly nonlinear and experience two different time constants, away and near points at impact. Utilizing hybrid dynamics, we can capture the salient features of these systems, periods of continuous motion punctuated by rapid jumps in velocity.

In Chapter 2, we showed for a system as simple as the billiard, there does not exist a compatible distance function for an extended, i.e. continuous, trajectory whenever the impact is not perfectly elastic. Importantly, this result means the notion of distance between two points along a trajectory undergoing impact is distinct from the distance along continuous trajectories. Hence, new control techniques are needed for systems undergoing impact. We developed two such tools, one for state estimation, in Chapter 3, and the other for control input generation, in Chapter 4. Future work in both cases is still needed, an online method for state (both continuous and discrete) estimation and a continuous feedback controller for piecewise–differentiable systems. It remains to be seen how precise the change in discrete state must be determined based on a given controller. We suspect, at least for legged robots, it will greatly depend on the continuous mode dynamics (and hence on how the physical robot is designed). Another possibility is designing the controller to be robust to hybrid mode switches, e.g. the change in continuous dynamics and resets. Another avenue for further research is better characterization of continuous extensions of trajectories undergoing

impact considering what are the trade offs between requiring exact projection to the original trajectory, continuous trajectories, or compatible distance functions. Perhaps relaxing the requirement of compatible distance functions around points of impacts will allow the use control methodologies similar to those used for continuous systems.

BIBLIOGRAPHY

[1] N. Aghannan and P. Rouchon. An intrinsic observer for a class of lagrangian systems. *IEEE Transactions on Automatic Control*, 48(6):936–945, June 2003.

[2] M. A. Aizerman and F. R. Gantmacher. Determination of Stability by Linear Approximation of a Periodic Solution of a System of Differential Equations with Discontinuous Right-Hand Sides. *The Quarterly Journal of Mechanics and Applied Mathematics*, 11(4):385–398, 1958.

[3] A. Alessandri, M. Baglietto, and G. Battistelli. Receding-horizon estimation for switching discrete-time linear systems. *IEEE Transactions on Automatic Control*, 50(11):1736–1748, November 2005.

[4] Angelo Alessandri, Marco Baglietto, and Giorgio Battistelli. Minimum-Distance Receding-Horizon State Estimation for Switching Discrete-Time Linear Systems. In *Assessment and Future Directions of Nonlinear Model Predictive Control*, number 358 in Lecture Notes in Control and Information Sciences, pages 348–366. Springer-Verlag Berlin Heidelberg, 2007.

[5] Aleksandr Aravkin, James V. Burke, Lennart Ljung, Aurelie Lozano, and Gianluigi Pillonetto. Generalized Kalman smoothing: Modeling and algorithms. *Automatica*, 86:63–86, December 2017.

[6] Aleksandr Aravkin, James V. Burke, and Gianluigi Pillonetto. Robust and Trend-Following Kalman Smoothers using Student's t. *IFAC Proceedings Volumes*, 45(16):1215–1220, July 2012.

[7] Aleksandr Aravkin, Dmitriy Drusvyatskiy, and Tristan van Leeuwen. Variable projection without smoothness. *arXiv preprint arXiv:1601.05011*, 2016.

[8] Aleksandr Y Aravkin, James V Burke, and Gianluigi Pillonetto. Robust and trend-following student's t kalman smoothers. *SIAM Journal on Control and Optimization*, 52(5):2891–2916, 2014.

[9] Laurent Bako and Stéphane Lecoeuche. A sparse optimization approach to state observer design for switched linear systems. *Systems & Control Letters*, 62(2):143–151, February 2013.

[10] Patrick Ballard. The Dynamics of Discrete Mechanical Systems with Perfect Unilateral Constraints. *Archive for Rational Mechanics and Analysis*, 154(3):199–274, September 2000.

[11] A. Balluchi, L. Benvenuti, M.D. Di Benedetto, and A.L. Sangiovanni-Vincentelli. Observability for hybrid systems. In *Proceedings of the IEEE Conference on Decision and Control*, volume 2, pages 1159–1164, Maui, Hawaii, USA, 2003. IEEE.

[12] Andrea Balluchi, Luca Benvenuti, Maria D. Di Benedetto, and Alberto Sangiovanni-Vincentelli. The design of dynamical observers for hybrid systems: Theory and application to an automotive control problem. *Automatica*, 49(4):915–925, 2013-04, 2013.

[13] Andrea Balluchi, Luca Benvenuti, Maria D. Di Benedetto, and Alberto L. Sangiovanni-Vincentelli. Design of Observers for Hybrid Systems. In *Proceedings of Hybrid Systems: Computation and Control (HSCC)*, volume 2289, pages 76–89, Berlin, Heidelberg, 2002. Springer Berlin Heidelberg.

[14] N. Barhoumi, F. Msahli, M. Djemaï, and K. Busawon. Observer design for some classes of uniformly observable nonlinear hybrid systems. *Nonlinear Analysis: Hybrid Systems*, 6(4):917–929, 2012-11, 2012.

[15] Amir Beck and Marc Teboulle. A fast iterative shrinkage-thresholding algorithm for linear inverse problems. *SIAM Journal on Imaging Sciences*, 2(1):183–202, 2009.

[16] A. Bemporad, D. Mignone, and M. Morari. Moving horizon estimation for hybrid systems and fault detection. In *Proceedings of the American Control Conference*, volume 4, pages 2471–2475 vol.4, June 1999.

[17] J. J. B. Biemond, N. van de Wouw, W. P. M. H. Heemels, and H. Nijmeijer. Tracking Control for Hybrid Systems With State-Triggered Jumps. *IEEE Transactions on Automatic Control*, 58(4):876–890, April 2013.

[18] H. A. P. Blom and E. A. Bloem. Exact Bayesian and particle filtering of stochastic hybrid systems. *IEEE Transactions on Aerospace and Electronic Systems*, 43(1):55–70, 2007-01, 2007.

[19] Henk A. P. Blom and Yaakov Bar-Shalom. The Interacting Multiple Model Algorithm for Systems with Markovian Switching Coefficients. *IEEE Transactions on Automatic Control*, 33(8), August 1988.

[20] Bernard Brogliato. *Nonsmooth Mechanics: Models, Dynamics and Control.* Springer, 1999.

[21] Bernard Brogliato and Daniel Goeleven. Singular mass matrix and redundant constraints in unilaterally constrained Lagrangian and Hamiltonian systems. *Multibody System Dynamics*, 35(1):39–61, September 2015.

[22] Francesco Bullo and Richard M. Murray. Tracking for fully actuated mechanical systems: A geometric framework. *Automatica*, 35(1):17–34, January 1999.

[23] Samuel A Burden. *A Hybrid Dynamical Systems Theory for Legged Locomotion*. PhD thesis, University of California, Berkeley, 2014.

[24] Samuel A. Burden, Humberto Gonzalez, Ramanarayan Vasudevan, Ruzena Bajcsy, and S. Shankar Sastry. Metrization and Simulation of Controlled Hybrid Systems. *IEEE Transactions on Automatic Control*, 60(9):2307–2320, September 2015.

[25] Samuel A. Burden, Shai Revzen, and S. Shankar Sastry. Model Reduction Near Periodic Orbits of Hybrid Dynamical Systems. *IEEE Transactions on Automatic Control*, 60(10):2626–2639, October 2015.

[26] Samuel A. Burden, S. Shankar Sastry, Daniel E. Koditschek, and Shai Revzen. Event–Selected Vector Field Discontinuities Yield Piecewise–Differentiable Flows. *SIAM Journal on Applied Dynamical Systems*, 15(2):1227–1267, January 2016.

[27] James V Burke. Descent methods for composite nondifferentiable optimization problems. *Mathematical Programming*, 33(3):260–279, 1985.

[28] M. Di Bernardo, C.J. Budd, A.R. Champneys, and P. Kowalczyk. *Piecewise-Smooth Dynamical Systems: Theory and Applications*. Number 163 in Applied Mathematical Sciences. Springer, London, 2008.

[29] A. Doucet, N. J. Gordon, and V. Krishnamurthy. Particle filters for state estimation of jump Markov linear systems. *IEEE Transactions on Signal Processing*, 49(3):613–624, 2001-03, 2001.

[30] Jindřich Duník, Ondřej Straka, Oliver Kost, and Jindřich Havlík. Noise covariance matrices in state-space models: A survey and comparison of estimation methods—Part I. *International Journal of Adaptive Control and Signal Processing*, 31(11):1505–1543, 2017.

[31] Nima Fazeli, Samuel Zapolsky, Evan Drumwright, and Alberto Rodriguez. Learning Data-Efficient Rigid-Body Contact Models: Case Study of Planar Impact. In *Proceedings of the Conference on Robot Learning*, page 10, 2017.

[32] G. Ferrari-Trecate, D. Mignone, and M. Morari. Moving horizon estimation for hybrid systems. *IEEE Transactions on Automatic Control*, 47(10):1663–1676, October 2002.

[33] G Ferrari-Trecate, D Mignone, and M Morari. Moving horizon estimation for hybrid systems. *IEEE transactions on automatic control*, 47(10):1663–1676, October 2002.

[34] A. F. Filippov. *Differential Equations with Discontinuous Righthand Sides*. Kluwer Academic Publishers, 1988.

[35] F. Forni, A. R. Teel, and L. Zaccarian. Follow the Bouncing Ball: Global Results on Tracking and State Estimation With Impacts. *IEEE Transactions on Automatic Control*, 58(6):1470–1485, June 2013.

[36] R J Full and D E Koditschek. Templates and Anchors: Hypotheses of legged locomotion on land. *Journal of Experimental Biology*, 202:8, 1999.

[37] S. Galeani, L. Menini, A. Potini, and A. Tornambè. Trajectory tracking for a particle in elliptical billiards. *International Journal of Control*, 81(2):189–213, February 2008.

[38] Eric Gerde and M. Marder. Friction and fracture. *Nature*, 413(6853):285–288, September 2001.

[39] R. Goebel, R.G. Sanfelice, and A. Teel. Hybrid dynamical systems. *IEEE Control Systems*, 29(2):28–93, April 2009.

[40] Rafal Goebel, Joao Hespanha, Andrew R. Teel, Chaohong Cai, and Ricardo Sanfelice. Hybrid systems: Generalized solutions and robust stability. *IFAC Proceedings Volumes*, 37(13):1–12, September 2004.

[41] D. Gómez-Gutiérrez, S. Čelikovský, A. Ramírez-Treviño, J. Ruiz-Léon, and S. Di Gennaro. Sliding mode observer for Switched Linear Systems. In *IEEE International Conference on Automation Science and Engineering*, pages 725–730, 2011-08, 2011.

[42] John Guckenheimer and Philip Holmes. *Nonlinear Oscillations, Dynamical Systems, and Bifurcations of Vector Fields*. Springer, 1983.

[43] J. P. Hespanha and A. S. Morse. Stability of switched systems with average dwell-time. In *Proceedings of the IEEE Conference on Decision and Control*, volume 3, pages 2655–2660, December 1999.

[44] Morris W. Hirsch, Stephen Smale, and Robert L. Devaney. *Differential Equations, Dynamical Systems, and an Introduction to Chaos*. Elsevier, 2013.

[45] George W. Housner. The behavior of inverted pendulum structures during earthquakes. *Bulletin of the Seismological Society of America*, 53(2):403–417, February 1963.

[46] Olivier Huber and Harshal B. Oza. Implicit numerical integration for the simulation and control of a non-smooth system with resets. In *2016 IEEE 55th Conference on Decision and Control (CDC)*, pages 6551–6556, December 2016.

[47] John D. Hunter. Matplotlib: A 2D Graphics Environment. *Computing in Science Engineering*, 9(3):90–95, May 2007.

[48] Dong Jin Hyun, Sangok Seok, Jongwoo Lee, and Sangbae Kim. High speed trot-running: Implementation of a hierarchical controller using proprioceptive impedance control on the MIT Cheetah. *The International Journal of Robotics Research*, 33(11):1417–1445, September 2014.

[49] A.P. Ivanov. The stability of periodic solutions of discontinuous systems that intersect several surfaces of discontinuity. *Journal of Applied Mathematics and Mechanics*, 62(5):677–685, January 1998.

[50] Aaron M Johnson, Samuel A Burden, and Daniel E Koditschek. A hybrid systems model for simple manipulation and self-manipulation systems. *The International Journal of Robotics Research*, 35(11):1354–1392, September 2016.

[51] Scott C Johnson. *Observability and Observer Design for Switched Linear Systems*. PhD thesis, Purdue University, December 2016.

[52] Gavin Kenneally, Avik De, and D. E. Koditschek. Design Principles for a Family of Direct-Drive Legged Robots. *IEEE Robotics and Automation Letters*, 1(2):900–907, July 2016.

[53] Jisu Kim, Hyungbo Shim, and Jin Heon Seo. State Estimation and Tracking Control for Hybrid Systems by Gluing the Domains. *IEEE Transactions on Automatic Control*, 64(7):3026–3033, July 2019.

[54] Krysztof C. Kiwiel. *Methods of Descent for Nondifferentiable Optimization*. Springer-Verlag, 1985.

[55] Scott Kuindersma, Robin Deits, Maurice Fallon, Andrés Valenzuela, Hongkai Dai, Frank Permenter, Twan Koolen, Pat Marion, and Russ Tedrake. Optimization-based locomotion planning, estimation, and control design for the atlas humanoid robot. *Autonomous Robots*, 40(3):429–455, March 2016.

[56] Vikash Kumar, Emanuel Todorov, and Sergey Levine. Optimal control with learned local models: Application to dexterous manipulation. In *2016 IEEE International Conference on Robotics and Automation (ICRA)*, pages 378–383, Stockholm, Sweden, May 2016. IEEE.

[57] Jerzy Kyparisis. Uniqueness and differentiability of solutions of parametric nonlinear complementarity problems. *Mathematical Programming*, 36(1):105–113, October 1986.

[58] Roger Labbe. FilterPy, 2014. https://github.com/rlabbe/filterpy.

[59] John M. Lee. *Introduction to Smooth Manifolds*. Number 218 in Graduate Texts in Mathematics. Springer, New York ; London, 2nd ed edition, 2013.

[60] John M. Lee. *Introduction to Riemannian Manifolds*. Springer Berlin Heidelberg, New York, NY, 2018.

[61] Remco I. Leine and Nathan van de Wouw. *Stability and Convergence of Mechanical Systems with Unilateral Constraints*. Number v. 36 in Lecture Notes in Applied and Computational Mechanics. Springer, Berlin, 2008.

[62] N J Lennes. On the Motion of a Ball on a Billiard Table. *The American Mathematical Monthly*, 12(8/9):5, August 1905.

[63] A.U. Levin and K.S. Narendra. Control of nonlinear dynamical systems using neural networks: Controllability and stabilization. *IEEE Transactions on Neural Networks*, 4(2):192–206, March 1993.

[64] Sergey Levine, Chelsea Finn, Trevor Darrell, and Pieter Abbeel. End-to-End Training of Deep Visuomotor Policies. *Journal of Machine Learning Research*, 17:40, April 2016.

[65] Andrew D. Lewis. Is it worth learning differential geometric methods for modeling and control of mechanical systems? *Robotica*, 25(6):765–777, November 2007.

[66] Per Lötstedt. Mechanical Systems of Rigid Bodies Subject to Unilateral Constraints. *SIAM Journal on Applied Mathematics*, 42(2):281–296, 1982.

[67] J. Lygeros, K.H. Johansson, S.N. Simic, Jun Zhang, and S.S. Sastry. Dynamical properties of hybrid automata. *IEEE Transactions on Automatic Control*, 48(1):2–17, January 2003.

[68] Saunders Mac Lane. Geometrical Mechanics v1. Accessed via https://harrydole.com/Mac%20Lane, 1968.

[69] R. Mallik, A. M. Pace, S. A. Burden, and B. Johnson. Accurate Small–Signal Discrete–Time Model of Dual Active Bridge using Saltation Matrices. In *2020 IEEE Energy Conversion Congress and Exposition (ECCE)*, pages 6312–6317, October 2020.

[70] L. Menini and A. Tornambe. Asymptotic tracking of periodic trajectories for a simple mechanical system subject to nonsmooth impacts. *IEEE Transactions on Automatic Control*, 46(7):1122–1126, July 2001.

[71] L. Menini and A. Tornambe. Asymptotic tracking of periodic trajectories for a simple mechanical system subject to nonsmooth impacts. *IEEE Transactions on Automatic Control*, 46(7):1122–1126, July 2001.

[72] Katja D. Mombaur, Richard W. Longman, Hans Georg Bock, and Johannes P. Schlöder. Open-loop stable running. *Robotica*, 23(1):21–33, January 2005.

[73] K.D. Mombaur, H.G. Bock, J.P. Schloder, and R.W. Longman. Self-stabilizing somersaults. *IEEE Transactions on Robotics*, 21(6):1148–1157, December 2005.

[74] Richard Montgomery. *A Tour of Subriemannian Geometries, Their Geodesics and Applications*, volume 91 of *Mathematical Surveys and Monographs*. American Mathematical Society, United States of America, 2002.

[75] Irinel Constantin Morărescu and Bernard Brogliato. Trajectory Tracking Control of Multiconstraint Complementarity Lagrangian Systems. *IEEE Transactions on Automatic Control*, 55(6):1300–1313, June 2010.

[76] James Munkres. *Topology*. Pearson, second edition, 2000.

[77] Marian Ioan Munteanu. Old and New Structures on the Tangent Bundle. In *Conference on Geometry, Integrability and Quantization*, Varna, Bulgaria, 2007. GIQ.

[78] Richard M. Murray, Zexiang Li, and S. Shankar Sastry. *A Mathematical Introduction to Robotic Manipulation*. CRC Press, 1994.

[79] Jorge Nocedal and Stephen J Wright. *Nonlinear Equations*. Springer, 2006.

[80] Lael U. Odhner, Leif P. Jentoft, Mark R. Claffee, Nicholas Corson, Yaroslav Tenzer, Raymond R. Ma, Martin Buehler, Robert Kohout, Robert D. Howe, and Aaron M. Dollar. A compliant, underactuated hand for robust manipulation. *The International Journal of Robotics Research*, 33(5):736–752, April 2014.

[81] Travis E. Oliphant. *A Guide to NumPy*. Trelgol Publishing, USA, 2006.

[82] Yizhar Or and Aaron D. Ames. Stability and Completion of Zeno Equilibria in Lagrangian Hybrid Systems. *IEEE Transactions on Automatic Control*, 56(6):1322–1336, June 2011.

[83] A. M. Pace and S. A. Burden. Decoupled limbs yield differentiable trajectory outcomes through intermittent contact in locomotion and manipulation. In *2017 IEEE International Conference on Robotics and Automation (ICRA)*, pages 2261–2266, May 2017.

[84] Andrew M. Pace and Samuel A. Burden. Piecewise - Differentiable Trajectory Outcomes in Mechanical Systems Subject to Unilateral Constraints. In *Proceedings of the 20th International Conference on Hybrid Systems: Computation and Control - HSCC '17*, pages 243–252, Pittsburgh, Pennsylvania, USA, 2017. ACM Press.

[85] David Pekarek, Vlad Seghete, and Todd D Murphey. The Projected Hamilton's Principle: Modeling Nonsmooth Mechanics as Switched Systems. unpublished, January 2017.

[86] Elijah Polak. *Optimization: Algorithms and Consistent Approximations*. Springer, 1997.

[87] C. David Remy, Keith Buffinton, and Roland Siegwart. Stability Analysis of Passive Dynamic Walking of Quadrupeds. *The International Journal of Robotics Research*, 29(9):1173–1185, August 2010.

[88] M. Rijnen, A. Saccon, and H. Nijmeijer. Reference Spreading: Tracking Performance for Impact Trajectories of a 1DoF Setup. *IEEE Transactions on Control Systems Technology*, pages 1–8, 2019.

[89] Mark Rijnen, Benjamin Biemond, Nathan Van De Wouw, Alessandro Saccon, and Henk Nijmeijer. Hybrid Systems with State-Triggered Jumps: Sensitivity-Based Stability Analysis with Application to Trajectory Tracking. *IEEE Transactions on Automatic Control*, pages 1–1, 2019.

[90] Mark Rijnen, Hao Liang Chen, Nathan van de Wouw, Alessandro Saccon, and Henk Nijmeijer. Sensitivity analysis for trajectories of nonsmooth mechanical systems with simultaneous impacts: A hybrid systems perspective. In *2019 American Control Conference (ACC)*, pages 3623–3629, July 2019.

[91] Stephen M. Robinson. Local structure of feasible sets in nonlinear programming, Part III: Stability and sensitivity. In *Nonlinear Analysis and Optimization*, volume 30, pages 45–66. Springer Berlin Heidelberg, Berlin, Heidelberg, 1987.

[92] R T Rockafellar. A Property of Piecewise Smooth Functions. *Computational Optimization and Applications*, page 4, 2003.

[93] R. Tyrrell Rockafellar and Roger J.-B. Wets. *Variational Analysis*. Springer Verlag, Heidelberg, Berlin, New York, 1998.

[94] Alessandro Saccon, Nathan van de Wouw, and Henk Nijmeijer. Sensitivity analysis of hybrid systems with state jumps with application to trajectory tracking. In *IEEE Conference on Decision and Control*, pages 3065–3070. IEEE, December 2014.

[95] M Schatzman. Uniqueness and continuous dependence on data for one–dimensional impact problems. *Mathematical and Computer Modelling*, 28(4—8):1–18, 1998.

[96] Stefan Scholtes. *Introduction to Piecewise Differentiable Equations*. SpringerBriefs in Optimization. Springer, New York, 2012.

[97] C E Seah and I Hwang. State Estimation for Stochastic Linear Hybrid Systems with Continuous-State-Dependent transitions: An IMM approach. *IEEE Transactions on Aerospace and Electronic Systems*, 45(1):376–392, January 2009.

[98] Vlad Seghete and Todd D. Murphey. A Propagative Model of Simultaneous Impact: Existence, Uniqueness, and Design Consequences. *IEEE Transactions on Automation Science and Engineering*, 11(1):154–168, January 2014.

[99] Alexander Spröwitz, Alexandre Tuleu, Massimo Vespignani, Mostafa Ajallooeian, Emilie Badri, and Auke Jan Ijspeert. Towards dynamic trot gait locomotion: Design, control, and experiments with Cheetah-cub, a compliant quadruped robot. *The International Journal of Robotics Research*, 32(8):932–950, July 2013.

[100] Robert R. Stengel. *Optimal Control and Estimation*. Dover, 1994.

[101] D. Stewart and J.C. Trinkle. An implicit time-stepping scheme for rigid body dynamics with Coulomb friction. In *2000 IEEE International Conference on Robotics and Automation*, pages 162–169, San Fransico, CA, 2000. IEEE.

[102] Richard Sutton and Andrew Barto. *Reinforcement Learning: An Introduction*. The MIT Press, second edition, 2018.

[103] E. Todorov. A convex, smooth and invertible contact model for trajectory optimization. In *2011 IEEE International Conference on Robotics and Automation*, pages 1071–1076, May 2011.

[104] Stefan van der Walt, S. Chris Colbert, and Gael Varoquaux. The NumPy Array: A Structure for Efficient Numerical Computation. *Computing in Science Engineering*, 13(2):22–30, March 2011.

[105] René Vidal, Alessandro Chiuso, Stefano Soatto, Shankar Sastry, Gerhard Goos, Juris Hartmanis, and Jan van Leeuwen. Observability of Linear Hybrid Systems. In *Hybrid Systems: Computation and Control*, volume 2623, pages 526–539. Springer Berlin Heidelberg, Berlin, Heidelberg, 2003.

[106] Jize Zhang. *Nonconvex Optimization Methods with Applications to Portfolio Selection and Hybrid Systems*. PhD thesis, University of Washington, Seattle, 2020.

[107] Jize Zhang, Andrew M. Pace, Samuel A. Burden, and Aleksandr Aravkin. Offline state estimation for hybrid systems via nonsmooth variable projection. *Automatica*, 115:108871, May 2020.

Appendix A

APPENDICES FOR CHAPTER 3

A.1 Switched and hybrid dynamical systems

A *hybrid dynamical system* is a tuple $H = (D, F, G, R)$ [25, 39] where

$$D = \coprod_{j \in J} D_j,\ F : D \to TD,\ G \subset D,\ R : G \to D.$$

With $\phi : [0, \infty) \times D \to D$ the *flow* of H, then a discrete-time switched nonlinear system is obtained by *sampling* H with timestep $\Delta > 0$:

$$x^+ = \phi(\Delta, x).$$

This equation may not immediately appear to be "switched", but the function ϕ is only piecewise-continuous; the switching structure can be exposed with reference to the flows $\phi_j : [0, \infty) \times D_j \to D_j$ and *time-to-guard* $\tau_j : D_j \to [0, \infty)$, $\tau_{j,k} : D_j \to [0, \infty)$ functions associated with each discrete state $j \in J$ and pair of discrete states $(j, k) \in J \times J$:

$$x^+ = \begin{cases} \phi_j(\Delta, x), & \tau_j(x) > \Delta; \\ \phi_k\left(\Delta - \tau_{j,k}(x), R_{j,k}\left(\phi_j(\tau_{j,k}(x), x)\right)\right), & \\ & \tau_j(x) = \tau_{j,k}(x) \leq \Delta. \end{cases}$$

This piecewise-defined equation, equivalent to (but much more explicit than) $x^+ = \phi(\Delta, x)$, is a discrete-time switched nonlinear system (in particular, each function in the piecewise definition is continuously differentiable) with model set indexed by $M = J \cup (J \times J)$ and switching rule determined as a function of x:

$$m(x) = \begin{cases} j, & \tau_j(x) > \Delta; \\ (j, k), & \tau_j(x) = \tau_{j,k}(x) \leq \Delta. \end{cases}$$

A.2 Linear Spring Double Mass Hopper

For more on the theory of modeling systems as mechanical systems subject to unilateral constraints, see [66]. To explicitly formulate the hybrid dynamical system given in Sec. 3.7.1, we use the hybrid dynamical system definition found in [50, §3.1].

$$\mathcal{J} = \{\mathrm{A}\downarrow, \mathrm{G}\downarrow, \mathrm{G}\uparrow, \mathrm{A}\uparrow\}$$

$$\Gamma = K_4$$

A completely connected graph with 4 vertices

$$D_{\mathrm{A}\downarrow} = \{(q, \dot{q}) \in \mathbb{R}^4 | q[2] \geq 0 \text{ and } \dot{q}[2] \leq 0\}$$

$$D_{\mathrm{G}\downarrow} = \{(q, \dot{q}) \in \mathbb{R}^4 | q[2] = 0 \text{ and } \dot{q}[2] \leq 0\}$$

$$D_{\mathrm{G}\uparrow} = \{(q, \dot{q}) \in \mathbb{R}^4 | q[2] = 0 \text{ and } \dot{q}[2] \geq 0\}$$

$$D_{\mathrm{A}\uparrow} = \{(q, \dot{q}) \in \mathbb{R}^4 | q[2] \geq 0 \text{ and } \dot{q}[2] \geq 0\}$$

$$G_{\{\mathrm{A}\downarrow,\mathrm{G}\downarrow\}} = \{(q, \dot{q}) | q[\mathrm{G}\downarrow] = 0 \text{ and } \dot{q}[\mathrm{G}\downarrow] \leq 0\}$$

$$G_{\{\mathrm{A}\downarrow,\mathrm{G}\uparrow\}} = \{(q, \dot{q}) | q[\mathrm{G}\downarrow] = 0 \text{ and } \dot{q}[\mathrm{G}\downarrow] \leq 0 \text{ and } \dot{q}[\mathrm{A}\downarrow] > 0\}$$

$$G_{\{\mathrm{A}\downarrow,\mathrm{A}\uparrow\}} = \{(q, \dot{q}) | \dot{q}[\mathrm{A}\downarrow] = 0 \text{ and } F_{\mathrm{A}\downarrow}(q, \dot{q})[\mathrm{G}\downarrow] \geq 0\}$$

$$G_{\{\mathrm{G}\downarrow,\mathrm{A}\downarrow\}} = \{(q, \dot{q}) | F_{\mathrm{G}\downarrow}(q, \dot{q})[\mathrm{G}\downarrow] \geq 0\}$$

$$G_{\{\mathrm{G}\downarrow,\mathrm{G}\uparrow\}} = \{(q, \dot{q}) | \dot{q}[\mathrm{A}\downarrow] > 0\}$$

$$G_{\{\mathrm{G}\downarrow,\mathrm{A}\uparrow\}} = \{(q, \dot{q}) | \dot{q}[\mathrm{A}\downarrow] > 0 \text{ and } F_{\mathrm{G}\downarrow}(q, \dot{q})[\mathrm{G}\downarrow] \geq 0\}$$

$$G_{\{\mathrm{G}\uparrow,\mathrm{A}\downarrow\}} = \{(q, \dot{q}) | \dot{q}[\mathrm{A}\downarrow] < 0 \text{ and } F_{\mathrm{G}\uparrow}(q, \dot{q})[\mathrm{G}\downarrow] \geq 0\}$$

$$G_{\{\mathrm{G}\uparrow,\mathrm{G}\downarrow\}} = \{(q, \dot{q}) | \dot{q}[\mathrm{A}\downarrow] > 0\}$$

$$G_{\{\mathrm{G}\uparrow,\mathrm{A}\uparrow\}} = \{(q, \dot{q}) | F_{\mathrm{G}\uparrow}(q, \dot{q})[\mathrm{G}\downarrow] \geq 0\}$$

$$G_{\{\mathrm{A}\uparrow,\mathrm{A}\downarrow\}} = \{(q, \dot{q}) | \dot{q}[\mathrm{A}\downarrow] < 0\}$$

$$G_{\{\mathrm{A}\uparrow,\mathrm{G}\downarrow\}} = \{(q, \dot{q}) | \dot{q}[\mathrm{A}\downarrow] < 0 \text{ and } q[\mathrm{G}\downarrow] = 0 \text{ and } \dot{q}[\mathrm{G}\downarrow] < 0\}$$

$$G_{\{\mathrm{A}\uparrow,\mathrm{G}\uparrow\}} = \{(q, \dot{q}) | q[\mathrm{G}\downarrow] = 0 \text{ and } \dot{q}[\mathrm{G}\downarrow] < 0\}$$

$$R_{\{i,j\}}(q, \dot{q}) = \begin{cases} (q, \dot{q}[1], 0) \text{ for } i \in \{\mathrm{A}\downarrow, \mathrm{A}\uparrow\} \text{ and } j \in \{\mathrm{G}\downarrow, \mathrm{G}\uparrow\} \\ (q, \dot{q}[1], \dot{q}[2] \text{ otherwise} \end{cases}$$

The vector fields are defined in (**??**).

A.3 Nonlinear double mass hopper hybrid system description

$$\mathcal{J} = \{\mathrm{A}, \mathrm{G}\}$$

$$\Gamma = K_2$$

A completely connected graph with 2 vertices

$$D_{\mathrm{A}} = \{(q, \dot{q}) \in \mathbb{R}^4 | q_{\mathrm{G}} \geq 0 \text{ and } \dot{q}_{\mathrm{A}} \leq 0\}$$

$$D_{\mathrm{G}} = \{(q, \dot{q}) \in \mathbb{R}^4 | q_{\mathrm{G}} = 0 \text{ and } \dot{q}_{\mathrm{A}} \leq 0\}$$

$$G_{\{\mathrm{A,G}\}} = \{(q, \dot{q}) | q[2] = 0 \text{ and } \dot{q}[2] \leq 0\}$$

$$G_{\{\mathrm{G,A}\}} = \{(q, \dot{q}) | F_{\mathrm{G}}(q, \dot{q})[2] \geq 0\}$$

$$R_{\{\mathrm{A,G}\}}(q, \dot{q}) = (q, \dot{q}[q], 0)$$

$$R_{\{\mathrm{G,A}\}}(q, \dot{q}) = (q, \dot{q})$$

The vector fields include a nonlinear of the spring force.

A.4 With measurement model $\mathcal{H}_{\text{relative}}$, the linear one foot robot described in 3.7.2 is unobservable.

PROPOSITION 1. *Given the discrete mode sequence, the switched linear system given by the dynamics $\dot{x} = A_i x$ and $y = Cx$ is continuous state unobservable, with A_i the forward Euler's approximation of* (**??**) *with $\Delta t = .01$ and $i \in \{1, 2, 3, 4\}$ and $C = \begin{bmatrix} 1 & 0 & -1 & 0 \\ 0 & 1 & 0 & -1 \end{bmatrix}$.*

Proof: For the system described in Sec. 3.7.1 and given more explicitly in App. A.2 the reset map is either I, the identity matrix, or $R = \text{diag}(1, 1, 1, 0)$. Let

$$T_O = \begin{bmatrix} \frac{1}{\sqrt{2}} & 0 & \frac{1}{\sqrt{2}} & 0 \\ 0 & \frac{1}{\sqrt{2}} & 0 & \frac{1}{\sqrt{2}} \end{bmatrix} \tag{A.1}$$

$$T_N = \begin{bmatrix} -\frac{1}{\sqrt{2}} & 0 & \frac{1}{\sqrt{2}} & 0 \\ 0 & -\frac{1}{\sqrt{2}} & 0 & \frac{1}{\sqrt{2}} \end{bmatrix} \tag{A.2}$$

$$T = \begin{bmatrix} T_O \\ T_N \end{bmatrix}. \tag{A.3}$$

T is an observable decomposition, with T_N being the unobservable transformation for all four discrete state. As such, for any discrete mode sequence, the unobservable subspace remains constant. As the nullspace of the reset map is not the unobservable subspace nor do either reset map R or I permute the statespace, the switched linear system defined by the above dynamics is unobservable. A more concise viewpoint is for any finite n, $(RT_N^T T_N)^n \neq 0$,

- $(T_N^T T_N)(T_N^T T_N) = T_N^T T_N$
- for any finite n, $(T_N^T R T_N)^n \neq 0$

hence the system is continuous state unobservable. □